Aus dem Adolf-Butenandt-Institut der
Ludwig-Maximilians-Universität München
Lehrstuhl: Stoffwechselbiochemie
Vorstand: Prof. Dr. rer. nat. Dr. h.c. Christian Haass

Characterization of the *C9orf72* Dipeptide Repeat Proteins in Frontotemporal Dementia and Amyotrophic Lateral Sclerosis

- Dissertation -

zum Erwerb des Doktorgrades der Naturwissenschaften (Dr. rer. nat)
an der Medizinischen Fakultät der Ludwig-Maximilians-Universität München

vorgelegt von
Stephanie May
aus Recklinghausen

2015

Gedruckt mit Genehmigung der Medizinischen Fakultät der Ludwig-Maximilians-Universität München

Betreuer: Prof. Dr. rer. nat. Dr. h.c. Christian Haass

Zweitgutachterin: Dr. Dorothee Dormann, Emmy Noether research group leader

Dekan: Herr Prof. Dr. med. dent. Reinhard Hickel

Tag der mündlichen Prüfung: 14.04.2016

Eidesstattliche Versicherung

Ich erkläre hiermit an Eides statt, dass ich die vorliegende Dissertation mit dem Thema *Characterization of the C9orf72 Dipeptide Repeat Proteins in Frontotemporal Dementia and Amyotrophic Lateral Sclerosis* selbständig verfasst, mich außer der angegebenen keiner weiteren Hilfsmittel bedient und alle Erkenntnisse, die aus dem Schrifttum ganz oder annähernd übernommen sind, als solche kenntlich gemacht und nach ihrer Herkunft unter Bezeichnung der Fundstelle einzeln nachgewiesen habe.
Ich erkläre des Weiteren, dass die hier vorgelegte Dissertation nicht in gleicher oder in ähnlicher Form bei einer anderen Stelle zur Erlangung eines akademischen Grades eingereicht wurde.

München, _____

_____

Stephanie May

Science is not only a disciple of reason

but, also, one of romance and passion

– Stephen Hawking

Summary

Amyotrophic lateral sclerosis (ALS) and frontotemporal dementia (FTD) are severe neurodegenerative diseases with overlapping clinical and pathological features. Recently, a GGGGCC hexanucleotide repeat expansion in the non-coding region of the *C9orf72* gene was discovered to be the most frequent pathogenic mutation in both diseases. Although lacking an ATG start codon, the repeat is translated into poly-GA, poly-GR and poly-GP dipeptide repeat (DPR) proteins. These DPR proteins form insoluble p62-positive inclusions distinct from the co-occuring TDP-43 positive inclusions that are also found in most other forms of ALS and FTD. It is unclear how DPR proteins are translated although the mutant allele is poorly expressed and, even more important, how they contribute to FTD/ALS.

My data shows that although the levels of the mature *C9orf72* mRNA are reduced in mutation carriers, the repeat containing transcripts are stabilized. Additionally, I discovered the antisense transcription of the repeat expansion and following it could be shown that the antisense RNA is translated into poly-PA, poly-PR and additional poly-GP DPR proteins.

To analyze the role of sense and antisense DPR proteins individually, I designed synthetic genes to express the DPR sequence with an ATG start codon but without GGGGCC repeats. Only poly-GA formed insoluble p62-positive aggregates similar to the neuropathological findings in patients. Additionally, aggregates in poly-GA transduced primary neurons had the same size and intensity as aggregates found in patients. Of the five DPR proteins, only poly-GA and poly-PR induced cell death in primary neurons. To elucidate the underlying toxicity mechanisms I used a mass spectrometry approach to identify poly-GA co-aggregating proteins. Although the poly-GA interactome showed a significant enrichment of proteins of the ubiquitin-proteasome system, I could not detect altered proteasome activity. Among the other interactors, Unc119, a factor controlling trafficking of lipidated cargo proteins, has been previously linked to neuromuscular function and axon maintenance in *C. elegans*.

Unc119 co-aggregates with poly-GA and the levels of soluble Unc119 were strongly reduced in neurons overexpressing poly-GA, indicating a loss of function. In patients, Unc119 is also partially sequestered into poly-GA aggregates. Unc119 knockdown in primary neurons inhibited dendritic branching and caused neurotoxicity similar to poly-GA overexpression. Importantly, Unc119 overexpression partially rescued poly-GA toxicity. Together, these findings support the hypothesis that Unc119 loss of function contributes to poly-GA toxicity. Apart from DPR inclusions, patients with *C9orf72* mutation show abundant aggregates of phosphorylated TDP-43, but TDP-43 and DPR inclusions rarely occur within the same cells. TDP-43 aggregation correlates with neurodegeneration, but it is unclear, how the *C9orf72* repeat expansion triggers TDP-43 pathology. In the neuronal expression model, poly-GA induced partial mislocalization of TDP-43 into small cytoplasmic aggregates, thus directly links both pathologies for the first time.

Taken together, I have established the first DPR protein cell culture system that replicates important features of *C9orf72* pathology and enables the prediction of novel pathological findings in patients such as Unc119 co-aggregation. The toxicity of poly-GA and poly-PR in primary neurons suggests that these proteins contribute to the pathogenesis of *C9orf72* ALS/FTD.

Zusammenfassung

Amyotrophe Lateralsklerose (ALS) und Frontotemporale Demenz (FTD) sind zwei schwerwiegende neurodegenerative Erkrankungen, welche überlappende klinische und pathologische Eigenschaften zeigen. Kürzlich wurde eine GGGGCC Hexanukleotid-Wiederholung außerhalb der kodierenden Sequenz des *C9orf72* Gens gefunden. Obwohl diese Wiederholungssequenz kein ATG Startcodon aufweist, wird sie in poly-GA, poly-GR und poly-GP Dipeptid Repeat (DPR) Proteine translatiert. Diese DPR Proteine bilden unlösliche p62-positive Einschlüsse, welche sich klar von den ebenso auftretenden TDP-43-positiven Einschlüssen in Patienten unterscheiden. Es ist allerdings unklar, warum DPR Proteine translatiert werden, obwohl das mutierte Allel schwach expremiert ist und wie sie zu FTD/ALS beitragen.

Die Daten meiner Arbeit zeigen, dass die Repeat-enthaltenden Transkripte stabilisiert sind, obwohl die gesplicte *C9orf72* mRNA in Mutationträgern reduziert ist. Des Weiteren konnte ich zeigen, dass die Antisense-Transkription der verlängerten Repeat-Region stattfindet und dies führte später zu der Entdeckung der Antisense Proteine poly-PA, poly-PR und poly-GP. Um den genauen Einfluss der Sense und Antisense DPR Proteine zu untersuchen habe ich synthetische Gene konzipiert, welche die DPR Sequenz mit einem ATG Startcodon, aber ohne die originale Repeatsequenz GGGGCC expremieren. Nur poly-GA zeigte die typischen unlöslichen p62-positiven Aggregate. Außerdem zeigen Aggregate in poly-GA transduzierten primären Neuronen die gleiche Größe und Intensität wie Aggregate in Patienten. Von den fünf DPR Proteinen induzierten nur poly-GA und poly-PR Apoptose in primären Neuronen. Mit Hilfe eines massenspektrometrischen Ansatzes wurden poly-GA co-aggregierende Proteine identifiziert. Unter den angereicherten Proteinen fanden sich besonders Proteine des Ubiquitin-Proteasom Systems und zusätzlich der Trafficking Faktor Unc119. Unc119 wurde bereits mit neuromuskulären Funktionen und der Instandhaltung von Axonen in Zusammenhang gebracht. Unc119 co-aggregiert mit poly-GA und die löslichen Level von Unc119

waren in meinem System stark reduziert und wiesen auf einen Verlust der Funktion hin. In Patienten, findet sich Unc119 ebenfalls in poly-GA Aggregaten, was zu einem Verlust des cytosolischen Unc119 führte. Unc119 Knockdown inhibiert die normale Verzweigung von Dendriten und verursacht Neurotoxizität, vergleichbar mit der Überexpression von poly-GA. Außerdem schwächt Unc119 Überexpression die poly-GA Toxizität deutlich ab. Zusammen unterstützen die Ergebnisse die Annahme, dass poly-GA die normale Unc119 Funktion stört.

Neben den DPR Protein Einschlüssen, finden sich weitere krankheitsrelevante Einschlüsse aus phosporyliertem TDP-43, die mit Neurodegeneration korrelieren. Weil TDP-43 und DPR Einschlüsse selten in der gleichen Zelle auftreten, ist unklar wie TDP-43 Veränderungen durch die *C9orf72* Mutation ausgelöst werden. In dem neuronalen Expressionssystem induziert poly-GA eine partielle Mislokalisation von TDP-43 in kleine cytoplasmatische Aggregate und verknüpft somit zum ersten Mal beide Arten von Pathologie.

Zusammengefasst, habe ich in dieser Arbeit das erste DPR Protein Zellkulturmodel etabliert, das viele wichtige Merkmale der Patienten reproduziert und erfolgreich Befunde in Patienten voraussagt, wie die Ko-Aggregation von poly-GA mit Unc119. Die Translation des *C9orf72*-Repeats in aggregierende DPR Proteine trägt höchstwahrscheinlich zur Pathogenese von ALS/FTD bei, da poly-GA und poly-PR das Absterben von Nervenzellen verursachen.

Table of Contents

List of Figures

List of Abbreviations

Aβ	Amyloid β
AD	Alzheimer´s disease
ALS	Amyotrophic lateral sclerosis
ALSci	ALS with FTLD cognitive impairment
ANOVA	Analysis of variance
APS	Ammonium persulfate
ASO	Antisense oligonucleotide
Atg5	Autophagy related 5
Atg7	Autophagy related 7
Bag6	Bcl2-associated athanogene 6
BS3	Bis-sulfosuccinimidyl suberate
BSA	Bovine serum albumin
Borax	Sodium borate decahydrate
bvFTD	Behavioral variant FTD
C9orf72	Chromosome 9 open reading frame 72
CA3/4	Cornu ammonis region 3/4
CBL	Cerebellar granular cell layer
CBP	CREB-binding protein
cDNA	Complementary DNA
CHMP2B	Charged multivesicular body protein 2b
CID	Collision-induced dissociation
CIP	Calf intestine phosphatase
CMA	Chaperone-mediated autophagy
CNS	Central nervous system
CSF	Cerebral spinal fluid
CT	Computer tomography
CTBP1	C-terminal binding protein 1
DAPI	4′,6-Diamidin-2-phenylindol
DENNL72	Differentially expressed in normal and neuoplastic cell like 72 (C9orf72 protein)
DG	Dentate gyrus
DIV	Days *in vitro*
DLDH	Dementia lacking distinctive histopathology
DMSO	Dimethylsulfoxide
DN	Dystrophic neurite
DNA	Desoxyribonucleic acid
dNTP	Deoxynucleotide
DPR	Dipeptide repeat
DTT	Dithiothreitol
E1	Ubiquitin activating enzyme
E2	Ubiquitin conjugation enzyme
E3	Ubiquitin ligase
E19	Embryonic day 19

E.coli	Escherichia coli
ECL	Enhanced chemiluminescence
EDTA	Ethylenediaminetetraacetic acid
EEG	Electro encephalogram
EMCCD	Electron-multiplying charged coupled device
EMG	Electromyography
EPDR1	Ependym-related 1
ER	Endoplasmic reticulum
FABP5	Fatty acid binding protein 5
fcMRI	Functional connectivity MRI
FCS	Fetal calf serum
FDA	US food and drug administration
FDG-PET	Fluordesoxyglucose-positron emission tomography
FDR	False discovery rate
fFTD	Familial frontotemporal dementia
FTD	Frontotemporal dementia
FTD-MND	Frontotemporal dementia with motor neuron disease
FTLD-U	Frontotemporal lobar degeneration (with ubiquitin pathology)
FUS	Fused-in-sarcoma
FXTAS	Fragile-x-tremor ataxia syndrome
GA	Glycine-Alanine
GFP/EGFP	Green fluorescent protein/enhanced GFP
GP	Glycine-Proline
GR	Glycine-Arginine
GRN	Progranulin
GST	Glutathione-S-transferase
HA	Human influenza hemaglutinin
HBSS	Hank´s balanced salt solution
HEK293 cells	Human embryonic kidney cells
HRP	Horse radish peroxidase
HSD17B4	Hydroxysteroid-(17-beta)-dehydrogenase 4
IAA	Iodoacetamide
IB	Immunoblot
IF	Immunofluorescence
IP	Immunoprecipitation
iPS cells	Induced pluripotent stem cells
IPTG	Isopropyl β-D-1-thiogalactopyranoside
kDa	Kilodalton
LB	Lysogeny broth
LC-MS/MS	Liquid chromatography-tandem mass spectrometry
LD	Linkage disequilibrium
LDH	Lactate dehydrogenase
LOAD	Late onset AD
LST4P	*C9orf72* yeast orthologe
MA	Macroautophagy
MAP	Microtubule-associated protein

MAPRE2	Microtubule-associated protein RP/EB family 2
MAPT	Microtubule-associated protein Tau
MD1	Myotonic dystrophy 1
MND	Motor neuron disease
MRI	Magnetic resonance imaging
MS	Multiple sclerosis
NA	Numeric aperture
NB	Neurobasal
NCI	Neuronal cytoplasmic inclusion
NEAA	Non-essential amino acids
NII	Neuronal intranuclear inclusion
NLS	Nuclear localization sequence
NMDAR	N-Methyl-D-aspartic acid receptor
NT	N-terminus
OD280	Optical density
OPTN	Optineurin
PA	Proline-Alanine
PBS	Phosphate-buffered saline
PCR	Polymerase chain reaction
PDL	Poly-D-lysine
PES	Polyehtersulfone
PFA	Paraformaldehyde
PNFA	Progressive nonfluent aphasia
PPA	Primary progressive aphasia
PR	Proline-Arginine
P/S	Penicillin/Streptamycin
PSD-95	Post-synaptic density protein 95
PSMC2	Proteasome 26S subunit ATPase 2
PSMC4	Proteasome 26S subunit ATPase 4
p-TDP-43	Phosphorylated TDP-43
PVDF	Polyvinylidene difluoride
qPCR	Quantitative PCR
RAN translation	Repeat associated non-ATG translation
RFP	Red fluorescent protein
RIPA	Radio immunoprecipitation assay
(m)RNA	(messenger) ribonucleic acid
RPL31	Ribosomal protein L31
rpm	Rounds per minute
RPS5	Ribosomal protein S5
RPT3	Regulatory particle triphosphatase
RT	Room temperature
RT-PCR	Reverse-transcriptase PCR
SBMA	Spinal and bulbar muscular atrophy
SCA1	Spinocerebellar ataxia type 1
SCA7	Spinocerebellar ataxia type 7
SCA8	Spinocerebellar ataxia type 8

SD	Semantic dementia
SDS-PAGE	Sodium dodecyl sulfate- polyacrylamide gel electrophoresis
SFG	Superia frontal gyrus
sFTD	Sporadic frontotemporal dementia
shRNA	Short hairpin RNA
SMA	Spinal muscular atrophy
SNP	Single nucleotide polymorphism
SOD1	Superoxide dismutase 1
SQSTM1	Sequestosome 1
SRB	Sulforhodamin B
SSRI	Selective serotonin reuptake inhibitor
STE	Sodiumchloride-Tris-EDTA
TARDBP/ TDP-43	Transactive response DNA-binding protein 43
TCA	Trichloric acetic acid
TEMED	Tetramethylethylendiamin
TMEM160	Transmembrane protein 160
TO-PRO-3	Quinolinium, 4-[3-(3-methyl-2(3H)-benzothiazolylidene)-1-propenyl]-1-[3-(trimethylammonio)propyl]-, diiodide
TUNEL	Terminal deoxynucleotidyl nick end labeling
UBQLN2	Ubiquilin 2
Unc119	Uncoordinated 119
UPS	Ubiquitin-proteasome system
UV	Ultraviolet
VCP	Valosin containing protein
wt	Wild-type
XTT	2,3-bis-(2-methoxy-4-nitro-5-sulfophenyl)-2H-tetrazolium-5-carboxanilide
YWHAZ	Tyrosine 3-monooxygenase/tryptophan 5-monooxygenase activation protein, zeta

1. Introduction

1.1. Frontotemporal dementia/Amyotrophic lateral sclerosis

Frontotemporal dementia (FTD) and amyotrophic lateral sclerosis (ALS) are two severe neurodegenerative diseases with no effective treatment so far. FTD is the second most common form of presenile dementia with a prevalence of 5-15 % of all dementia (Rademakers et al., 2012). First reports of FTD-like cases were described in 1892 by the neuropsychiatrist Arnold Pick (Pick, 1892). Especially during the last 20 years, a broader knowledge on genetic and molecular basics of the disease was gained and the link to another neurodegenerative disease, ALS, was described.

ALS also termed Charcot's disease or Lou Gehrig's disease is the most frequent motor neuron disorder (MND) with a worldwide prevalence of 1-2 people affected per 100,000 (Bennion Callister and Pickering-Brown, 2014; Ferrari et al., 2011; Rademakers et al., 2012). It is characterized by a severe loss of motor neurons that leads to death due to respiratory paralysis within 1-5 years after the onset of symptoms. As ALS and FTD share common genetic and pathological features they are classified as a spectrum of disease with ALS or FTD as the extreme ends of the spectrum (Bennion Callister and Pickering-Brown, 2014; Ferrari et al., 2011; Ng et al., 2015).

1.1.1. Clinical features

1.1.1.1. Frontotemporal Dementia (FTD)

FTD is comprised of three different syndromes, behavioral variant frontotemporal dementia (bvFTD), semantic dementia (SD) and progressive non fluent aphasia (PNFA). It has an average age of onset of mid to late 50s and can be further distinguished in familial and sporadic cases that occur equally common in men and women. Interestingly, 40 % of all FTD cases are familial with a clear genetic background (Snowden et al., 2002).

The three clinical syndromes are usually overlapping but a clear dominant feature of one of the three is often present. All three are characterized by the loss of neurons in the frontotemporal lobe (Josephs et al., 2011). In contrast to Alzheimer's disease (AD), memory and visuospatial abilities remain intact initially.

Behavioral variant FTD (bvFTD) is the most frequent of the three subtypes (Bennion Callister and Pickering-Brown, 2014). It is mainly characterized by changes in personality, deterioration of behavior and social conduct that can show through disinhibition, binge eating, emotional blunting or loss of insight (Bennion Callister and Pickering-Brown, 2014; Ferrari et al., 2011; Ng et al., 2015).

In contrast, patients with semantic dementia have severe naming and word comprehension impairments while speech output in general is still fluent. Additionally, they often show loss of facial recognition (prosopagnosia). Dependent on the temporal lobe affected first, semantic dementia can be classified in right or left SD variant. Moreover, behavioral changes can be observed in these patients, however, they manifest differently than the classical bvFTD (Rosen et al., 2006).

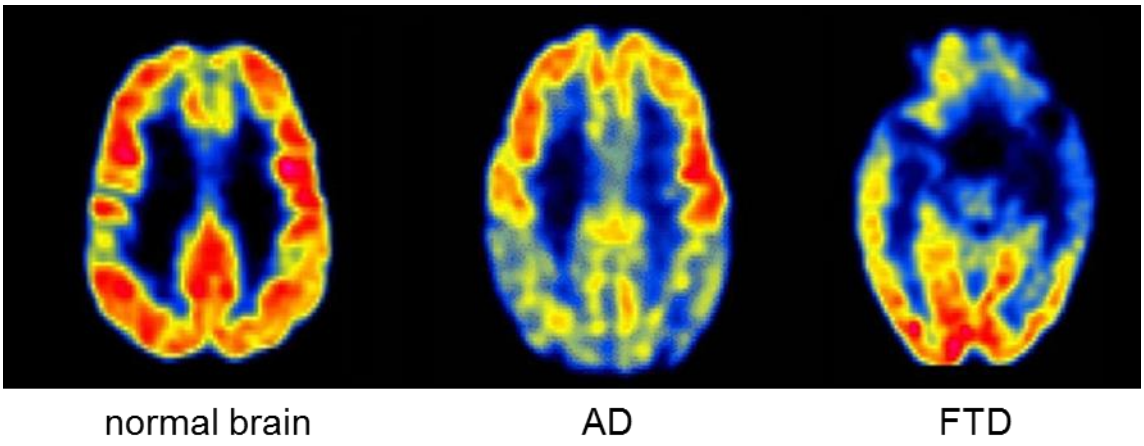

Figure 1: Typical hallmark of an FTD patient.
^{18}FDG PET scans showing the brain activity of a control brain, an Alzheimer disease patient (AD) and a patient with frontotemporal dementia (FTD). Highly active areas are depicted in red, whereas areas of low activity are depicted in blue. In contrast to a healthy person and an AD patient, patients with FTD show remarkably reduced activity in the frontal temporal lobes of the brain. Figure adapted from Dementia Today (Project, 2006).

Patients suffering from progressive non fluent aphasia show non fluent speech production, phonologic and grammatical errors and most pronounced, word retrieval

difficulties as well as problems in reading and writing. Behavioral changes, however, are less common in this subtype (Rosen et al., 2006).

The clinical diagnosis of the three different subtypes is obtained based on the observed clinical features and neuroimaging techniques. In magnetic resonance imaging (MRI) and computer tomography (CT) the atrophy of the frontal lobes can be detected. Additionally, positron emission tomography can be used to visualize glucose metabolism a direct measure for brain activity (Figure 1). Furthermore, it is important to exclude other types of dementia such as Alzheimer's disease or psychiatric conditions resulting in similar abnormal behavior. However, a definite diagnosis can only be achieved post mortem through neuropathological findings or mutation analysis.

Up until now there is no cure for FTD and treatment strategies are only symptomatic. Apart from serotonin reuptake inhibitors (SSRI) to reduce behavioral symptoms, memantine, an NMDA receptor antagonist, cholinesterase inhibitors or antidepressants are used. However, all of these drugs were originally developed for the application in other diseases such as AD and there is only minimal evidence for a beneficial effect in FTD.

1.1.1.2. Amyotrophic lateral sclerosis (ALS)

Amyotrophic lateral sclerosis is a disease of the upper and lower motor neurons and the corticospinal tract (Kiernan et al., 2011). So far it is not known why specifically these types of neurons are affected and whether upper or lower motor neurons are impaired first. While the upper motor neuron degeneration causes symptoms of hyperreflexia and spasticity, progressive muscle weakness and muscle wasting are a result of degeneration of the lower motor neurons (Van Damme and Robberecht, 2009). Consequently, patients suffer from progressive paralysis and respiratory failure may occur 1-5 years after disease onset. ALS is the most frequent form of motor neuron disease. It was first described by Jean-Martin Charcot in 1869 (Ferrari et al., 2011; Kiernan et al., 2011).

The average onset of ALS is 55 years of age but it can also occur quite early in life. Only 10 % of the cases are familial, whereas the rest is classified as sporadic with

unknown genetic predisposition (Ferrari et al., 2011; Ng et al., 2015). However, not all familial cases might be classified as such, due to missing familial medical history or the occurrence of recessive inherited

Figure 2: Characteristic features of ALS.
ALS is a disease of the upper and lower motor neurons and typically manifests in the disproportionate wasting of muscles. (A) The 'split hand', is a typical symptom of ALS patients in which disproportionate wasting of the abductor pollicis brevis and the first dorsal interossei muscle of the hand is present. This type of wasting is consistent with a cortical, motor neuronal origin seen in ALS. (B) The image depicts a limb-onset ALS. The patient shows prominent bilateral wasting of the shoulder girdles, pectoral muscles and the proximal upper arms. Figure adapted from (Kiernan et al., 2011).

mutations. Familial cases tend to show an earlier age of onset but are otherwise not distinguishable through symptoms or disease progression.

The final diagnosis of ALS is achieved through a combination of physical examination and neurological tests such as electromyography (EMG) or nerve conduction velocity. Typical phenotypes are the split hand, a clear sign for disproportionate wasting of muscles consistent with a cortical, motor neuron origin of ALS (Figure 2A), or prominent bilateral wasting of shoulder and upper arm muscles (Figure 2B) (Kiernan et al., 2011). For a clear diagnosis of ALS, other muscle affecting diseases showing similar phenotypes for instance spinal muscular atrophy (SMA) or multiple sclerosis (MS) have to be excluded through differential diagnosis.

Unfortunately, there is no effective treatment for ALS so far. The only Food and Drug Administration (FDA) approved drug is riluzole that is thought to protect neurons from glutamate mediated excitotoxicity (Miller et al., 2007). However, survival of patients can be only prolonged by few months. Otherwise only symptomatic treatment options are available to alleviate pain, cramps or depression

symptoms. Thus, there is a pressing need to develop new affective treatment alternatives and biomarker tools to increase survival and life quality for these patients.

1.1.1.3. FTD/ALS

As mentioned earlier, symptoms of ALS and FTD can be present in the same patient with one of the disease being diagnosed first and following, the patient develops additional symptoms of the other disease. Those types are classified as FTD with motor neuron disease (FTD-MND) if FTD is the disease diagnosed first or ALS with cognitive impairment (ALSci) if ALS symptoms are predominant. Typically, the mixed disease is more severe and has a considerable poorer prognosis (Ng et al., 2015). Motor neuron disease is often associated with the behavioral variant FTD, but rarely with semantic dementia or progressive non fluent aphasia (Josephs et al., 2005; Josephs, 2008). Approximately 15 % of FTD patients also develop motor neuron symptoms (Lomen-Hoerth et al., 2002). Moreover, the frequency of FTD symptoms in ALS patients is 5-50 % depending on the literature source (Lomen-Hoerth et al., 2002; Strong, 2008).

Additional evidence for a connection is found in families where both diseases occur within the same family (Ferrari et al., 2011; Josephs, 2008). The strongest evidence, however, comes from a mutation in the *C9orf72* gene that can cause both diseases depending on the circumstances.

1.1.2. Neuropathology

Beside clinical evidence for the connection between FTD and ALS, the pathology seen in the patients clearly shows that there is a link between the two diseases on a molecular level (Figure 3). Specifically, there are distinct neuronal protein inclusions that are associated with both diseases such as the Tar DNA binding protein (TDP-43) or the Fused in Sarcoma (FUS) protein inclusions (Chen-Plotkin et al., 2010; Ng et al., 2015). Additionally, there is evidence that both diseases share some affected brain regions (Ferrari et al., 2011).

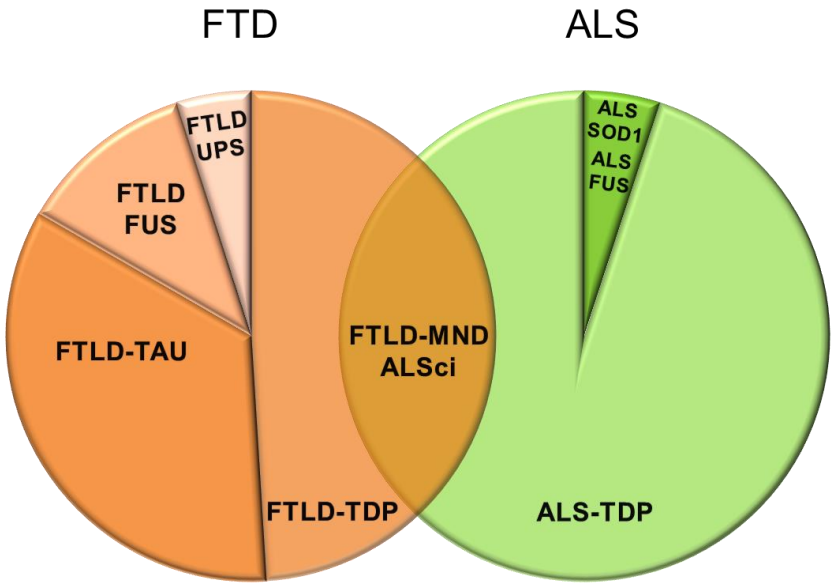

Figure 3: Pathological classification of FTD and ALS.
FTD (orange) and ALS (green) can be classified based on the protein inclusions found in the patients. 97 % of all ALS cases and nearly 50 % of all FTD cases show TDP-43 positive cytoplasmic and nuclear inclusion (FTLD-TDP/ALS-TDP). Adapted from (Chen-Plotkin et al., 2010).

1.1.2.1. Frontotemporal Lobar Degeneration (FTLD)

Frontotemporal lobar degeneration (FTLD) is the underlying pathology occurring in patients with FTD and is describing the typical atrophy of the frontal and temporal lobes. Shrinkage and spongiform morphology of the affected brain regions are a result of the massive neuronal loss being present through the progression of disease. Pathologically, FTLD can be divided into two major subtypes based on the aggregating proteins found in patients. First, cases with inclusions of the hyperphosphorylated protein Tau (FTLD-TAU) and second, cases showing ubiquitin-positive but tau negative inclusions (FTLD-U) (Mackenzie et al., 2010). Currently 1/3 of all FTD cases are FTLD-Tau associated, whereas 2/3 are FTLD-U cases.

The FTLD-U cases can be further subdivided into 3 major categories FTLD-TDP, FTLD-FUS and FTLD-UPS (Figure 3) (Mackenzie et al., 2011; Mackenzie et al., 2010).

In 2006, TDP-43 was discovered as the main inclusion protein in both FTD and ALS in sporadic and familial cases. FTLD-TDP is the most common pathological

subtype. TDP-43 pathology is present in 90 % of all FTLD-U cases. Based on the inclusion types found in patients, TDP pathology can be divided into 4 major subtypes FTLD-TDP type A-D (Mackenzie et al., 2011).

The second FTLD-U subtype, FTLD-FUS, is characterized by cytosolic inclusions of the normally nuclear protein Fus. Cases are characterized by a young age of onset, and mostly present with bvFTD (Seelaar et al., 2010). Furthermore, a negative family history often exists and caudate atrophy is detected in MRI (Josephs, 2010).

FTLD-UPS is the rarest of the three subtypes, showing only ubiquitin and p62-positive but TDP-43 and Tau negative inclusions. They are also classified as dementia lacking distinctive histopathology (DLDH) and many are associated with multivesicular body protein 2b (Chmb2b) mutations (Holm et al., 2009).

1.1.2.2. Motor Neuron Disease (MND)

In contrast to the frontotemporal degeneration of FTD, typical neuropathological hallmarks of ALS include the loss of anterior horn cells, degeneration of the brain stem motor nuclei as well as of the descending corticospinal tract (Strong et al., 2009). Additionally, Bunina body like intracellular inclusions, hyaline conglomerates and ubiquitin positive intracellular inclusions are found (van Welsem et al., 2002). 97 % of all familial and sporadic ALS cases show TDP-43 pathology (ALS-TDP) and the regional spreading from spinal and cortical motor neurons and glia to other cortical regions is used to stage ALS progression (Mackenzie et al., 2007; Maekawa et al., 2009). Cases without TDP-43 pathology mostly show inclusions of misfolded SOD1 protein (ALS-SOD1) always related to a mutation in SOD1 (Maekawa et al., 2009). Additionally, very rare cases negative for TDP-43 show inclusions of the Fus protein (ALS-FUS) (Vance et al., 2009).

1.1.2.3. FTLD/MND

Beside several clear FTD or ALS pathological characteristics, there are also pathological features that are associated with mixed forms of the two diseases. These cases are often accompanied by spongiform degeneration in frontal and

precentral gyrus (cortical layers II and III) and subcortical gliosis (Strong et al., 2009; Yoshida, 2004). Neuronal loss is most pronounced in the anterior cingulate gyrus, substantia nigra and amygdala (Strong et al., 2009). They are either classified as ALSci or, if the frontal cortex is majorly involved, as FTD-MND. Apart from typical TDP-43 positive inclusions, many cases with mixed clinical and pathological features show additional NCI and dystrophic neurites that are ubiquitin/p62-positive but TDP-43 negative (Ng et al., 2015).

1.1.3. Genetics

As the pathology, genetics of the disease spectrum FTD-ALS are highly complex. Whereas some mutations can be clearly associated with one disease and therefore can be found at the extreme ends of the FTD-ALS continuum, others can be the cause of either diseases, or even mixed forms.

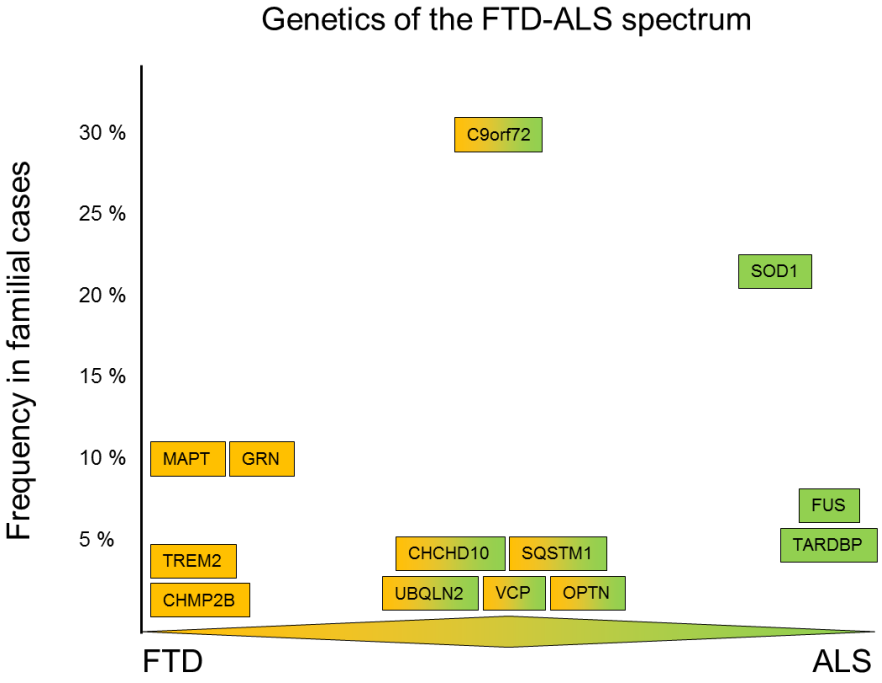

Figure 4: Summary of the main genes linked to ALS and FTD and their frequency.
FTD (orange) and ALS (green) are depicted as extreme ends of a disease spectrum. Genes linked specific to FTD are illustrated in orange on the left with their frequency in familial cases. ALS related genes are shown in green on the right. Genes associated with both diseases can be found in the middle with mixed coloring and arranged based on their frequency. *C9orf72* is the most common known cause for both FTD and ALS. Adapted from (Guerreiro et al., 2015)

Figure 4 illustrates the main known genes that are currently associated with the clinical FTD-ALS spectrum.

1.1.3.1. C9orf72

The newest addition to genes associated with both FTD and ALS came in 2006. Two groups independently reported a locus on chromosome 9 in the 9p21.2-p13.3 region to be associated with a substantial amount of autosomal dominant FTD-ALS cases (Morita et al., 2006; Vance et al., 2006). The following paragraph will discuss *C9orf72* and its role in FTD/ALS in more detail.

Identification as most common pathogenic mutation

In 2011, 11 years after the initial discovery (Hosler et al., 2000), two research groups independently discovered *C9orf72* on the locus of chromosome 9 to be the most common genetic cause of frontotemporal dementia and amyotrophic lateral sclerosis (DeJesus-Hernandez et al., 2011; Renton et al., 2011). The mutation was mapped to an intronic region of the gene and was identified to be a hexanucleotide repeat expansion (GGGGCC). Patients with the mutation have up to several thousand repetitions of the repeat sequence, whereas healthy controls show less than 30. However, the repeat length can vary among different tissues due to somatic mutations as a patient that showed only 90 repeats in blood cells had a much higher repeat length in the brain (Fratta et al., 2015). So far, it is also unknown which minimum repeat length is sufficient to cause disease.

The frequency of the mutation in FTD is about 25 % in familial FTD and 6 % in sporadic cases, whereas *C9orf72* mutation accounts for roughly 40 % of familial ALS (Majounie et al., 2012; Renton et al., 2011). Although *C9orf72* is the most frequent genetic cause for both ALS and FTD, there are particular geographical regions that have a high mutation frequency such as Finland. Furthermore, it has been debated whether all *C9orf72* patients stem from one single founder disseminated in Northern Europe. However, since *C9orf72* mutations are also rarely found in Asian and African populations, a second theory of a predisposing haplotype is more likely (van der Zee et al., 2013). Descriptions concerning repeat

expansions increasing from 100 to over 1000 within one generation and somatically in the CNS support this hypothesis (Dols-Icardo et al., 2014).

Function

So far not much is known about the C9orf72 protein. There are 3 transcripts variants and two potential protein isoforms. Depending on the transcript, the hexanucleotide repeat expansion can be either found in the promotor region or the first intron (DeJesus-Hernandez et al., 2011; Renton et al., 2011).

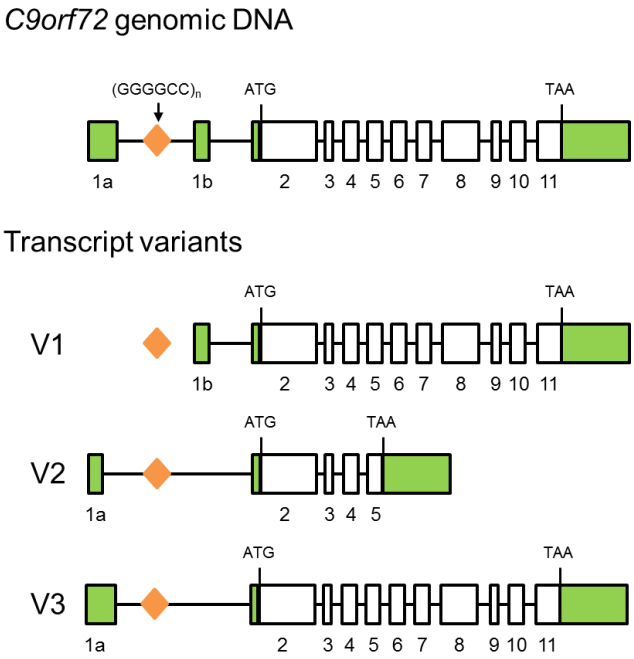

Figure 5: *C9orf72* gene structure and transcription variants.
Schematic overview of the *C9orf72* gene and its three transcription variants. Variants two and three may lead to transcription of the hexanucleotide repeat expansion. The expansion is depicted as orange rhombus, whereas exons are shown as white boxes and untranslated regions as green boxes. The figure was adapted from (DeJesus-Hernandez et al., 2011).

The C9orf72 protein, also called DENNL72 is predominantly expressed in neuronal cell populations that are vulnerable to ALS and FTD such as hippocampus, dentate gyrus, striatum, thalamus, brain stem nucleus, cerebellum, the cortex and the spinal cord (Suzuki et al., 2013). Structurally, it has been found to be similar to Differentially Expressed in Normal and Neoplasia (DENN) family of guanidine nucleotide exchange factors that activate Rab-GTPases. These proteins are

important regulators of membrane traffic (Levine et al., 2013; Zhang et al., 2012). In accordance to that, the yeast orthologous gene of *C9orf72*, Lst4p, has been found to prevent lysosomal delivery of cargo by redirecting endosome localized proteins to the cell surface (Rubio-Texeira and Kaiser, 2006). Therefore, loss of function might hamper with lysosomal degradation of particular cargos. However, this still needs to be proven experimentally in mammalian cells.

Clinical phenotypes and pathology

The mutation in *C9orf72* is most commonly associated with bvFTD, ALS or a combination of both. These cases have a high frequency of psychosis especially hallucinations and delusions, which often leads to a wrong diagnosis of schizophrenia or bipolar disorder at the beginning (Galimberti et al., 2014; Meisler et al., 2013). Patients also often present with an impaired episodic memory which may correlate with brain atrophy of the post cingulate gyrus and the parietal lobes seen in those patients. In comparison to other mutations, progressive non fluent aphasia and semantic dementia are quite rare in *C9orf72* mutation carriers and half of ALS patients with *C9orf72* mutation also show cognitive and behavioral impairment, which is much more frequent than in other mutations (Millecamps et al., 2012; Montuschi et al., 2015). Additionally, Parkinsonism can sometimes be seen in patients with *C9orf72* mutation that initially showed FTD symptoms (Lesage et al., 2013; O'Dowd et al., 2012). Also noticeable is that, compared to other FTD cases, *C9orf72* patients show increased subcortical involvement, especially thalamic and cerebellar involvement (Mahoney et al., 2012a). The age of onset and disease duration, however, are highly variable, even in one family, and can vary from 27 to 83 years and a duration ranging from 3 to 264 month (Majounie et al., 2012; Sabatelli et al., 2012; Stewart et al., 2012). Current studies suggest that ALS patients with *C9orf72* mutation have a shorter survival than sporadic ALS (Byrne et al., 2012; Cooper-Knock et al., 2012; García-Redondo et al., 2013).

Neuropathological analysis shows p-TDP-43-positive inclusions in almost all *C9orf72* patients. Atrophy of the frontal and temporal cortex, hippocampus, pyramidal motor system, amygdala, striatum, thalamus and midbrain is

symmetrically (Mackenzie et al., 2013). However, *C9orf72* patients tend to show less frontotemporal atrophy but rather increased parieto-occipital, thalamic and cerebellar atrophy compared to other genes (Mahoney et al., 2012a). Overall, the region specific neurodegeneration correlates with p-TDP-43 inclusion incidence and of the four TDP-43 pathological subtypes *C9orf72* is associated with type A and B. In type A specifically compact or granular neuronal cytoplasmic inclusions (NCI), dystrophic neurites and occasional neuronal intranuclear inclusions (NII) are found in layer 2 of the cortex and cortical white matter. In contrast, type B is classified through granular NCIs in all cortical layers with only a few dystrophic neurites or NIIs. However, there are also cases reported without any TDP-43 pathology (Mackenzie et al., 2013; Mackenzie et al., 2011).

In addition to TDP-43, p62-positive characteristically star-shaped neuronal inclusions are reported, that are most dominant in hippocampus, cerebellum and neocortical regions. These inclusions were reported to be the most defining characteristic of *C9orf72* patients (Al-Sarraj et al., 2011). In 2013, the predominant proteins in these inclusions could be identified as dipeptide repeat proteins resulting from the unconventional translation of the hexanucleotide repeat expansion in the *C9orf72* gene (Ash et al., 2013; Mori et al., 2013c).

Disease mechanisms

Since the discovery of the *C9orf72* mutation, there is a huge discussion in the field whether it results in a loss of function or a gain of toxic function. Three potential disease mechanisms are discussed. First, repeat expansion might lead to reduction in *C9orf72* transcription and translation, therefore causing a loss of function of the C9orf72 protein. Several groups could find evidence that transcript variant 1 (see Figure 5) is decreased in blood, cortex, cerebellum and spinal cord of mutation carriers compared to controls (Belzil et al., 2013a; Donnelly et al., 2013; Mori et al., 2013c; Renton et al., 2011). There is also evidence of hypermethylation of a CpG island upstream of the repeat potentially responsible for the downregulation of the gene (Belzil et al., 2014; Liu et al., 2014; Xi et al., 2013). Furthermore, knockdown of *C9orf72* in neuronal cell lines showed defects in endocytosis and

autophagy and knockdown or knockout in *C. elegans* and zebrafish lead to motor dysfunction and axonopathy (Ciura et al., 2013; Farg et al., 2014; Therrien et al., 2013). However, no phenotype could be found in knockout mouse models questioning the importance of the C9orf72 protein and its relevance in disease.

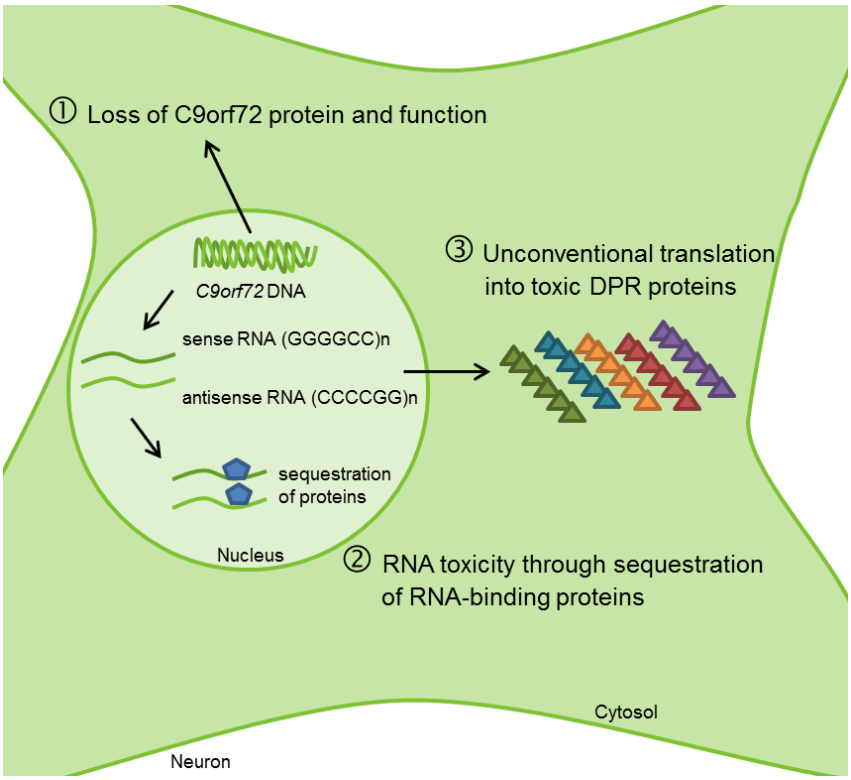

Figure 6: Possible disease mechanisms of *C9orf72* hexanucleotide repeat expansion mutation.
Three potential disease mechanisms are discussed. (1) The expansion might lead to a reduction in *C9orf72* expression and, thus, to a loss of C9orf72 protein function. (2) The repeat RNA may cause toxicity through sequestering important RNA-binding proteins, resulting in a toxic gain of function or (3) the repeat is unconventionally translated into five potential dipeptide repeat proteins, poly-GA, poly-GR, poly-GP, poly-PA and poly-PR leading to a toxic protein gain of function. Adapted from (Rohrer et al., 2015a).

As a second hypothesis, the repeat RNA might sequester RNA binding proteins and the loss of these proteins might cause disease. RNA foci containing sense and antisense repeat RNA can be found in patients in affected brain regions and the burden in these areas correlates with clinical phenotypes (Mizielinska et al., 2013). By now, several proteins have been identified to be sequestered by *C9orf72* repeat RNA (Almeida et al., 2013; Gendron et al., 2013; Mizielinska et al., 2013; Mori et

al., 2013b). However, variable sequestration of some has been observed and the role of RNA-binding proteins in the disease needs to be further elucidated.

Finally, the repeat is translated through unconventional translation into 5 potential dipeptide repeat (DPR) proteins, poly-glycine-alanine (GA), poly-glycine-arginine (GR), poly-glycine-proline (GP), poly-proline-alanine (PA) and poly-proline-arginine (PR). In 2013, two groups could independently show that sense and later also antisense proteins can be found in neuronal cytoplasmic inclusions in the brain of *C9orf72* mutation carriers (Ash et al., 2013; Gendron et al., 2013; Mori et al., 2013a; Mori et al., 2013c). However, toxicity and their relative role are unclear.

DPR proteins

The role that DPR proteins might play in disease is still unclear. Nonetheless, their presence in *C9orf72* mutation carriers is undisputed. Since the repeat is located in an intronic region of the *C9orf72* gene and does not carry an ATG start codon, canonical translation should not occur. Two rare possibilities of non-ATG translation have been reported. First, there is evidence that alternative start codons with a good Kozak sequence can initiate transcription (Ivanov et al., 2011; Peabody, 1989; Touriol et al., 2003). Second, repeat-associated non-ATG (RAN)-dependent translation has been shown to occur in other repeat expansion disorders with non-coding expansions such as fragile X tremor ataxia syndrome (FXTAS) or myotonic dystrophy type 1 (MD-1) (Cleary and Ranum, 2013; Todd et al., 2013). RAN translation was initially discovered in spinocerebellar ataxia type 8 (SCA8) by Zu and colleagues showing that CAG expansions lacking an ATG start codon are translated in all three reading frames, rendering this hypothesis for translation the most likely (Zu et al., 2011). The underlying machinery of RAN translation is so far unknown. At present, the mechanism of translation in *C9orf72* is not elucidated.

Apart from overall translation it is very interesting to analyze if and how DPR proteins contribute to disease. It is also an open question, whether one of the five proteins is more important than the other or if one protein is preferentially produced in patients. So far, all studies show that poly-GA is the most abundant species in patients, but if poly-GA is also the species underlying the disease mechanisms still

needs to be elucidated (Mackenzie et al., 2013; Mori et al., 2013c). Additionally, it is very important to discriminate between RNA and protein disease mechanisms and to identify their individual contributions. Therefore, good cellular models are needed to help answering these questions.

1.1.3.2. Other genetic causes for FTD/ALS

As can be seen in Figure 4, many mutations have been already identified that can cause either FTD or ALS. In this part, I will focus on mutations that are potentially in the same pathway as the mutation in *C9orf72*.

TARDBP

The TAR DNA binding protein (TARDBP) gene encodes for the 414 amino acids long TDP-43 protein that is responsible for the primary pathology in both FTD and ALS. Mutations were first discovered in 2008 and have a prevalence of 4-6 % in familial ALS and 1 % in sporadic ALS (Andersen and Al-Chalabi, 2011). So far, only one FTD patient with a TARDBP mutation was identified, suggesting a mainly ALS-related role of the TARDBP mutations (Borroni et al., 2009). The 33 known pathogenic mutations are almost all missense substitutions affecting the last exon of TARDBP which encodes the Gly-rich low complexity (prion-like) domain. The pathogenic mutations lead to a redistribution of the protein to the cytosol and to the loss of its nuclear function (Neumann et al., 2006). Physiologically, TDP-43 is a ubiquitously expressed DNA-/RNA-binding protein which plays an important role in RNA splicing and microRNA biogenesis.

SQSTM1

Sequestosome 1 (SQSTM1), also known as p62, is a major component of cytoplasmic neuronal inclusions in FTD and ALS. Mutations associated with the FTD-ALS continuum, however, were discovered relatively late. Currently, 20 mutations are identified in FTD (Le Ber et al., 2013; Rubino et al., 2012). The frequency is roughly 1-3 % in FTD and ALS. SQSTM1 is an important protein in the ubiquitin-proteasome system and autophagy (Bennion Callister and Pickering-

Brown, 2014; Hardy and Rogaeva, 2014; Ng et al., 2015). The mutations found in FTD are associated with TDP-43 pathology. In ALS, increased levels of p62 and TDP-43 can additionally be found in the spinal cord. ALS patients with SQSTM1 mutation also frequently show atrophy of the frontal lobe (Hardy and Rogaeva, 2014).

UBQLN2

Ubiquilin 2 is a member of the ubiquitin-like protein family. However, it's exact function is still unknown (Lee and Brown, 2012). It is an intronless gene on chromosome Xp11.21. Autosomal dominant missense mutations were identified in either ALS or FTD, however, there is a high phenotypic variability within the same family (Vengoechea et al., 2013). Most mutations affect the proline residues in the ProXX repeat region leading to deficient protein degradation (Gellera et al., 2012; Synofzik et al., 2012). Regarding pathology, UBQLN2 mutations are associated with ubiquitin, p62, TDP-43, Fus and Optineurin inclusions (Hardy and Rogaeva, 2014). Moreover, UBQLN2-positive inclusions are found in the hippocampus of ALS patients with dementia but are absent in ALS cases without dementia, suggesting a link to neurodegeneration (Deng et al., 2011).

1.2. Protein aggregation in neurodegeneration

The presence of aggregated protein species is a common feature of neurodegenerative diseases that often comes along with toxicity and cellular damage. The central nervous system (CNS) is particularly susceptible for the misfolding of proteins. However, the reasons for the specific vulnerability of distinct neuronal populations still needs to be elucidated (Saxena and Caroni, 2011). Although many diseases are classified by a specific aggregating protein, there is an overlap between diseases and most aggregates do contain components of the cellular protein quality control system such as ubiquitin or p62 (Swart et al., 2014).

1.2.1. Characteristics of protein aggregates

Protein aggregates can be classified into two groups, amorphous aggregates or structured amyloid fibrils. Whereas amorphous aggregates appear granular and mostly consist of disordered and unstructured polypeptide tangles, amyloids are highly ordered and repetitive assemblies that have a so called cross β structure (Swart et al., 2014). Amyloids or amyloidogenic proteins further have a high β sheet content and are resistant against most proteolytic and denaturing agents. Additionally, they are also known to be selftemplating meaning a pathogenic protein can transmit its misfolded state to the wildtype protein. In general, the process of aggregate formation can be described as nucleation – elongation – polymerization, where fibrils can undergo continuous fragmentation and reassembly (Chiti and Dobson, 2006; Harper and Lansbury Jr, 1997; Jarrett and Lansbury, 1993). This continuous process may affect turnover and recycling of aggregates, thus possibly adding to the toxic production line. Generally, it is very interesting that proteins forming aggregates in neurodegenerative diseases differ structurally and functionally, however, they all share the potential to form aggregates, suggesting that the formation of aggregates is unlikely to be random in these diseases. The inclusion bodies seen in patients, also called aggresomes are formed through the transport of cellular aggregates along dynein motors to the microtubule organization center where they are packaged into inclusion bodies. This is likely a response to proteostatic stress initiated to eliminate misfolded or toxic proteins to minimize obstruction of cellular processes and target them for macroautophagy (Fortun et al., 2003; Iwata et al., 2005; Rideout et al., 2004; Swart et al., 2014). It is, however, still under discussion if the formation of aggregates is a protective action of the cell to hide the toxic species or if the aggregates themselves are toxic through various mechanisms.

1.2.2. Toxicity of aggregating proteins

Over the past decades evidence for the involvement of aggregated proteins in disease initiation and progression of neurodegenerative diseases has been accumulating. As a first hint, insoluble proteins accumulate in affected brain

regions and are described as hallmarks of the individual diseases. Furthermore, many mutations that are disease causing, such as mutations in TDP-43, SOD1 and MAPT increase the propensity for aggregation of the underlying proteins (Li et al., 2001). Experimental evidence has come from animal models overexpressing disease associated mutant proteins that mirror some disease characteristics. Moreover, *in vitro* produced aggregates have shown toxicity in numerous cell culture systems (Bucciantini et al., 2002; Price et al., 2000). Following these lines of evidence, it is highly likely that protein aggregates either directly contribute to cell death or are an epiphenomenon of an earlier pathologic event. Early studies in Alzheimer's disease Amyloid β (Aβ) research showed that intracerebral microinjections of old rhesus monkeys with Aβ fibrils but not soluble Aβ lead to neuronal loss and tau phosphorylation (Guela et al., 1998). Additionally, switching off expression of aggregating proteins can rescue the phenotypes in conditional mouse models of spinocerebellar ataxias type 1 and 7 (SCA1, SCA7) and Huntington's disease (Ramachandran et al., 2014; Yamamoto et al., 2000; Zu et al., 2004).

To fully elucidate whether the inclusion bodies, intermediate aggregates or oligomeric species confer toxicity it is very important to understand the underlying toxicity mechanisms.

1.2.2.1. Mechanisms of toxicity

For the development of potential therapeutic approaches it is crucial to understand the exact molecular events leading to cell death. Increasing amounts of pathogenic proteins may cause toxicity through multiple mechanisms such as inhibition of the protein degradation machinery, mitochondrial dysfunction, oxidative stress or sequestration of important proteins.

Insoluble proteins may further interfere with microtubule transport, autophagic trafficking or impair cellular functions through the recruitment of essential functional components such as proteasomal machinery, chaperones and transcription factors or cytoskeletal proteins (Cummings et al., 1998; Ii et al., 1997). The depletion of these factors may, in combination, lead to a multiple-systems neurotoxicity. Additional, the propagation of aggregated protein material may

further enhance toxicity. Overall, many studies have already implicated some of the above mentioned mechanisms (Blokhuis et al., 2013; Chhangani and Mishra, 2013; Hara et al., 2006).

Protein sequestration

A mechanism of toxicity of aggregating proteins may be the sequestration of important proteins. First of all, the cytoplasmic aggregation of disease relevant proteins may prevent them to execute their normal function. Knockout studies from zebrafish and drosophila indicate that the loss of TDP-43 and Fus may be toxic for neuronal cells (Feiguin et al., 2009; Kabashi et al., 2010; Lin et al., 2011; Sasayama et al., 2012; Wang et al., 2011). However, the more likely hypothesis is that the aggregated proteins may recruit other proteins like chaperones or RNAs to the inclusions and thus, lead to a loss of function of the respective proteins (Blokhuis et al., 2013). This entrapment may remove important proteins from critical cellular processes such as protein degradation or RNA metabolism. In spinal and bulbar muscular atrophy (SBMA), caused by a CAG repeat expansion, polyglutamine protein aggregates sequester an important transcriptional activator CREB-binding protein (CBP) leading to loss of function and neuronal toxicity. Overexpressing CBP could rescue these phenotypes in neuronal cell culture, supporting sequestration as an important disease mechanism in proteinopathies (McCampbell et al., 2000).

Impairment of protein degradation

Impairment of the protein degradation system has been discussed in many neurodegenerative diseases. A lot of evidence exists, suggesting that this is the main disease mechanism in many of these diseases (Lim and Yue, 2015; Swart et al., 2014). One of the strongest arguments for this theory is the existence of ubiquitin-positive inclusion bodies in all of them. Specifically, the ubiquitin proteasome system has been found to be impaired through Huntingtin, Aβ oligomers and α-synuclein (Jana et al., 2001; Lindersson et al., 2004; Tseng et al., 2008). Furthermore, the second protein degradation system, the autophagy-lysosome-

pathway has also been found to be impaired in AD, Parkinson's disease (PD) and Huntington's disease (HD). Interestingly, impairment of the autophagic system in mice leads to neurodegeneration and the formation of ubiquitin-positive inclusions (Hara et al., 2006; Komatsu et al., 2006). Further reports support that ubiquitin is also a relevant protein in selective autophagy, as it is involved in the degradation of mitochondria and protein aggregates through signaling the initiation of autophagosome formation (Ishihara and Mizushima, 2009; Kirkin et al., 2009). Thus, the clearance of protein aggregates may be a very important mechanism in the development of neurodegenerative diseases.

Mitochondrial dysfunction

Mitochondria have an essential role in cell viability, specifically in neurons as they have a high energy consumption. Impairments in the mitochondrial function have been found in several neurodegenerative diseases such as AD, HD and PD (Browne et al., 1997; Caspersen et al., 2005; Crouch et al., 2005; Gu et al., 1996; Manczak et al., 2006; Nicklas et al., 1985; Schapira et al., 1990). Mouse models, overexpressing α-synuclein, an aggregating protein in AD and specifically PD, support the involvement of mitochondrial dysfunction in neurodegenerative diseases, as they show degenerated mitochondria and reduction in complex IV activity of the respiratory chain (Martin et al., 2006; Song et al., 2004).

Aggregate propagation

The spreading of aggregated protein material in a stereotypical staging pattern along axonal connections is well documented for most neurodegenerative diseases (Braak and Braak, 1991; Braak et al., 2003; Deng et al., 2004; Guo and Lee, 2014; Holmes and Diamond, 2012). Furthermore, many proteins found in neuronal inclusions show prion-like properties *in vitro* and *in vivo* suggesting this to be a highly common feature of neurodegeneration. Prion-like domains have self-aggregating properties and are able to convert native proteins into the toxic prion type. This recruitment of native protein and misfolding that would not take place otherwise, may be an important disease mechanism of aggregating proteins and is

called the prion hypothesis (Jucker and Walker, 2013). Evidence has been found in several cell culture and animal models (Holmes and Diamond, 2012). Moreover, *in vivo* seeding and spreading has been shown for aggregate prone proteins Aβ (Eisele et al., 2010; Meyer-Luehmann et al., 2006), Tau (Frost et al., 2009; Sanders et al., 2014) and Huntington's polyQ (Ren et al., 2009). The most striking evidence proceeds from PD patients that received striatal grafts of fetal neuronal tissue, where α-synuclein lewy body pathology was also present in the implanted grafts (Kordower et al., 2008; Li et al., 2008). Thus, propagation of proteins may be an important mechanism of toxicity in neurodegenerative diseases.

1.2.3. Clearance of protein aggregates

The clearance of aggregated protein species is typically executed through either the ubiquitin-proteasome system (UPS) or the autophagy-lysosome-pathway, which can be subdivided into macroautophagy (MA), microautophagy and chaperone-mediated autophagy (CMA). These mechanisms can also work hand in hand and even compensate for one another to a certain amount if one system fails. For example, α-synuclein is normally degraded via the UPS system, however, with increased burden, the autophagy machinery is recruited and supports the overstrained system (Ebrahimi-Fakhari et al., 2011). Additionally, chemicals inhibiting lysosomal degradation also compromise the UPS function suggesting that autophagy may also be required for the proper function of the UPS (Korolchuk et al., 2009). Typically, the ubiquitin-proteasome system is responsible for the clearance of single monomeric proteins, whereas larger aggregates are cleared through bulk autophagy.
The ubiquitin-proteasome system consists of the core protease machinery, the 26S proteasome and specific enzymes controlling substrate recognition, selection and targeting. In the initial step multiple ubiquitin proteins are covalently attached to the substrate protein with the help of the ubiquitin activating enzyme (E1), the ubiquitin ligase (E3) and the ubiquitin conjugation enzyme (E2). In the next step, ubiquitin chains are recognized by the 26S proteasome, consisting of the 20S core machinery and the 19S regulatory particles. The 26S proteasome degrades the poly-ubiquitinated substrate protein through unfolding the protein and cleavage into

short peptides. Peptides are further processed into amino acids by cellular aminopeptidases and ubiquitin is released for further reuse (Dantuma and Bott, 2014).

As mentioned before, many proteins found in inclusion bodies are ubiquitinated. For α-synuclein, Tau, SOD1 and Huntingtin it is known that they are degraded via the ubiquitin-proteasome system and inhibition of the system leads to their accumulation (Dantuma and Bott, 2014).

In the autophagy-lysosomal-pathway both CMA and MA might help in the clearance of aggregated proteins. Whereas the chaperone-mediated autophagy rather targets polypeptides to the surface of lysosomes for the translocation through the membrane and subsequent degradation, MA is used to eliminate larger aggregates or inclusion bodies. Therefore, the selected cargo is engulfed into double membrane vesicles and subsequent fused with lysosomes or endosomes. These mechanisms clearly have an important role in neurodegeneration as increasing autophagy results in the enhanced clearance of disease related proteins and increased survival of neuronal cells (Caccamo et al., 2010; Ravikumar et al., 2004; Sarkar et al., 2007).

1.2.3.1. The ubiquitin-proteasome system (UPS) in neurodegeneration

The proteasome plays a central role in neurodegeneration. A lot of evidence has accumulated showing that the inhibition of the UPS can lead to neurodegenerative phenotypes. However, it still needs to be elucidated whether the UPS is really impaired in neurodegenerative diseases. It is known that the UPS is actively involved in maintaining and resolving inclusion bodies (Schipper-Krom et al., 2014) and there is an ubiquitin-dependent transport of proteins to aggresomes (Kawaguchi et al., 2003). Therefore it may well be that the UPS is important in the development of neurodegenerative diseases but it may still be functional in those diseases. Another important hint for a role of the UPS in neurodegeneration came from the discovery of mutations in several genes with a function in the UPS such as Parkin, Ubiquilin1 or VCP (Chan et al., 2011; Ju and Weihl, 2010; Zhang and Saunders, 2009). However, these proteins also have other important cellular

functions apart from the UPS (Dantuma and Bott, 2014). Thus, further evidence is needed to link the dysfunction of those proteins to the UPS.

To provide an hypothesis on the UPS state in neurodegenerative disease, activity measurements of the three individual enzymatic activities of the proteasome, the trypsin-like, chymotrypsin-like and the caspase-like activity are necessary. These measurements can be difficult, as for example, the chymotrypsin-like activity needs to be reduced by 80 % before an effect on protein clearance can be detected. On the other hand, stress conditions may lead to an earlier effect (Dantuma et al., 2000). Initial studies on proteasome activity in human post mortem tissue showed a reduced proteasome activity in several neurodegenerative diseases (Keck et al., 2003; Keller et al., 2000; McNaught and Jenner, 2001; Seo et al., 2004). The following cell line and animal studies, unfortunately, were not very consistent. Whereas some studies could replicate the reduced activity, others did find no effect or even an increased proteasomal activity (Dantuma and Bott, 2014). Nonetheless, there is evidence directly linking aggregating proteins to a dysfunctional proteasome. A-synuclein and the prion protein both directly bind to and inhibit the UPS function *in vitro* and *in vivo* (Chen et al., 2006; Kristiansen et al., 2007; Snyder et al., 2003). The polyQ protein can also inhibit the UPS *in vitro* and *in vivo* however the inhibitory activity does not compromise the UPS function *in vivo* as the 26S proteasome is still able to degrade ubiquitinated substrates (Hipp et al., 2012). Mouse models, where the Huntingtin expression can be regulated via Doxycyclin show an effect on UPS activity, however, this effect is transient and UPS restoration coincides with inclusion body formation in these mice (Mitra et al., 2009; Ortega et al., 2010). Thus, the formation of inclusion bodies may be a protective mechanism of neurons to secure general UPS function.

To draw a conclusion from the results achieved so far, there is not enough evidence supporting the theory of a global inhibition of the ubiquitin-proteasome system as a universal feature in all neurodegenerative diseases in general. There is, however, evidence for the involvement of the UPS in several neurodegenerative diseases. Whether it is impaired or can be used as a possible therapeutic strategy needs further investigations.

1.2.4. Protein aggregation and degradation mechanisms in FTD/ALS

There is explicit evidence that protein aggregation is central in the pathology of FTD and ALS. Several studies point to a clear involvement of protein aggregates in neurotoxicity. Expression of wildtype or mutant TDP-43 leads to mislocalization and aggregation in the cytosol and a toxic gain of function in primary neurons (Barmada et al., 2010; Fallini et al., 2012). Transgenic mouse lines with cytoplasmic TDP-43 show a motor phenotype and a reduced life span (Guo et al., 2011; Stallings et al., 2010; Xu et al., 2010). Additionally, the distribution of TDP-43 aggregates in patients correlates with neurodegeneration, as aggregates can be found in the motor neurons in ALS and more wide spread in the brains of FTD patients (Baloh, 2011; Mackenzie et al., 2013).

Several potential toxicity mechanisms for the existing protein aggregates are discussed in the literature. As for several other neurodegenerative diseases, the involvement of the ubiquitin-proteasome system is considered. The UPS has been linked to FTD and ALS by several functional studies (Blokhuis et al., 2013), UPS impairment in SOD1 mutant mice being just one of them (Cheroni et al., 2009). Further evidence comes from disease causing mutations in the Ubiquilin-2 gene as the overexpression of mutant Ubqln2 results in the impairment of UPS function (Deng et al., 2011). Interestingly, Ubqln2 positive inclusions in the hippocampus are absent in ALS patients without dementia suggesting a link to neurodegeneration (Deng et al., 2011). More evidence for the impairment in proteasome function comes from mice with a motor neuron specific knockout of the proteasome subunit Regulatory Particle Triphosphatase (Rpt3), which results in the loss of spinal cord motor neurons and locomotor dysfunction. Additionally, those mice show inclusion bodies positive for TDP-43, Fus, Ubqln2 and Optineurin (Tashiro et al., 2012). Apart from the proteasome, the second protein degradation pathway, autophagy, might also be involved in the pathology of FTD and ALS. Heat shock proteins, p62 and other chaperones are upregulated in the spinal cord and present in patient aggregates (Basso et al., 2009; Watanabe et al., 2001). Furthermore, mice lacking the important autophagy proteins, Autophagy protein 5 and 7 (Atg5, Atg7) in the

CNS show movement disorders, neurodegeneration and p62 and ubiquitin-positive inclusions (Hara et al., 2006; Komatsu et al., 2006).

All of these results further strengthen the importance of protein aggregation as a central hallmark in FTD and ALS and establish the components of the protein degradation system as important modulators of protein aggregation and toxicity in FTD/ALS. Recent studies have enlarged the knowledge on the molecular composition of the aggregates and provided a starting point for future investigations. Although current available disease models confirm a role for aggregated proteins in the pathology of FTD and ALS, those models often do not fully recapitulate the disease. Thus, new models are a crucial tool to achieve a clearer picture. Novel mutations triggering protein aggregation such as the *C9orf72* mutation causing FTD/ALS may be the perfect opportunity to help further dissect the underlying effects and mechanisms of action of protein aggregation in ALS and FTD.

2. Aim of the study

The massively expanded GGGGCC repeat in *C9orf72* mutation carriers is translated in all three reading frames resulting in aggregating DPR proteins poly-GA, poly-GR and poly-GP, however the role of these proteins in the disease is still elusive (Ash et al., 2013; Mori et al., 2013c). Based on these initial findings, the overall aim of my thesis was to evaluate the contribution of the different DPR proteins to the pathophysiology of ALS/FTD.

As several other microsatellite expansion disorders are bidirectionally transcribed (Belzil et al., 2013b), I first aimed to investigate whether antisense transcripts of the *C9orf72* repeat expansion are present in the cerebellum of mutation carriers and how poor transcription of the mutant allele and abundant DPR expression can be reconciled.

Second, I aimed to develop a cell culture system in HEK293 cells and primary neurons to investigate the expression and toxicity of the five different proteins (poly-GA, poly-GR, poly-GP, poly-PA and poly-PR) and compare the results to the known characteristics seen in FTD and ALS patients.

Understanding the downstream mechanisms of potential DPR protein toxicity is crucial to elucidate the pathophysiology of ALS/FTD. Accordingly, the third aim of my study was to identify cellular proteins co-aggregating with DPR proteins by LC-MS/MS, since loss of function of these proteins may contribute to toxicity mechanisms. Furthermore, I aimed to validate the role of these interactors in DPR toxicity and confirm co-aggregation in patient brain.

Another important goal in understanding how DPR proteins contribute to disease progression is to uncover a potential connection of DPR and TDP-43 pathology. To this end, the final aim of my thesis was to analyze if DPR proteins can initiate TDP-43 mislocalization in my cell culture model.

Thus, the results of my thesis may help to identify novel therapeutic strategies for the devastating symptoms of *C9orf72* FTD/ALS.

3. Materials and Methods

3.1. Materials

3.1.1. Equipment and tools

3.1.1.1. General equipment

Name	Company
Analytical scale	Mettler-Toledo
Autoclave	Systec
Balance	Mettler-Toledo
Bunsen burner	Heraeus
CFX384 Real-Time System quantitative PCR	Biorad
CO_2-incubator	Thermo Scientific
Cooling centrifuge 5417R	Eppendorf
DNA electrophoresis gel system	Thermo Scientific
Dynabeads magnet	Life technologies
Film cassette	G. Kisker
Film developer	CaWo
Filter trap slot blot	Hoefer Scientific Instruments
Freezer (-20 °C)	Liebherr
Freezer (-80 °C)	Heraeus
Fridge	Liebherr
Glassware	VWR
Incubator	B. Braun Biotech International
Lamina flow	Heraeus
Microsurgical instruments (Dumont forceps and scissors)	Microwave
Milli Q plus filtration system	Merck Millipore
N_2-tank	Messer Griesheim

Nano Drop	Implen
Oven	Memmert
PCR thermal cycler	Eppendorf
pH meter	Thermo Scientific
Pipette boy	Brand
Power suppliers	Bio-Rad, Major Science
Powerwave XS plate reader	BioTek
Protein electrophoresis gel system	Bio-Rad
Rotors (TLA-55, SW28)	Beckmann Coulter
Scanner	Epson
UV lamp	Intas
Vortexer	Scientific Industries
Water bath	GFL

3.1.1.2. Microscope equipment

Name	**Company**
Confocal laser scanning microscope (LSM 710)	Zeiss
Epifluorescence microscope (Axiovert.A2)	Zeiss
Immersol 518 F	Zeiss
Light microscope (Wilovert S)	Hund Wetzlar
Microscope cover glasses (18 mm, 20 mm)	VWR
Microscope slides Superfrost plus	Thermo Scientific
Objective (Plan Apochromat, 20x/1 air DIC)	Zeiss
Objective (Plan Apochromat, 40x/1.4 oil DIC)	Zeiss
Objective (Plan Apochromat, 63x/1.4 oil DIC)	Zeiss
Phase contrast microscope (CKX41)	Olympus
Vectashield H-1000 mounting medium	Vectorlabs

3.1.1.3. Mass spectrometry equipment

Name	Company
Easy-nLC 1000 HPLC system	Thermo Fisher Scientific
Inhouse 1.9 µm C18 particle packed columns 75 µm inner diameter, 20 cm length	Dr. Maisch GmbH
Orbitrap Elite	Thermo Fisher Scientific

3.1.2. Consumables

Name	Company
Cell culture dish (3.5 cm, 6 cm, 10 cm)	Nunc
Cell culture plate (12 well, 96 well)	Nunc
Cell culture flask (75 cm^2)	Nunc
Cell culture plate black (96 well)	BD Falcon
Cellulose acetate filter membrane 0.2 µm	GE Healthcare
Centrifuge tubes (1.5 ml for TLA-55)	Beckmann Coulter
Centrifuge tubes for rotor SW28	Beckmann Coulter
Gloves (Latex)	Semperit
Gloves (Nitrile)	Meditrade
Hard shell PCR plates 384 well	Bio-Rad
Immobilon-P membrane, PVDF, 0.45 µm	Merck Millipore
Parafilm “M”	Pechiney Plastic Packaging
PCR tubes, strips, 96 well plates	Sarstedt
PES membrane filters, 0.45 µm	VWR international
pH indicator strips	Merck Millipore
Pipette tips (10 µl, 200 µl, 1000 µl)	Sarstedt, VWR
Pipettes	Gilson, Raynon, Eppendorf
Serological pipettes (2 ml, 5 ml, 10 ml, 25 ml)	Sarstedt
Tricine gels 10-20 %	Invitrogen
Tubes (1,5 ml, 2 ml)	Sarstedt

Tubes (15 ml, 50 ml)	Sarstedt
Whatman paper	Schleicher & Schüll
X-ray films	Fuji

3.1.3. Software and online tools

Name	**Company/Link**
Adobe Illustrator	Adobe Systems
APE	Wayne Davis
AxioVision	Zeiss
Bio-Rad CFX manager	Bio-Rad
BLAST	NCBI, http://blast.ncbi.nlm.nih.gov/Blast.cgi?CMD=Web&PAGE_TYPE=BlastHome
Ensembl	EMBL-EBI, Sanger Centre http://www.ensembl.org/index.html
GraphPad Prism	GraphPad Software, Inc
ImageJ	NIH
iScore designer	KAKENHI, http://www.med.nagoyau. ac.jp/neurogenetics/i_Score/i_score.html
LSM	Zeiss
MetaMorph	Molecular Devices
NCBI	http://www.ncbi.nlm.nih.gov/
Primer3	Whitehead Institute for Biomedical Research, http://bioinfo.ut.ee/primer3/
Spidey	NCBI, http://www.ncbi.nlm.nih.gov/spidey/

3.1.4. Services

Name	**Company**
Antibody production	Eurogentec

DNA sequencing	GATC Biotech
Oligonucleotide synthesis	Sigma-Aldrich

3.1.5. Chemicals

Name	**Company**
4-(2-hydroxyethyl)-1-piperazineethanesulfonic acid (HEPES)	Biomol
Acrylamide (19:1 / 40 % (w/v))	Serva
Agarose ultrapure	Life technologies
Ammonium persulfate (APS)	Roche
Ampicillin	Boehringer Mannheum
Boric acid	Merck Millipore
Bovine serum albumin	Sigma-Aldrich
Bromphenol blue	Merck Millipore
$CaCl_2$	AppliChem
DAPI	Roche
DMSO	Roth
DTT	Biomol
ECL	Thermo Scientific
ECL plus	Thermo Scientific
EDTA	USB
Ethanol	Sigma Aldrich
Ethidiumbromide	Roth
Fish gelatin	Sigma-Aldrich
Gelatin	Sigma-Aldrich
Glycerol	USB
Glycine	Biomol
I-Block	Tropix
IPTG	Roth

Isopropanol	Merck Millipore
Kanamycin	Roth
KCl	USB
KH_2PO_4	Merck Millipore
Methanol	Merck Millipore
$MgCl_2$	Roth
$MgSO_4$	Sigma-Aldrich
$Na_2[B_4O_5(OH)_4]$	Sigma-Aldrich
Na_2HPO_4	Merck Millipore
NaCl	Merck Millipore
NaH_2PO_4	Sigma-Aldrich
$NaHCO_3$	Merck Millipore
NaN_3	Merck Millipore
Paraformaldehyde	SERVA
Sodium borate decahydrate (Borax)	Sigma-Aldrich
Sodium deoxycholate	Sigma-Aldrich
Sodium dodecyl sulfate (SDS)	Roth
Staurosporine	Sigma-Aldrich
Suberic acid bis(3-sulfo-N-hydroxysuccinimide- ester) sodium salt (BS3)	Sigma-Aldrich
Sucrose	Sigma-Aldrich
Tetramethylethylenediamine (TEMED)	USB
TO-PRO-3	Life technologies
Tris base	AppliChem
Triton-X-100	Merck Millipore
Tryptone	BD Bioscience
Yeast extract	BD Bioscience
ß-mercaptoethanol	Roth

3.1.6. Kits

Name	Company
Caspase 3/7 Glo	Promega
DNase digest Kit	Qiagen
Endofree Plasmid Maxi Kit	Qiagen
Gel and PCR clean-up Kit	Marcherey-Nagel
LDH assay	Promega
NucleoBond Xtra Midi EF	Marcherey-Nagel
Nucleospin Plasmid Kit	Marcherey-Nagel
Proteasome activity assay	Promega
RNeasy Mini Kit	Qiagen
RT-PCR Kit TaqMan MicroRNA Reverse Transcription Kit	Applied Biosystems
SsoFast™ EvaGreen® Supermix	Bio-Rad
TUNEL assay	Roche
XTT assay	Roche

3.1.7. Reagents

Name	Company
Benzonase	Sigma-Aldrich
Calf-intestinal alkaline phosphatase (CIP)	NEB
DNA ladder	Life technologies
DNA polymerase (Pfu)	Agilent
DNA Polymerase (Taq)	Promega
DNAse	Sigma-Aldrich
Deoxyribonucleotides (dNTPs)	Roche
Glutathione sepharose 4B	GE Healthcare
Lysozyme	Merck Millipore
Phosphatase inhibitor cocktail	Sigma-Aldrich

Protein A Sepharose beads	GE Healthcare
Protein G Dynabeads	Life technologies
Proteinase inhibitor cocktail	Sigma-Aldrich
Restriction enzymes	NEB
RNA Later	Ambion
RNAse A	Sigma Aldrich
SeaBlue Prestained Protein Ladder Plus2	Life technologies
T4-Ligase	NEB

3.1.8. Antibodies

Name	**Company**
ß-Actin, clone AC-15	Sigma-Aldrich
Alexa secondary antibodies	Life technologies
Poly-AP, clone 14E12	Elisabeth Kremmer
Anti-mouse-HRP	Promega
Anti-rabbit-HRP	Promega
Anti-rat-HRP	Santa-cruz
Calnexin	Proteintech
Poly-GA, clone 1A12	Elisabeth Kremmer
GFP, clone N86/8	Neuromab
GFP, clone N38/8	Neuromab
GFP	Clonetech
HA	Sigma-Aldrich
HA, clone R001	Elisabeth Kremmer
Myc, clone 9E10	Elisabeth Kremmer
MAP2, clone AP-20	Sigma-Aldrich
Myc, clone A-14	Santa-cruz
P62	Cell signaling
P62	MBL

PSD-95, clone K28/43	Neuromab
PSMC2	Bethyl laboratories
PSMC4	Bethyl laboratories
pTDP-43, Ser409/410 clone 1D3	Elisabeth Kremmer
TDP-43	Cosmo
TDP-43	Sigma-Aldrich
Unc119#1	Eurogentec
Unc119#2	Thermo Scientific
V5	Life technologies

3.1.9. Cloning vectors and oligonucleotides

3.1.9.1. Cloning vectors

Name	**Company**
Fu3a	Dieter Edbauer
FhSynW2	Dieter Edbauer
FUW2 lentivirus vector	Dieter Edbauer
pEF6/V5-His	Life technologies
pCS2-Q_{102}-GFP	Betina Schmid
pEGFP-N1	Clonetech
pSPAX	(Salmon and Trono, 2007)
pVSVg	(Kuhn et al., 2010)

3.1.9.2. Oligonucleotides for shRNA cloning

Oligonucleotides were cloned into Fu3a vector.

Name	Species	Sequence sense	Sequence antisense
shUnc	mr	gatccccGAGAGGCACTACTTTCGAAttcaagagaTTCGAAAGTAGTGCCTCTCtttttggaaa	agcttttccaaaaaGAGAGGCACTACTTTCGAAtctcttgaaTTCGAAAGTAGTGCCTCTCggg
shLuc	ff	gatccccCGTACGCGGAATACTTCGAttcaagagaTCGAAGTATTCCGCGTACGttttttggaaa	agcttttccaaaaaCGTACGCGGAATACTTCGAtctcttgaaTCGAAGTATTCCGCGTACGgggg

h= human, m= mouse, r= rat, ff= firefly

3.1.9.3. Cloning primers

cDNA was cloned AscI/EcoRI or AscI/NotI into FUW2 vector.

Name	Species	Sense	Antisense
Bag6	r	ataggcgcgcctATGGAGCCGAGTGATAGTACCAGTACCGCT	tatgcggccgcCTAGGGGTCATCAGCAAATGCCCGGTGGGC
Ctbp1	h	aGGCGCGCCTatgggcagctgcacttgctca	ataGCGGCCGCCTACAACTGGTCACTGGCGTGGT
Epdr1	r	ataggcgcgcctATGCTCACACGCGCTCCCCGCCG	tatgcggccgcTCACAGGGAGCAGTTCTCTTTCATCTTCTCTG
Fabp5	h	ataggcgcgcctATGGCCAGCCTTAAGGACCTGGAAGG	actgaatTCATTGTACCTTCTCATAGACCCGAGTACAGATG
Hsd17b4	r	ataggcgcgcctATGGCTTCGCCTCTGAGGTTCGACGGGC	tatgcggccgcTCAGAGCTTGGCATAGTCTTTCAGAATCATCTGT
Mapre2	h	aGGCGCGCCTatgcctgggccgacccaaacc	ataGCGGCCGCTCAGTACTCTTCCTGCTGCGGGG
Rpl31	r	ataggcgcgcctATGGCTCCCGCAAAGAAGGGTGGCGAG	actgaattcTTAGTTCTCATCCACATTGACTGTCTGTAGATTT

Rps5	r	ataggcgcgcctATGACTGAA TGGGAAACAGCCACACC CGCG	actgaattcTCAGCGGTTAGACTTGGCC ACACGCTCCAG
Tmem160	r	ataggcgcgcctATGGGAGGC GGCTGGTGGTGGGCTC	actgaattcTTACTCGGGGGGTGGCCGG CCCGCTTC
Unc119	h	aGGCGCGCCTATGAAGG TGAAGAAGGGCGGCG	ataGCGGCCGCtcagggtgtcccgctgtaggaat a
Unc119	r	aaaggcgcgcctATGAGCGGG TCGAACCCGAAGGCTAC G	atagaattcGCTTACTGGCCTCCGTTAT AGGCATAGTCGG

3.1.9.4. qPCR primers

Name	Species	Sense	Antisense
C9orf72 intron	h	AAGAGGCGCGGGTAGAA G	AGTCGCTAGAGGCGAAAGC
C9orf72 exon 1b-2	h	CTGCGGTTGCGGTGCCTG C	AGCTGGAGATGGCGGTGGGC
C9orf72 exon 2-3	h	ACTGGAATGGGGATCGC AGCA	ACCCTGATCTTCCATTCTCTCTGT GCC
C9orf72 specific RT	h	CAATTCCACCAGTCGCT AGA	CTGCGGTTGCGGTGCCTGC
Unc119	r	GCGCTTTGTTCGATACCA GT	TGTTCTTGCTGCTGGGAATG
YHWAZ	h	TGAACAAAAGACGGAAG GTGCTG	TCTGATAGGATGTGTTGGTTGCA
GAPDH	r	CCGCATCTTCTTGTGCAG TGCC	AGACTCCACGACATACTCAGCA CC

3.1.10. Cell culture

3.1.10.1. Reagents

Name	Company
B27 supplement	Life technologies
Bovine serum albumin (BSA)	Sigma-Aldrich
DMEM glutamax-I	Life technologies
Fetal bovine serum	Life technologies
Laminin	Roche
L-glutamate	Sigma-Aldrich
L-glutamine	Sigma-Aldrich
Lipofectamine 2000	Life technologies
Neurobasal	Life technologies
Non-essential amino acids (NEAA)	Life technologies
OptiMEM	Life technologies
Penicillin/Streptomycin (P/S)	Life technologies
Poly-D-lysine (PDL)	Sigma-Aldrich
Trypsin (2.5 %)	Life technologies
Trypsin EDTA	Life technologies

3.1.10.2. Cell lines and bacteria strains

Name	Company
DH5α *E. coli* competent cells	Life technologies
HEK293-FT	Life technologies
Stble 3 *E. coli* competent cells	Life technologies

3.1.11. Patient material

Case number	GGGGCC expansion	Gender	Clinical and neuropathological diagnosis	Age of death
Ctrl-1	-	female	control, no neurological or psychiatric disease	47
Ctrl-2	-	male	control, no neurological or psychiatric disease	60
Ctrl-3	-	female	control, no neurological or psychiatric disease	60
Ctrl-4	-	male	control, no neurological or psychiatric disease	70
Ctrl-5	-	male	ALS	65
Ctrl-6	-	male	ALS/FTLD	61
Ctrl-7	-	male	FTLD-(MND)	55
C9-1	+	female	FTLD-MND	65
C9-2	+	female	FTLD-MND	59
C9-3	+	female	ALS/beginning FTLD	47
C9-4	+	male	FTLD/Parkinson	65
C9-5	+	female	ALS	63

3.1.12. Buffers and Media

All buffers were prepared with MilliQ water unless specified otherwise

3.1.12.1. Antibody purification

Name	Composition
100x lysozyme stock	20 mg/ml lysozyme stock in STE buffer
100x NaN_3 for antibody dilutions	10 % NaN_3

Acid elution buffer	0.1 M Glycine-HCl 150 mM NaCl adjust to pH 2.5
BS3 stock solution (25 mM)	25 mg BS3 in 1.75 ml 20 mM sodium-phosphate buffer adjust to pH 7.4
Column wash buffer	0.1 M Tris-HCl 0.5 M NaCl Adjust to pH 8
Conjugation buffer	20 mM sodium phosphate Na_2HPO_4 0.15 M NaCl adjust to pH 7 to 9
Neutralization buffer	1 M Tris adjust to pH 9.5
Quenching buffer for antibody purification	1 M Tris adjust to pH 7.5
STE	10 mM Tris-HCl 150 mM NaCl 1 mM EDTA adjust pH 8

3.1.12.2. Biochemistry

Name	**Composition**
20x SB agarose gel buffer (100 mM)	38.17 g sodium borate decahydrate (Borax) 33 g boric acid 1L dH_2O adjust to pH 8.0

4x Laemmli buffer	4 % SDS 20 % glycerol 5 % ß-mercaptoethanol 200 mM Na2HPO4 bromophenol blue adjust to pH 7.4
4x SDS PAGE running buffer	1.5 M Tris base 0.4 % (w/v) SDS adjust to pH 8.8
4x SDS PAGE stacking buffer	0.5 M Tris base 0.4 % (w/v) SDS adjust to pH 6.8
5x DNA loading buffer	50 % glycerol 50 mM Na_2EDTA 0.05 % bromophenol blue adjust to pH 8.0
Acrylamide-Schägger buffer	49.5 % acrylamide 3 % bisacrylamide
Anode buffer	0.2 M Tris-HCl adjust to pH 8.9
Basic buffer	150 mM NaCl 50 mM Tris pH 7.5 5 % Glycerol
Blotting buffer	25 mM Tris 0.2 M Glycine
Cathode buffer	0.1 M Tris-HCl 0.1 M Tricine 0.1 % SDS
I-Block buffer	0.2 % I-Block in TBSTx

RIPA buffer	137 mM NaCl 20 mM Tris, pH 7.5 0.1 % SDS 10 % glycerol 1 % Triton-X-100 0.5 % sodium deoxycholate 2 mM EDTA
SDS PAGE running buffer 1x with SDS	25 mM Tris 0.2 M glycine 0.1 % SDS
SDS filter trap cell culture	2 % SDS 100 mM Tris adjust to pH 7
SDS filter trap brain	1 % SDS 100 mM Tris adjust to pH 7
Seperating gel buffer	1.5 M Tris 0.4 % (w/v) SDS adjust to pH 8.8
Stacking gel buffer	0.5 M Tris 0.4 % (w/v) SDS adjust to pH 6.8
TBSTx	20 mM Tris 0.14 M NaCl 0.2 % Triton-X-100 adjust to pH 7.6
Tricine-Schägger gel buffer	3 M Tris-HCl 0.3 % SDS adjust to pH 8.45

Triton filter trap	1 % Triton-X-100 50 mM MgCl2 0.2 mg/ml DNAse I

3.1.12.3. Cell and bacterial culture

Name	**Composition**
Borate buffer	40 mM boric acid 10 mM sodium tetra borate $Na_2B_4O_7 \bullet 10H_2O$ adjust to pH 8.5
Coating solution for cover glasses	1.5 % PDL 0.5 % laminin dissolve in borate buffer
Coating solution for plastic culture plates	1.5 % PDL dissolve in borat buffer
Cortical primary neuron medium	0.25 % L-glutamine (200 mM stock) 2 % B27 1 % penicillin/streptomycin in Neurobasal medium
HBSS	0.14 M NaCl 5.4 mM KCl 0.25 mM Na_2HPO_4 5.6 mM glucose 0.44 mM KH_2PO_4 1.3 mM $CaCl_2$ 1.0 mM $MgSO_4$ 4.2 mM $NaHCO_3$

HEK293 cell medium	1 % penicillin/streptomycin 1 % NEAA 10 % FCS in DMEM Glutamax
High BSA HEK293 medium	6.4 % high BSA stock in HEK293 cell medium prepare fresh
High BSA stock	20 % BSA in DMEM medium filter through 0.2 µm sterile filter
Hippocampal primary neuron medium	2 % B27 0.25 % L-glutamine (200 mM stock) 0.125 % L-glutamate (10 mM stock) 1 % penicillin/streptomycin in Neurobasal medium
LB agar	1.5 % agar dissolve in LB medium
LB medium	1 % tryptone 0.5 % yeast extract 86 mM NaCl
Phosphate-buffered saline (PBS)	0.14 M NaCl 10 mM Na_2HPO_4 2.8 mM KH_2PO_4 2.7 mM KCl adjust to pH 7.4
Poly-D-lysine stock	10 g/ml in borate buffer

3.1.12.4. Immunofluorescence

Name	Composition
2x GDB	0.2 % gelatin powder 0.33 M Na_2HPO_4 0.9 M NaCl 0.6 % Triton-X-100 adjust to pH 7.4
Immunofluorescence blocking buffer	2 % fetal bovine serum 2 % bovine serum albumin 0.2 % fish gelatin dissolve in PBS
Permeabilisation/quenching buffer	0.2 % Triton-X-100 50 mM NH_4Cl dissolve in PBS
PFA-fix	4 % PFA 0.15 mM NaOH 0.13 mM NaH_2PO_4 0.12 mM sucrose adjust to pH 7.5

3.1.12.5. Mass spectrometry

Name	Composition
Resuspension buffer 1	8 M Urea 10 mM HEPES adjust to pH 8.0
Resuspension buffer 2	6 M Urea 2 M Thiourea 10 mM HEPES adjust to pH 8.0

3.2. Methods

3.2.1. Molecular Biology

3.2.1.1. Molecular Cloning

Subcloning

The insert fragment of interest was cut from the plasmid using two restrictions enzymes. 3 µg plasmid were digested in optimal buffer and temperature conditions for the respective enzymes for 1 h. Afterwards, enzyme activity was terminated via heat inactivation (65 °C/20 min) and the insert was isolated on a 1 % agarose gel containing 1 µg/ml Ethidiumbromide. After excising the band containing the insert fragment, the DNA was purified with the NucleoBond Gel Extraction kit and eluted in 50 µl H_2O. The backbone of choice was cut with the same restriction enzymes and additionally dephosphorylated with 1 µl calf intestinal phosphatase (CIP) for 1 h at 37 °C to prevent religation. The following purification steps were performed as described for the insert. Following, 9 µl insert and 3 µl backbone were ligated with 1 µl T4 ligase and 2 µl ligase buffer and 5 µl MilliQ water for 1 h at room temperature. The ligation mix was then transformed in competent bacteria as described below.

Oligonucleotide cloning

To design shRNAs with a unique seed region for a target of interest, the iScore designer (http://www.med.nagoya-u.ac.jp/neurogenetics/i_Score/i_score.html) and the NCBI Blast web tool (http://blast.ncbi.nlm.nih.gov/Blast.cgi) were used. Final Oligonucleotides with restriction sites flanking sense and antisense pairs were made to order at Sigma Aldrich. Oligonucleotides were dissolved to 100 µM with MilliQ water. Annealing was carried out by mixing 1 µl of sense and antisense oligonucleotides with 2 µl NEB buffer 4 and 16 µl MilliQ water and heating the reaction mix to 95 °C for 4 min. The backbone was prepared as described above in “subcloning” but without CIP dephosphorylation. 2 µl annealed Oligonucleotides were ligated with 2 µl backbone, 2 µl ligase buffer, 13 µl MilliQ water and 1 µl T4

Ligase at room temperature for 1 h. Transformation was performed as described below.

PCR Product cloning

Primers for PCR product cloning were designed manually with similar annealing temperatures for forward and reverse primer and restriction sites flanking both ends. The PCR reaction-mix was prepared as follows:

Component	**Amount**
DNA template	100 ng
Forward primer (20 µM)	1 µl
Reverse primer (20 µM)	1 µl
dNTPs (10 mM each)	1 µl
10x Pfu buffer	5 µl
Pfu DNA Polymerase	1 µl
MilliQ water	ad 50 µl

For a standard PCR the following program was applied:

Step	**Temperature [°C]**	**Time**	**# of cycles**
Initial denaturation	95	2 min	1
Denaturation	95	20 s	30
Annealing	$T_{m(primer)}$-5	20 s	
Extension	72	1 min/1 kb	
Final extension	72	8 min	1

Following PCR, the samples were loaded on a 0.7-2 % Agarose, supplemented with 1 µg/ml Ethidiumbromide, depending on the PCR product length. The gel was run in

SB buffer at 250 V for 15 min. Afterwards, the band on the correct height was cut from the gel and DNA was isolated with the Nucleobond Gel extraction kit. To obtain the restriction site sticky ends for ligation, the PCR product DNA was digested overnight with the respective enzymes at optimal buffer and temperature conditions. On the next day a heat kill was performed and ligation was carried out as described above in "subcloning".

Transformation

Chemical competent DH5α or Stable3 (for recombination prone inserts) *E. coli* bacteria were freshly thawed on ice. 100 µl were added to the ligation mixture and incubated on ice for 30 min. Afterwards, bacteria were heat shocked at 42 °C for 1 min to facilitate DNA uptake. For recovery bacteria were shortly incubated on ice for 2 min and 400 µl LB media were added. The DH5α mix was incubated at 300 rpm and 37 °C for 1 h, whereas Stable3 bacteria were incubated at 30 °C for 2 h. Following, the whole sample was plated on a LB agar plate containing selection antibiotics. For re-transformation of a construct only 200 µl of the mixture were plated on LB plates with antibiotics. DH5α bacteria plates were incubated at 37 °C overnight, whereas Stable3 bacteria plates were incubated at 30 °C for 24 h. On the following day, clones were picked and grown in LB media with respective antibiotics at 37 °C (DH5α) or 30 °C (Stabl3) overnight.

DNA preparation

Bacteria cultures were centrifuged at 3000 g for 10 min at 4 °C. The supernatant was discarded and DNA was purified from the pellet with the NucleoBond Plasmid kit (miniprep.) or the NucleoBond Xtra Midi EF kit (midiprep.) according to the manufacturer's instructions. The DNA was eluted in 50 µl MilliQ water.

Control digest

A control digest with respective restriction enzymes was carried out to verify the cloning success. Therefore, restriction enzymes were chosen to achieve a specific digest pattern. 2 µl of the purified DNA were added to 0.5 µl of each enzyme. The

digest was carried out in the optimal buffer and temperature conditions for the respective enzymes for 1 h. Loading dye was added 1:5 to each sample and depending on the length of the DNA fragments, samples were loaded on a 0.7-2 % agarose gel supplemented with 1 µg/ml Ethidiumbromide. The gel was run in SB buffer at 250 V for 15 min. Afterwards, the restriction pattern was detected with an UV-lamp.

Sequencing

To assess the final construct for small deletions, insertions or point mutations, 100 ng of the purified plasmid were sequenced forward and/or reverse with appropriate primers at the GATC Biotech AG (Konstanz).

3.2.1.2. Real time quantitative PCR (qRT-PCR)

Quantitative PCR primer design

For primer design the cDNA sequence of the gene of interest provided by Ensembl was used as a template. Primers were designed using the Primer3 web tool (http://bioinfo.ut.ee/primer3/) around exon-intron boarders spanning large introns (>1000 bp) to avoid the amplification of genomic DNA. Primers were chosen to yield a product size of 200-300 bp and an optimal annealing temperature of 60 °C.

RNA isolation

To isolate RNA from primary neurons and HEK293 cells the Qiagen RNAeasy Mini kit was used according to the manufacturer's instructions. For patient samples the same kit was used with an additional DNAse digestion step as recommended in the manufacturer's instructions to avoid interference of residual genomic DNA. RNA samples were stored at -80 °C.

Reverse transcription RT-PCR

Depending on the experiment conditions the isolated RNA was diluted with RNAse-free H_2O prior to RT-PCR. The RT-PCR to generate complementary DNA (cDNA) was carried out with the TaqMan MicroRNA Reverse Transcription kit with random

hexamer primers (N6) according to the manufacturer's instructions. For C9orf72 patient experiments, specific RT-PCR primers were used to specifically amplify the sense and antisense repeat pre-mRNA/mRNA (see 3.1.9.4). A standard was generated by pooling equal amounts from all RNA samples and a dilution series was produced by diluting the pool 1:2 and three subsequent 1:10 dilutions. The exact composition of the final reaction mix for one RNA sample is depicted in the table below.

Component	**Amount**
100 mM dNTPs	0.45 µl
MultiScribeTM Reverse Transcriptase (50 U/µl)	3 µl
RNase inhibitor	0.56 µl
10x RT buffer	4.5 µl
N6 primer (50 ng/µl)	4.5 µl
diluted RNA	15 µl
nuclease-free H_2O	ad 45 µl

The final mix was incubated on ice for 5 min and the standard RT-PCR program was set as follows:

Temperature	**Time**
16 °C	30 min
42 °C	30 min
85 °C	5 min
4 °C	hold

Quantitative PCR

The qPCR was performed with the SsoFastTM EvaGreen reagent according to the manufacturer's instructions. After RT-PCR the cDNA was diluted 1:5 in nuclease

free H_2O and 2 µl of each sample were pipetted in triplicates as technical replicates to a 384-well plate. Gene specific qPCR primers were added to the SsoFast TM Eva Green reagent to a final concentration of 400 nM. 3 µl of the primer mix were added per sample. The final reaction mixture for one sample is described below.

Component	**Amount**
SsoFast^{TM} EvaGreen	2.5 µl
Forward primer (400 nM)	0.05 µl
Reverse primer (400 nM)	0.05 µl
cDNA template	2 µl
Nuclease free H_2O	ad 5 µl

The standard qPCR program was set to a total of 50 cycles as follows:

Step	**Temperature**	**Time**	**# of cycles**
Initial denaturation	95 °C	30 s	1
Denaturation	95 °C	5 s	50
Annealing + extension	60 °C	5 s	
Extension	95 °C	10 s	
Melt curve	65-95 °C	5 s	1

The relative mRNA expression was calculated with the BioRad CFX manager software using the Δ-Δ-Ct method with Tyrosine 3-monooxygenase/tryptophan 5-monooxygenase activation protein zeta (YWHAZ or Y1) as a housekeeping gene.

3.2.2. Cell culture and lentivirus production

3.2.2.1. HEK293-FT culture

Cultivation

Human embryonic kidney cells (HEK293 cells) were cultivated in DMEM Glutamax medium supplemented with 10 % FCS, 1 % P/S and 1 % MEM NEAA (HEK293 culture medium) at 37 °C and 5 % CO_2. Cells were splitted at 80 % confluency. Medium was removed and cells were washed with PBS once. Afterwards the cells were detached with 0.05 % Trypsin/EDTA for 1 min at 37 °C. Following, the cells were carefully resuspended in fresh medium and plated at the desired amount in cell culture dishes or splitted 1:10 for further cultivation.

Transfection

For transfection 200,000 cells were seeded in 1 ml HEK293 culture medium per 12-well. On the next day cells were transfected with lipofectamine 2000 according to the manufacturer's instructions.

Component	**Amount per well**
Total DNA	1 µg
in OptiMEM	0.125 µl
After 5 min combine with:	
Lipofectamin 2000	2.5 µl
in OptiMEM	0.125 µl

The final transfection mixture was incubated for 30 min at room temperature. Following the incubation, the transfection mixture was added to the cells and cells were incubated at 37 °C and 5 % CO_2. After 48 h cells were harvested for further experiments.

Lentivirus production

To produce lentivirus, a new HEK293 cell batch was freshly thawed and expanded. Full confluency was avoided to increase virus titer. One day prior to seeding, cells were splitted 1:2. Cells were seeded with a density of 5.5 million cells per 10 cm dish. On the following day HEK293 cells were transfected with Lipofectamine 2000 with three constructs as described below:

Component	**Amount per 10cm dish**
LTR vector	18.6 µg
pSPAX2	11 µg
pVSVg	6.4 µg
Total DNA	36 µg
in OptiMEM	4.5 ml
After 5 min combine with:	
Lipofectamin 2000	108 µl
in OptiMEM	4.5 ml

Whereas pVSVg and pSPAX allow for the formation of the virus particle, the LTR vector contains the construct of interest. After preparation, the transfection mixture was incubated for 20 min at room temperature. In the meantime, medium was exchanged to 5 ml prewarmed OptiMEM supplemented with 10 % FCS. Following incubation, 3 ml of the transfection mixture were slowly added to each 10 cm dish. On the next day medium was exchanged to 10 ml High BSA packaging medium and cells were further incubated for 24 h. The virus containing medium was collected subsequently and centrifuged at 600 g for 10 min at room temperature. The supernatant was filtered through a sterile 0.45 µm PES membrane filter and the filtrate was centrifuged at 66,000 g for 2.5 h at 4 °C. Afterwards the supernatant was discarded and the virus pellet was resuspended in 120 µl NB medium. The virus was stored in aliquots at -80 °C.

3.2.2.2. Primary neuron culture

Preparation of cover slips and cell culture dishes

Prior to the preparation of primary neuron cover slips and culture dishes were pretreated to improve culture conditions. Therefore, 18 mm cover slips were treated with 65 % nitric acid for two days to remove lipids. Afterwards they were washed four times with MilliQ water and sterilized in an oven at 200 °C for 6 h. Following, cover slips were transferred into 12-well culture plates and coated with 1.5 % PDL and 0.625 % laminin in 0.1 M borate buffer for at least 4 h. Culture dishes and plates without cover slips were coated with 1.5 % PDL in 0.1 M borate buffer for the same amount of time. After coating, the culture dishes and plates were washed three times with sterile MilliQ water and in a final step fresh NB medium was added. Cell culture dishes and plates were kept at 37 °C in 5 % CO_2 until plating of neurons.

Preparation of primary neurons

To prepare primary cortical and hippocampal neurons an embryonic day 18/19 (E18/19) pregnant Sprague-Dawly rat was sacrificed with CO_2 treatment and subsequent cervical dislocation. The embryos were collected from the mother's body and decapitated. Following, the brain was prepared from the embryo heads and transferred into a 10 cm cell culture dish containing ice cold HBSS. Afterwards the hippocampi and cortices were prepared by microdissection and collected separately in a 10 ml tube with ice cold HBSS. The hippocampi and cortices were washed three times with cold HBSS and afterwards hippocampi were incubated in 5 ml HBSS containing 150 µl of 2.5 % trypsin for 15 min at 37 °C. Cortices were incubated in 5 ml HBSS containing 500 µl of 2.5 % trypsin and 350 µl DNAse (2,000 U/mg). Afterwards, the hippocampi and cortices were washed three times with prewarmed HBSS and neurons were dissociated gently by carefully pipetting up and down. The cell number was counted with a Neubauer cell counting chamber and 85,000 hippocampal neurons were seeded in 1 ml NB medium supplemented with 2 % B27, 1 % penicillin/streptomycin, 0.25 % glutamine, 0.125 % glutamate per 12-well. For

cortical neurons 400,000 cells were seeded in 1 ml NB medium supplemented with 2 % B27, 1 % penicillin/streptomycin, 0.25 % glutamine per 12-well. Other cell culture dishes were seeded with adapted cell numbers according to the 12-well standard plates.

Cultivation of primary neurons

Primary cortical neurons were cultivated in NB medium supplemented with 2 % B27, 1 % penicillin/streptomycin, 0.25 % glutamine (cortical neuron medium) and hippocampal neurons were cultured in the same medium with additional 0.125 % glutamate (hippocampal neuron medium) at 37 °C and 5 % CO_2. After 7 days in culture or 1 day after transduction 1 ml fresh NB medium with 2 % B27, 1 % penicillin/streptomycin, 0.25 % glutamine was added to a 12-well to feed the cells. For other plate formats the volume was adjusted accordingly.

Transfection of primary neurons

Prior to the transfection, NB medium containing 1 % penicillin/streptomycin and 0.25 % glutamine was prepared and prewarmed in a new 12-well plate. The transfection mixture was prepared as noted below and incubated for 20 min at room temperature:

Component	**Amount**
Total DNA	1.8 µg
in NB medium	100 µl
After 5 min combine with:	
Lipofectamin 2000	3.2 µl
in NB medium	100 µl

At the end of the incubation period the hippocampal neurons on the glass cover slips were dipped once in prewarmed NB medium and transferred into the prepared 12-well plate. Afterwards, the transfection mixture was added drop wise and the neurons were incubated for 45 min at 37 °C and 5 % CO_2. Following the incubation,

cover slips were dipped in warm NB medium twice and transferred back into the original plate. Neurons were analyzed 3 or 5 days after transfection.

Transduction of primary neurons

Primary neurons were transduced on day 6 in vitro (DIV 6). Therefore, 1 µl virus was added to a 12-well plate. On the following day 1 ml cortical neuron medium was added and cells were incubated for 10 to 17 days until analysis. A 10 cm dish cortical neurons was transduced with 10 µl virus and 5 ml cortical neuron medium were added the following day. Cells were harvested for IP-Mass spectrometry experiments 17 days after transduction.

3.2.3. Cellular assays

3.2.3.1. Toxicity assays

Caspase 3/7 assay

Caspase-3 activation plays a crucial role in the execution phase of apoptosis and therefore measuring Caspase-3 activity with a luminescence based assay can be used to determine cell viability in cultured cells. Thus, primary cortical neurons were cultured in a white 96-well plate to support maximum luminescence output. The assay was performed according to the manufacturer's instructions. Medium was exchanged to 50 µl freshly prepared cortical neuron medium and 50 µl caspase activity reagent were added. The plate was shortly mixed at room temperature (400 rpm, 1 min), followed by an incubation at room temperature for 1 h. Luminescence was directly measured using the Microlumat plus 96 V. Relative Caspase 3/7 activity was calculated through normalization to a respective control. 1 µM Staurosporine treatment for 4 h was used as a positive control.

LDH activity assay

Lactate dehydrogenase (LDH) is a cytosolic enzyme. Its presence in the cell culture media is a marker for cytotoxicity. The LDH toxicity assay detects extracellular LDH through an enzymatic reaction producing a red formazan dye that can be

measured spectrophotometrically. For detection of cytotoxicity primary cortical neurons or HEK293 cells were cultured in 96-well plates. The complete supernatant was collected and transferred to a new 96-well plate. Afterwards, the cells were frozen at -80 °C for 30 min for cell lysis. 100 µl of fresh culture media were added and the cells were thawed at 37 °C for 15 min. After cell resuspension the plate was centrifuged at 4 °C and 250 g for 4 min. 50 µl of both supernatants were transferred into a new 96-well plate and 50 µl substrate mix were added. Following, the plates were incubated for 30 min at room temperature in the dark. To stop the enzymatic reaction 50 µl stop solution were added and the emission was measured at 490 nm with a plate reader. Subsequent the relative toxicity was calculated by substracting the background and then following the formula % toxicity = experimental LDH release/maximum LDH release. The results were normalized to the respective control. Staurosporine treatment (1 µM, 4 h) was used as a positive control.

SRB assay

Sulforhodamine B (SRB) is a protein binding dye that can be used to determine cell density. The assay was set up according to (Vichai and Kirtikara, 2006). Primary cortical neurons or HEK293 cells were cultured in a 96-well plate. For fixation cell culture medium was removed and 50 µl of 10 % Trichloricacid (TCA) were added followed by incubation on ice for 30 min. Fixed samples were washed with MilliQ water three times and dried at room temperature overnight. On the following day, cells were stained with 75 µl 0.4 % SRB in 1 % acetic acid for 15 min at room temperature. To remove unbound SRB dye, cells were washed repeatedly with 1 % acetic acid and the washed plate was dried at room temperature overnight. 200 µl of 10 mM Tris in MilliQ water were added and the plate was incubated at 200 rpm at room temperature until the SRB dye was dissolved completely. Afterwards, the absorption was measures with a plate reader at 510 nm. Relative cell viability was calculated by normalizing to the respective control. Staurosporine was used as a positive control (1 µM, 4 h).

TUNEL assay

Terminal deoxynucleotidyl nick end labeling (TUNEL) is used to detect DNA fragmentation that occurs during apoptosis. For the detection of apoptosis, primary cortical neurons were cultured in a black 96-well plate and fixed with 50 µl PFA-fix solution (15 min, room temperature). Afterwards cells were washed three times with PBS and subsequently permeabilized with 50 µl permeabilization/quenching buffer on ice for two minutes. Enzyme solution and labeling solution were mixed 1:10 and 25 µl of the mixture were added per well. The plate was incubated at 37 °C in the dark for 1 h. Afterwards, cells were washed again three times with PBS and stained with DAPI as a nuclear marker (0.2 mg/ml PBS) for 15 min. After a final washing step with PBS, images were acquired automatically in tile scans with the Zeiss LSM 710 confocal microscope. Image analysis was performed manually with the ImageJ cell counter plugin, blinded to the experimental conditions. At least 400 cells were counted per condition. Staurosporine was used as a positive control (1 µM, 4 h).

XTT assay

The 2,3-bis-(2-methoxy-4-nitro-5-sulfophenyl)-2H-tetrazolium-5-carboxanilide (XTT) assay is used to assess cell viability through the colorimetric reduction of the tetrazolium salt XTT by cellular enzymes. For this purpose cortical neurons were cultivated in a 96-well plate. According to the manufacturer's instructions, freshly thawed XTT labeling reagent and Electron-coupling reagent were mixed 50:1. Following, 50 µl of the mix were added per well and the plate was incubated for 24 h at 37°C and 5 % CO_2. The absorption was measured spectrophotometrically with a plate reader at 480 nm and a reference wavelength of 650 nm. Relative cell viability was calculated by substraction of A_{650} from A_{480} and subsequent normalization to the respective control. 1 µM Staurosporine treatment for 4 h was used as a positive control.

3.2.3.2. Other assays

Proteasome activity assay

Proteasome activity was measured by evaluating all three major proteolytic activities (Trypsin-like, Chymotrapsin-like and Caspase-like) independently with a Luciferase based detection system. HEK293 cells were cultivated in a white 96-well plate (PerkinElmer). Prior to cultivation, cells were washed with medium twice after trypsination to get rid of remaining trypsin before measuring proteasome. Two days after transfection, medium was exchanged to 50 µl medium-reagent mixture containing 25 µl fresh medium and 25 µl of the respective Proteasome-Glo cell based reagent equilibrated to room temperature. Additionally, a no cell containing medium control was prepared. Afterwards, the plate was sealed and incubated at room temperature while shaking at 400 rpm for 4 min. The plate was further incubated for 30 min at room temperature and luminescence was measured directly following incubation using the Microlumat plus 96 V. Proteasome activity was determined via subtraction of the medium control and subsequent sample normalization to the experiment control. Epoxomycin (8 µM, 2 h) was used as a positive control for impaired proteasome activity.

3.2.4. Protein biochemistry

3.2.4.1. Generation and purification of Unc119 rabbit polyclonal antibody

Antigen purification

For affinity purification with the corresponding Gluthatione-S-Transferase (GST)-fusion protein, *E.coli* bacteria were transformed with GST-hUnc119 coding vectors and bacteria were expanded in 800 ml LB media. Upon an OD_{600} of 0.6 the culture was induced with 1 mM IPTG at 30 °C. Following centrifugation at 600 *g* for 10 min at 4 °C the resulting pellet was resuspended in STE buffer. To disrupt the cells and extract the antigen, 100 µg/ml lysozyme were added and incubated on ice for 15 min. Afterwards, 5 mM DTT was added and the lysate was sonicated for 1 min. The samples were centrifuged at 10,000 *g* for 10 min at 4 °C. Following, the supernatant

was incubated with 4 ml maltose beads under vigorous shaking for 30 min. The beads were washed three times in STE buffer and the antigen was eluted with glutathione elution buffer and collected in 1 ml fractions. The protein concentration was measured using OD_{280}. Samples from all steps of the purification protocol were taken to check purity of the antigen by SDS-PAGE and subsequent Coomassie staining. Protease and phosphatase inhibitor were present in all steps of the purification.

Antibody production

Polyclonal antibodies were generated at Eurogentec SA, Belgium through the immunization of rabbits with the GST-tagged antigens. The serum of several large bleeds and the final bleed of immunized rabbits was collected and stored at -20°C until affinity purification of the antibodies.

Antibody purification

For affinity purification of the antibodies glutathione-S-transferase (GST)-fusion proteins with the corresponding antigen or GST alone, generated as described above, were incubated with 4 ml glutathione beads while shaking for 30 min. Afterwards the beads were washed with 0.5 % Triton-X-100 in STE buffer three times. Washed beads were transferred into a column and washed another four times with conjugation buffer. Subsequent, the beads were crosslinked to the antigen with 5 mM BS3. Protease and phosphatase inhibitor were present throughout all steps.

For negative selection the serum from immunized rabbits was diluted 1:1 with PBS and passed over the GST-only column three times. The flow through was collected and subsequently passed over the GST-Unc119 fusion protein column thrice.
Following, beads were washed with column buffer thrice. Finally, the antibody was eluted with glycine elution buffer and collected in 1 ml fractions. Fractions were neutralized with 100 µl 1M Tris pH 9.5 and the protein concentration was measured using OD_{280}. Samples from all steps of the purification protocol were taken to check purity of the antibody by western blotting.

3.2.4.2. Immunoblotting

HEK293 lysate preparation

HEK293 cells were washed once with PBS and 300 µl RIPA buffer substituted with Protease inhibitor cocktail (1:500) was added to a 12-well. Following, cells were incubated on ice for 20 min. Cells were detached from the well bottom with a pipette and transferred into a 1.5 ml tube. Afterwards, cells were incubated again for 20 min on ice and subsequent centrifuged at 1,000 g for 10 min. 4x Laemmli was added to the lysate to obtain a 1x solution and samples were boiled at 95 °C for 10 min. Samples were used immediately or stored at -20 °C until further use.

Neuron lysate preparation

Primary neuron lysates were prepared by adding 150 µl 2x Laemmli directly to each well after washing the cells with PBS once. The lysate was transferred to 1.5 ml tubes and boiled at 95 °C for 10 min. Samples were used immediately or stored at -20 °C until further use.

SDS-polyacrylamid gel electrophoresis (SDS PAGE)

To separate proteins according to their molecular weight, lysates were run under denaturizing conditions on a discontinuous SDS polyacrylamide gel electrophoresis system. Polyacryamide gels consisted of a 12.5 % acrylamide separating gel and a 4 % stacking gel. The detailed composition is described below.

Gel type	Composition of a 12.5 % gel
Stacking gel	6.5 ml H_2O 2.5 ml stacking gel buffer 1 ml acrylamide added for polymerization: 100 µl 10% APS 10 µl TEMED
Separating gel	8.75 ml H_2O 5 ml separating gel buffer 6.25 ml acrylamide added for polymerization: 200 µl 10% APS 20 µl TEMED

Gels were loaded with 25 µl lysate and 5 µl of the Seeblue Protein 2 marker and run at 80 V in running buffer for the first 20 min and 130 V afterwards until the dye front began running out of the gel.

Tricine-SDS-Schägger gels

Ready to use 10-20% Tricine gels were loaded with 20 µl lysate and 5 µl Seeblue Protein 2 marker and run at 80 V in cathode buffer for approximately 3 h.

Immunoblotting and immunodetection of proteins

Proteins were blotted on an isopropanol activated polyvinylidene difluoride (PVDF) membrane in blotting buffer at 400 mA for 75 min. After blotting, membranes were blocked in 0.2 % I-Block in TBSTx to saturate all unspecific binding sites for at least 1 h. Primary antibody diluted in 0.2 % I-Block in TBSTx was added and the membranes were incubated at 200 rpm and 4 °C overnight. On the following day, membranes were washed in TBSTx every ten minutes for approximately 1 h. Afterwards, a HRP coupled secondary antibody diluted 1:1000 in 0.2 % I-Block in

TBSTx was added and the membrane was incubated at 200 rpm and room temperature for 1 h.

3.2.4.3. Filter trap

Cultured cells

For filter trap assays primary cortical neurons or HEK293 cells were cultured in 12-well plates. Medium was removed and cells were washed with PBS once. Following cells were harvested in 600 µl 1 % Triton-X-100 in PBS substituted with DNAse (0.2 mg/ml) and 50 mM $MgCl_2$. The lysate was centrifuged at 18,000 g for 30 min (4 °C). Afterwards, the supernatant was discarded and the pellet was dissolved in 200 µl 2 % SDS in 100 mM Tris pH 7 and incubated for 1 h at room temperature. After incubation, the mixture was diluted 1:5 three times and filtered through a 0.2 µm cellulose acetate membrane. The membrane was blocked in 0.2 % I-Block in TBSTx for 1 h. Following, primary antibody was added and the membrane was incubated at 4 °C and 200 rpm overnight. The following steps were performed as described in immunodetection of proteins.

Patient material

The brain samples were homogenized in RIPA buffer containing 0.2 mg/ml DNAse. After centrifugation at 4 °C and 186,000 g for 30 min, the pellet was resuspended in 1 % SDS in 100 mM Tris pH 7. The following steps were performed as described above for cultured cells.

3.2.4.4. Immunoprecipitation of poly-GA aggregates

IP from HEK293 cells

HEK293 cells were harvested two days after transfection from a 10 cm dish in 1 ml RIPA buffer substituted with 0.2 mg/ml DNAse I and 10 µl Protease Inhibitor cocktail. Afterwards, samples were rotated at 4 °C for 30 min and centrifuged at 1,000 g for 15 min. Meanwhile, 5 µg GFP antibody (Neuromab) were pre-incubated with 25 µl Protein G Dynabeads for 1 h at 4 °C. After centrifugation 2 % of the

supernatant were kept as input control and the rest was mixed with the beads and rotated at 4 °C for 3 h. Following, the beads were washed with basic buffer thrice. Protein was released from the beads by boiling in 25 µl 4x Laemmli at 95 °C for 10 min. The Laemmli-mix was then diluted 1:1 with MilliQ water and 25 µl of each sample were used for immunoblotting.

Neuron IP for Mass spectrometry

Primary cortical neurons were harvested from 10 cm dishes after 17 days *in vitro* in 1 ml RIPA buffer substituted with 67 U/ml Benzonase and 10 µl Protease Inhibitor cocktail. Following, samples were rotated at 4 °C for 30 min and centrifuged at 1,000 g for 15 min. In the meantime, 50 µl Protein G Dynabeads were incubated with 10 µg GFP antibody for 1 h at 4 °C. 2 % of the sample supernatant were kept as input control and the rest was added to the pre-incubated dynabeads. The mix was rotated at 4 °C for 3 h. Afterwards, the beads were washed with 1 ml basic buffer thrice. 1/5 of the beads was kept for immunoblotting and protein was released from the beads by boiling at 95 °C in 20 µl 4x Laemmli for 10 min. The rest of the sample was further processed for mass spectrometry analysis.

3.2.4.5. Mass spectrometry (in collaboration with Daniel Hornburg)

Sample preparation

The bead-mix from the neuron-IP was resuspended in 50 µl 8 M Urea, 10 mM Hepes pH 8.0. The protein cysteines were reduced with DTT and alkylated with iodoacetamide (IAA), followed by quenching of IAA with thiourea. Proteins were digested with LysC for 4 h and the bead-mix was centrifuged for 5 min at 16,000*g*. The supernatant was removed and diluted with 4 volumes of 50 mM ammonium bicarbonate. The pellet was resuspended in 1 volume 6 M urea, 2 M thiourea, 10 mM Hepes pH 8.0, 4 volumes 50 mM ammonium bicarbonate. For overnight digestion LysC and Trypsin were added and the digest was carried out for 16 h. The resulting peptide mix was desalted on C18 StageTips and analyzed in single shots.

LC-MS/MS

Peptides were separated on a Thermo Scientific EASY-nLC 1000 HPLC system with in-house packed columns (75 µm inner diameter, 20 cm length, 1.9 µm C18 particles) in a 100 min gradient from 2 % acetonitrile, 0.5 % formic acid to 80 % acetonitrile, 0.5 % formic acid at 400 nl/min. The column temperature was set to 50 °C. An Orbitrap mass spectrometer was directly coupled to the LC through a nano electrospray source. The Orbitrap Elite was operated in a data-dependent mode. The survey scan range was set from 300 to 1,650 m/z, with a resolution of 120,000. Up to five of the most abundant isotope patterns with a charge ≥2 were subjected to collision-induced dissociation fragmentation at a normalized collision energy of 35, an isolation window of 2 Th and a resolution of 15,000 at m/z 200. Data was acquired with the Xcalibur software.

Data analysis

The MS raw files, were processed with the MaxQuant software (v 1.4.0.4) and Andromeda search engine , against the UniProtKB Rat FASTA database (06/2012) using default settings. Enzyme specificity was set to trypsin allowing cleavage N-terminally to proline and up to 2 miscleavages. Carbamidomethylation was set as fixed modification. Acetylation (N-terminus) and methionine oxidation were set as variable modifications. A false discovery rate (FDR) cutoff of 1 % was applied at the peptide and protein level. 'Match between runs', allowing the transfer of peptide identifications in the absence of sequencing, was enabled with a maximum retention time window of 1 min. For protein identification at least one razor peptide was required and data were filtered for common contaminants (n = 247). Peptides only identified by site modification were excluded from further analysis. A minimum of two valid quantifications was required in either GA_{149}-GFP or GFP quadruplicates. The PERSEUS environment (Maxquant/R-framework) was used for bioinformatics analysis and visualization. Imputation of missing values was performed with a normal distribution (width = 0.3; shift = 1.8). For pairwise comparison of proteomes and determination of significant differences in protein abundances, *t*-test statistics were applied with a permutation-based FDR of 2 % and

S0 of 2. For poly-GA-aggregate interacting proteins 1D annotation enrichment on the Welch-test difference using Uniprot Keywords with a Benjamini–Hochberg corrected FDR of 2 % was applied.

3.2.5. Immunofluorescence

Standard Immunostaining

Cells on cover slips were fixed with 500 µl PFA-fix for 15 min at room temperature. Cells in black 96-well plates were fixed with 50 µl PFA-fix and also incubated for 15 min at room temperature. Afterwards cells were washed with PBS three times. Meanwhile the primary antibody solution was prepared. Therefore 2x GDB buffer was mixed with equal amounts of MilliQ water and the primary antibodies were added. For each cover slip, 50 µl of the solution were placed on a parafilm in a wetchamber. The cover slips were dipped in MilliQ water once and carefully placed onto the antibody solution with the cell side down. Following, the cover slips were incubated overnight at 4 °C in the dark. On the next day cover slips were transferred back into a 12-well plate and washed with PBS thrice. The secondary antibody dilution was prepared by mixing 2x GDB buffer with MilliQ water as described above and the Alexa-tagged secondary antibodies were added 1:400 to the mix. 50 µl of the final mix were again placed on a parafilm in a wetchamber and the coverslip was placed on top. Incubation was carried out in the dark for 1 h at room temperature. Following the incubation, the cover slips were again transferred into a 12-well plate and washed once. Afterwards 1 ml PBS containing the nuclear marker DAPI (1:5000) was added and cells were incubated in the dark at room temperature for 15 min. Following, cells were washed with PBS twice and mounted on a glass slide with a drop of vectashield mounting medium. Finally, cover slips were fixated on the glass slide with clear nail polish.

Immunostaining of TDP-43

For TDP-43 immunostaining, cells grown on cover slips were fixed with 500 µl PFA-fix at room temperature for 15 minutes. Afterwards cells were washed with

PBS twice. To permeabilize the nucleus, cells were incubated in 500 µl permeabilisation/quenching buffer (0.2 % Triton-X-100, 50 mM NH_4Cl in PBS) on ice for 2 min. Next, cells were washed with PBS twice and incubated in 50 µl blocking buffer in a wetchamber on a parafilm at room temperature for 1 h in the dark. Cover slips were transferred to a fresh parafilm with 50 µl primary antibody dilution (blocking buffer diluted 1:10 in MilliQ water containing primary antibody, (Cosmo TDP-43)) and incubated at room temperature for 1 h in a wetchamber in the dark. Subsequently, cover slips were transferred back into the 12-well plate and washed with PBS thrice. The secondary antibody dilution was prepared adding Alexa-tagged antibodies 1:400 to the 1:10 dilution of blocking buffer in MilliQ water. 50 µl of the mix were pipetted on a parafilm and the cover slips were added on top and incubated in a wetchamber for 1 h at room temperature. The following steps were conducted as described in standard immunostaining.

Immunostaining of patient material (in collaboration with Martin Schludi)

Before staining, patient tissue slides were deparafinized. Therefore slides were quickly rinsed with xylol 10x. Afterwards 10x rinsing was repeated with 100 % ethanol twice, followed by 96 % ethanol once and 70 % ethanol washing steps twice and kept in MilliQ water afterwards. For antigen retrieval slides were incubated in citrate buffer in the microwave at 750 W for 4 min. This procedure was repeated 4 times. Afterwards, slides were washed with Brij washing buffer for 5 min twice. Slides were blocked with 2 % FCS in PBS for 5 min. Primary antibodies were diluted in blocking buffer (Anti-GA and Unc119 #1 1:1000) and slides were incubated at 4 °C overnight. Following, the slides were washed with Brij washing buffer twice. Secondary antibody solutions with Alexa antibodies were prepared 1:500 in blocking buffer and slides were incubated for one hour in the dark. Slides were washed in Brij washing buffer twice and subsequent stained with DAPI, diluted 1:5000 in Brij washing buffer, for 20 min in the dark. To reduce background and autofluorescence slides were also briefly incubated with Sudan black for 30 sec. Slides were washed again twice. Afterwards, a third washing step was conducted

with MilliQ water for 5 minutes. Slides were mounted with mounting media and fixed with clear nail polish.

Image acquisition

Images were acquired using the Zeiss LSM 710 confocal microscope and the Zeiss ZEN 2010 software. Depending on the experiment, either the 20x, 40x, or 63x objectives, as specified in the material sections, were used. The pinhole was set to 1 Airy unit for the longest wavelength and maintained for all others. For the filter setting and excitation/emission spectra the preset software adjustments for the specific dyes were used. To be in a linear range and to avoid oversaturation of pixels, laser intensity and detector gain were set accordingly. To achieve an optimal resolution in z-direction, the distance between two adjacent confocal planes of a z-stack was set that every pixel was covered by two confocal planes. Images were acquired in a x-y-resolution of at least 1024x1024 pixels and the scanning speed was chosen according to the experiment purpose. For quantitative and semi quantitative measurements all settings were maintained for every image of the respective experiment.

Image analysis

All images were analyzed blinded to the experimental conditions. For cell countings, images were analyzed with the Fiji cell counter plugin and at least 200 cells were counted per conditions. For exact numbers see corresponding figure legends. For neuron morphology analysis, maximum intensity projections Sholl analysis was performed with the MetaMorph software.

3.2.6. Statistical analysis

All statistical analyzes were performed with the GraphPad Prism software. Depending on the data set, t-test, one-Way-ANOVA or two-way-ANOVA with appropriate post-tests was conducted. All morphological analyzes and quantifications were performed blinded to the experimental conditions. Statistical significance was set as follows. * $p < 0.05$; ** $p < 0.01$; *** $p < 0.001$

4. Results

4.1. Expanded repeat RNA is stabilized in *C9orf72* mutation carriers

The initial discovery of non-ATG translation of the intronic *C9orf72* hexanucleotide repeat expansion mutation raised questions about the inter-connection and relative role of the proposed pathomechanisms. For instance, how can the expanded repeat be translated, if the expression of the mutant allele is reduced? To what extend is the transcript of the repeat-containing intron expressed, compared to non-repeat carriers? Is the antisense strand also transcribed and translated into the additional DPR species poly-PA, poly-PR and more poly-GP in patients?

To address these questions, I performed RT-qPCR analysis from the cerebellum of three *C9orf72* mutation carriers aged 41 to 65 and 6 aged matched controls that showed ALS or FTD pathology, but did not carry a *C9orf72* mutation. In the RT-qPCR, I used specific primer sets for both sense and antisense transcripts and intron-spanning primers amplifying exon 2 to 3 of *C9orf72* to detect all isoforms as well as primers spanning intron 1b to 2 amplifying only transcripts lacking the repeat (Figure 7A and compare Figure 5).

The total expression of *C9orf72*, normalized to the housekeeping gene *YWHAZ*, is downregulated by about 50 % in mutation carriers, compared to controls (Figure 7B). This observation is in line with the findings of other groups, investigating the expression of *C9orf72* in mutation carriers (DeJesus-Hernandez et al., 2011; Renton et al., 2011). Using strand-specific reverse transcription with either sense or antisense primers followed by qPCR analysis (Figure 7A), I investigated the expression of both transcripts. The expression levels were normalized to sense transcripts levels in control patients and PCR products were sequence verified. Strikingly, the expression of the repeat expansion transcripts, sense as well as antisense, is increased about 8-fold compared to control patients (Figure 7C), suggesting a stabilization of the containing repeat RNA species and first establishing the presence of the antisense transcript in *C9orf72* mutation carriers.

This data may reconcile *C9orf72* haploinsufficiency with RNA and protein toxicity and was the first step in the discovery of antisense derived DPR species (Mori et al., 2013c).

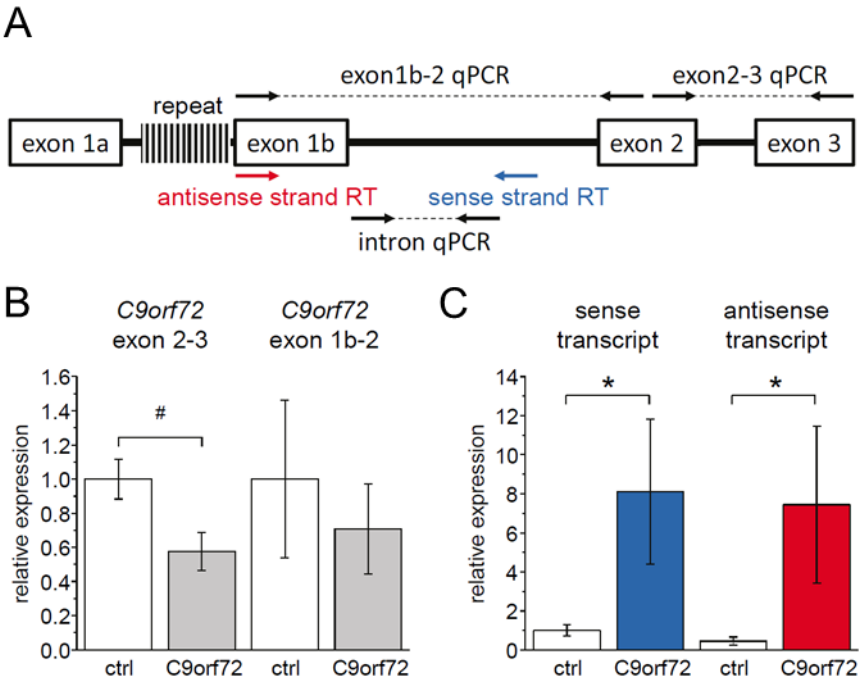

Figure 7: *C9orf72* transcripts are differentially expressed in mutation carriers.
(A) *C9orf72* genomic structure and primer settings for the RT/qPCR experiment. (B) Mature *C9orf72* mRNA levels are downregulated in the cerebellum of mutation carriers compared to control. Intron-spanning primers amplifying exon 2 to 3 detect all isoforms, whereas primers amplifying exon 1b to 2 detect the isoform lacking the repeat sequence. Data represent mean ± SEM; # = $p < 0{,}058$. (C) *C9orf72* sense and antisense transcript of the *C9orf72* are transcribed to a higher extend in mutation carriers compared to controls. Mean ± SEM; * = $p < 0{,}05$ One-way-ANOVA with Bonferoni correction; N=3 for cerebellum from *C9orf72* mutation carriers and N=6 for cerebellum from controls.

4.2. A cell culture model for DPR protein expression

4.2.1. DPR expression system

To address the role of DPR proteins in *C9orf72* FTD/ALS, I established a cell culture expression system. Even though the existence of DPR proteins in *C9orf72* mutation carriers is now widely accepted (Ash et al., 2013; Mori et al., 2013c; Zu et al., 2013), the contribution of DPR proteins to the development of *C9orf72* FTD and ALS is still an open question. Thus, one of my major aims was to decipher the individual characteristics of the different DPR species and their contribution to

disease development. Here, I used ATG-initiated epitope-tagged expression constructs for all possible reading frames of the G_4C_2 hexanucleotide repeat (Figure 8). The synthetic constructs encode 149 to 175 repeats of the distinct dipeptides. A mixture of alternative codons helped to prevent genomic repeat instability in E. coli observed with the GGGGCC repeats and a good expression in mammalian cell culture systems was achieved. Furthermore, the lack of a GGGGCC repeat allows to largely exclude RNA based toxicity and to focus on protein-based toxicity in my experiments. The poly-GP construct gene synthesis, however, failed repeatedly. Therefore, an ATG-initiated construct from the endogenous repeat sequence with about 80 GP repeats was designed (Figure 8).

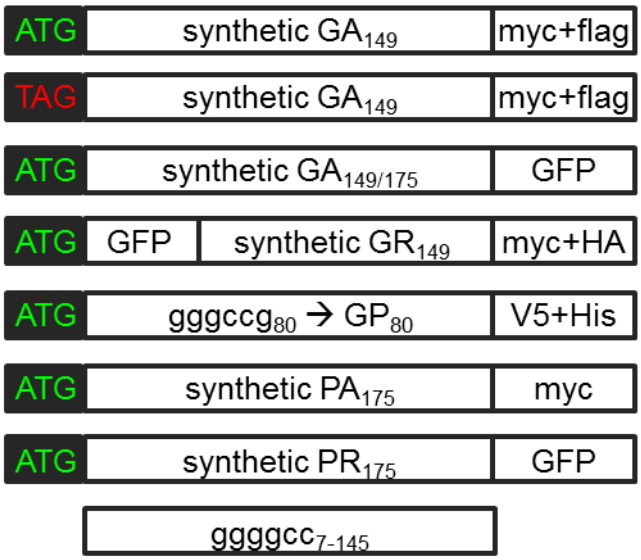

Figure 8: Schematic illustration of the DPR constructs used in this thesis.
For all possible reading frames almost GGGGCC-free synthetic genes were designed with an ATG start codon. For the poly-GR constructs, the GFP-Tag position had to be changed because GR_{149}-GFP was not expressed, whereas GFP-GR_{149} could be expressed nicely. The poly-GP synthetic gene construct could not be synthesized despite several attempts, therefore the original GGGGCC repeat was used for the construct design. For analysis of repeat sequence toxicity apart from protein toxicity non-ATG versions with the original repeat sequence from 7-145 repeats were designed. To further exclude toxicity of the synthetic gene RNA, a TAG-GA_{149} construct was prepared.

To additionally analyze, if the original repeat sequence induces RNA toxicity in a cell culture system, I used constructs containing 7 to 145 repeats of the original repeat sequence without an ATG start codon (Figure 8). A GFP or empty vector was used as a control in all experiments (Figure 8).

In summary, I could establish an expression system for all DPR proteins to further analyze their characteristics in cell culture systems.

4.2.2. Poly-GA forms p62-positive inclusions in HEK293 cells

All five DPR species co-aggregate into mainly cytosolic and p62-positive star-shaped inclusions in patients (Mori et al., 2013a; Mori et al., 2013c). To analyze the expression of the individual DPR proteins and their aggregation pattern in cell culture, HEK293 cells were transfected with GA_{175}-GFP, GFP-GR_{149}, GP_{80}-V5, PA_{175}-myc, PR_{175}-GFP or GFP as a control.

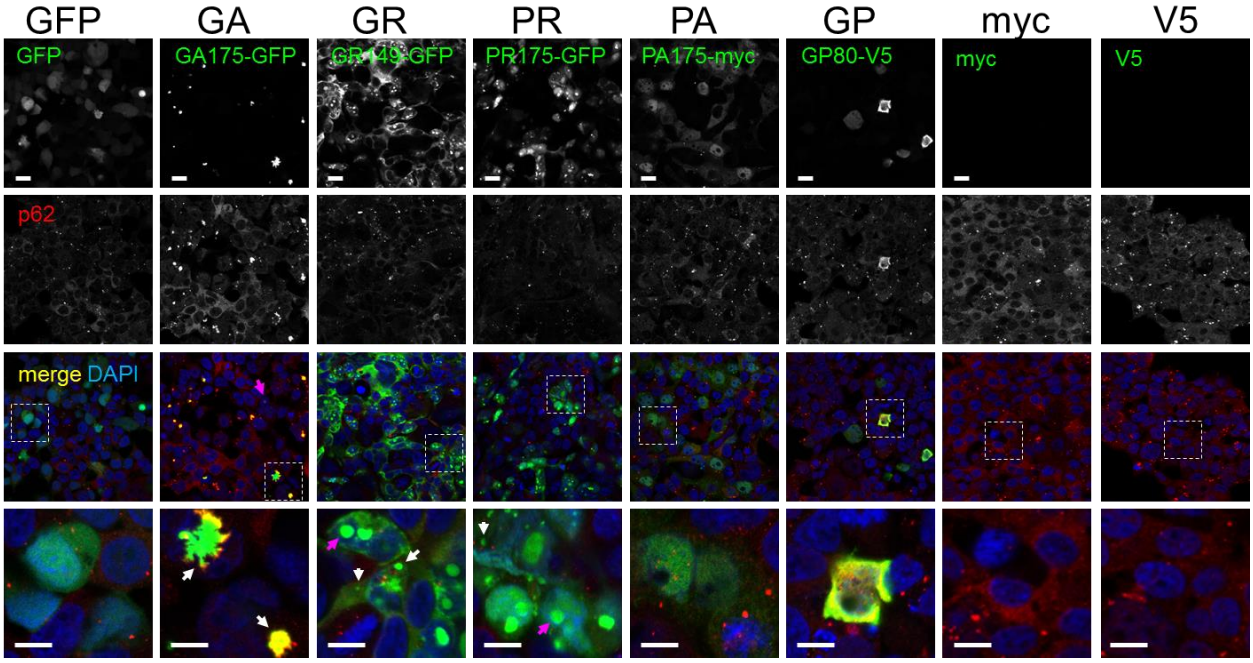

Figure 9: DPR proteins aggregate differently in HEK293 cells.
HEK293 cells were transfected with GA_{175}-GFP, GFP-GR_{149}, GP_{80}-V5, PR_{175}-GFP, PA_{175}-myc as well as a GFP, V5 tag or myc-control. Two days after transfection, cells were analyzed by GFP fluorescence, V5 or myc antibody in the case of GP_{80}-V5 and PA_{175}-myc. DAPI was used as a nuclear marker. Only GA_{175}-GFP transfected cells show cytosolic aggregates that are p62-positive. GFP-GR_{149} mainly shows nuclear aggregates and no aggregation could be detected for GP_{80}-V5. Since the AP_{175}-GFP construct also produced free GFP, the tag had to be changed to a myc-tag for proper analysis. PR_{175}-GFP mainly showed nuclear aggregates, whereas no aggregation could be detected for PA_{175}-myc. *White arrows* indicate cytosolic aggregates and *magenta arrows* nuclear aggregates. Bottom panels show close-ups indicated in the merge column. Scale bars depict 15 µm in overviews and 5 µm in close-ups.

Immunofluorescence of GFP was analyzed 2 days after transfection. Whereas poly-GA forms cytosolic inclusions, positive for the proteasomal marker p62, poly-GR and poly-PR mainly show large nuclear aggregates and no co-staining with p62

(Figure 9). Poly-GP and poly-PA were distributed throughout the whole cell and no aggregates could be detected. Moreover, no p62 co-localization could be observed for poly-PA and only a few poly-GP expressing cells showed co-localization with p62 (Figure 9).

In addition to p62-positive cytosolic inclusions, small nuclear aggregates of poly-GA are present in patients (Mackenzie et al., 2013). In my HEK293 cell culture model, these aggregates could also be seen in a low frequency. However, not all nuclear aggregates were found to be p62-positive (Figure 10).

Thus, poly-GA is the only of the five DPR proteins that shows a typical aggregation pattern comparable to patients in HEK293 cells.

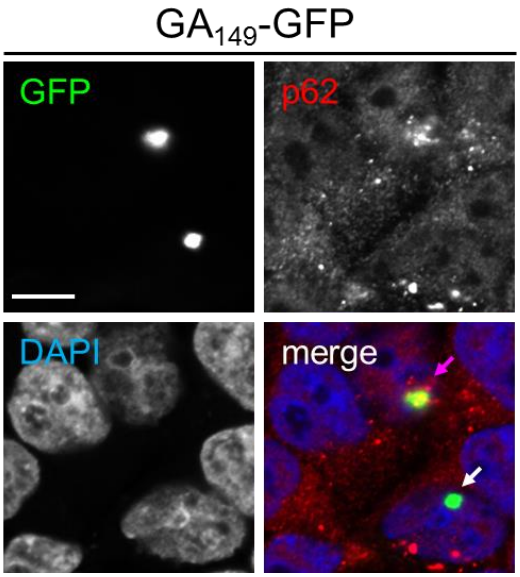

Figure 10: Poly-GA additionally forms less common nuclear aggregates.
HEK293 cells transfected with GA_{175}-GFP for three days. A part of nuclear poly-GA aggregates is p62-positive. *Magenta arrows* mark p62-positive and *white arrows* p62-negative nuclear aggregates. Scale bar = 5 µm

4.2.3. Biochemical properties of DPR proteins differ in HEK293 cells

Following, immunostaining of the DPR proteins, running behavior and expression levels of the different proteins were evaluated. GA_{175}-GFP, GFP-GR_{149} and PR_{175}-GFP could be detected at the top of the gel, whereas PA_{175}-myc ran on a higher molecular weight than expected, suggesting the formation of higher molecular

weight species. Only GP_{80}-V5 could be detected at the expected height of 20 kDa (Figure 11A).

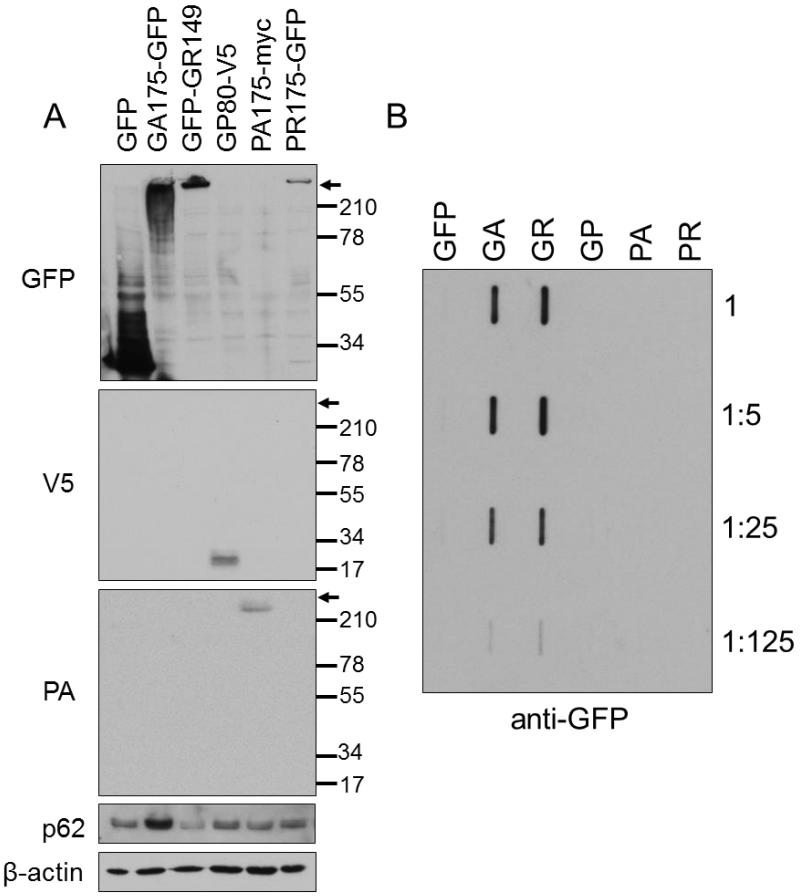

Figure 11: DPR proteins show differential biochemical properties.
HEK293 cells were transfected with GA_{175}-GFP, GFP-GR_{149}, GP_{80}-V5, PA_{175}-myc, PR_{175}-GFP or GFP as a control. After 2 days cells were harvested for immunoblotting or filter trap analysis. (A) Immunoblotting with indicated antibodies shows expression of DPR proteins and GFP control. GA_{175}-GFP, GFP-GR_{149}, PA_{175}-myc and PR_{175}-GFP are detected at the top of the gel (arrow), whereas GP_{80}-V5 runs at its expected height of 20 kDa. P62 levels are only elevated in GA_{175}-GFP transfected cells. (B) Filter trap assay for insoluble proteins. Only GA_{175}-GFP and GFP-GR_{149} form insoluble aggregates. Immunoblotting was carried out with a GFP antibody. Immunoblotting with anti-V5 for poly-GP or anti-myc for poly-PA showed no insoluble aggregates (Data not shown).

To analyze the solubility of the different proteins, a filter trap assay was performed. Only GA_{175}-GFP and GFP-GR_{149} were insoluble in 2 % SDS and could be detected on the filter, thereby exhibiting the same features as the patient aggregates (Figure 11B).

4.3. DPR proteins are not toxic in HEK293 cells

The key question is, if and how the DPR proteins contribute to disease pathophysiology in *C9orf72* cases. Therefore, the next step was to analyze toxicity of all five DPR proteins in the HEK293 cell culture system. For detecting dead cells, I performed an LDH assay. LDH is an intracellular enzyme that is only released upon cell death. The amount of LDH in the media is measured through the conversion of a colorimetric substrate. After three days of transfection with the different DPR proteins no toxicity was observed (Figure 12A). Staurosporine, which was used as a positive control, however, showed a marked reduction in cell viability of 20 % after 4 h treatment with 1 µM Staurosporine and a 95 % reduction after 24 h treatment.

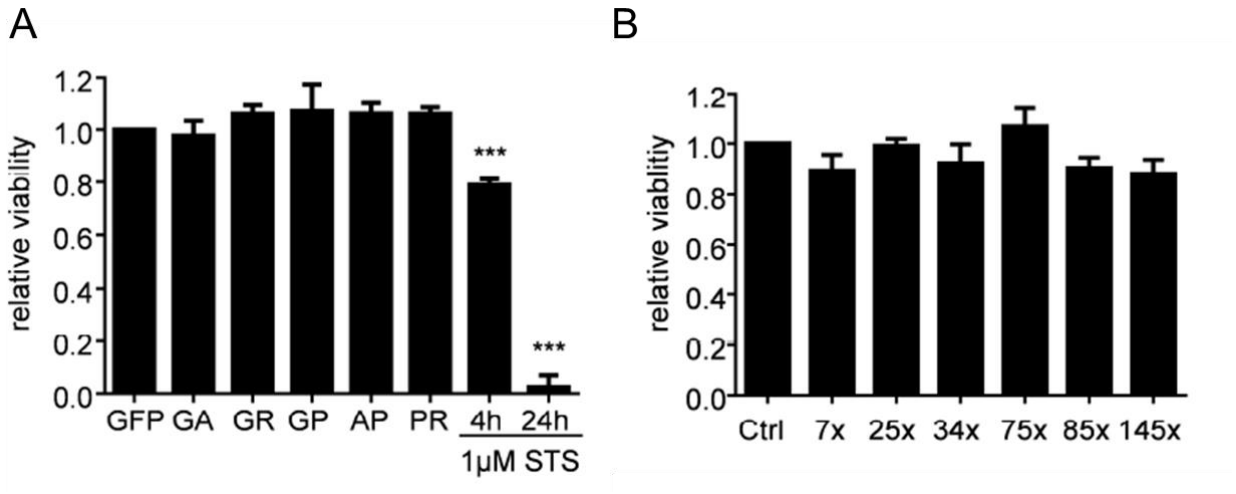

Figure 12: DPR proteins and RNA are not toxic in HEK293 cells.
HEK293 cells were transfected with the DPR protein constructs (GA_{175}-GFP, GFP-GR_{149}, GP_{80}-V5, PR_{175}-GFP, PA_{175}-myc) or GGGGCC-repeat expressing constructs in various length for 3 days. (A) LDH release assay detects no significant toxic effect upon DPR expression compared to GFP control in HEK293 cells. Treatment with 1 µM Staurosporine was used as a positive control. n=3 experiments with 10 replicates each; mean ± SD, *** $p<0.001$ in one-way ANOVA with Dunett's post-test. (B) Cell viability of HEK293 cells transfected with GGGGCC-repeat expressing constructs of increasing length (lacking an ATG start codon) was measured by XTT assay on day 3. No significant toxicity compared to an empty vector control (Ctrl) was observed (one-way ANOVA, Dunett's post-test).

Since the synthetic constructs showed no toxicity, I checked whether constructs with the original repeat sequence of *C9orf72* in various lengths without an ATG start codon show toxicity(Figure 8). However, no toxicity could be detected in the

tetrazolium dye based XTT assay measuring mitochondrial activity after 3 days of transfection in the HEK293 cell culture system (Figure 12B).

4.4. Poly-GR and poly-PR decrease proliferation of HEK293 cells

During my previous experiments I noticed, that although poly-GR and poly-PR did not show an effect on cell viability, there appeared to be fewer cells than in control conditions. Therefore, I used a XTT assay to investigate if poly-GR and poly-PR influence proliferation. Notably, after three days of transfection, poly-GR significantly reduced the number of cells to 80 % and poly-PR to 87 % compared to the GFP control (Figure 13A).

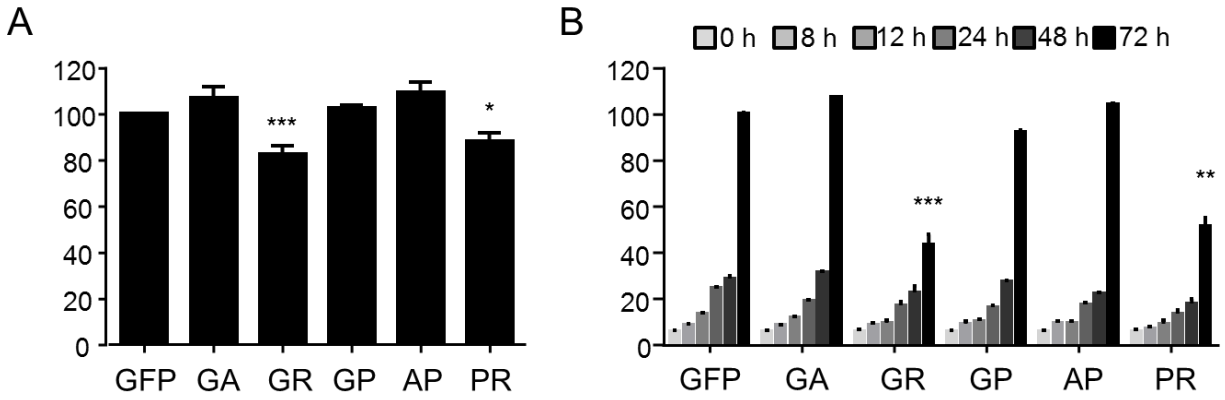

Figure 13: Poly-GR and poly-PR decrease proliferation in HEK293 cells.
HEK283 cells were transfected with GA_{175}-GFP, GFP-GR_{149}, GP_{80}-V5, PR_{175}-GFP, PA_{175}-myc or GFP as a control for three days. (A) XTT proliferation assay detects a significant decreased in proliferation in poly-GR and poly-PR expressing cells. N=3 with 10 replicates each. Mean ± SD are depicted. *p<0,05; ***p<0.001 in a one-way ANOVA with Dunetts post test. (B) Growth curves of DPR protein expressing HEK293 cells measured by SRB assay. Compared to GFP control poly-GR and poly-PR expressing cells grow significantly slower over time. Timepoints depicted are 0 h, 4 h, 8 h, 12 h, 24 h, 48 h, 72 h. N=3 with 10 replicates each. Mean ± SD are depicted. **p<0,01; ***p<0.001 in a two-way ANOVA.

To further corroborate, if the effect is really based on decreased proliferation and not on additional toxicity, I conducted a time-course series in a Sulforhodamine B (SRB) assay, analyzing cell number 0, 8, 12, 24, 48 and 72 hours after transfection with all five DPR proteins and GFP as a control. The SRB assay is based on total protein content and therefore is an additional approach to investigate cell number after DPR construct transfection. The proliferation over time clearly showed that cells transfected with poly-GR and poly-PR did not proliferate as fast as GFP

control cells and the other DPR expressing cells. 72 h after transfection 50 % less poly-GR expressing cells and 40 % less poly-PR expressing cells were present, compared to GFP control cells (Figure 13B). The other DPR proteins poly-GA, poly-GP and poly-PA had no significant effect on HEK293 cell proliferation.
In summary, HEK293 cells recapitulate some important features of the patient situation, however, cell death cannot be observed in this model. Since DPR proteins in patients are mostly expressed in quiescent neurons that probably cannot be compared with immortalized cell lines, I established a lentiviral DPR expression system in primary rat neurons for further investigations.

4.5. Lentiviral poly-GA expression system in primary neurons

4.5.1. Lentiviral poly-GA expression in primary neurons is comparable to patient levels

As poly-GA expression in HEK293 cells resembled the patient situation most, I first focused my investigations on poly-GA in primary neurons. To verify if the lentiviral expression system is comparable to the aggregate load detected in patients, I used primary cortical neurons, transduced with GA_{149}-myc (DIV 6+15) and a thin smear of frontal cortex tissue from a *C9orf72* patient (Figure 14A) to allow identical fixation and staining conditions.

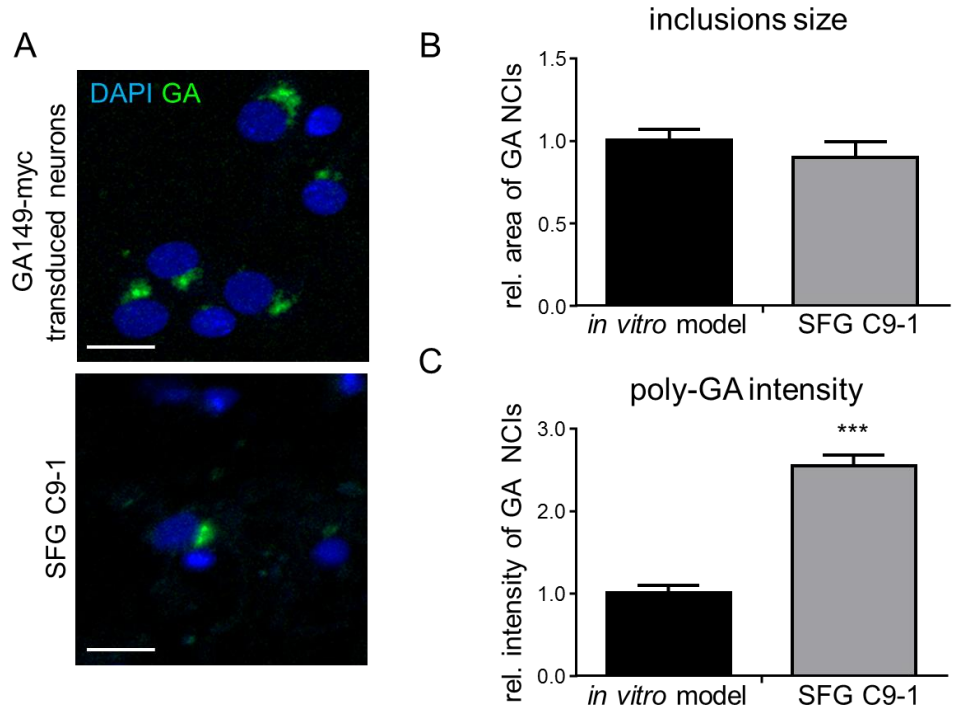

Figure 14: Expression levels of lentiviral poly-GA in neuronal culture are comparable to levels in *C9orf72* patients.

Primary cortical neurons (DIV 6+15) transduced with GA_{149}-myc or a thin smear of cortical tissue from a *C9orf72* patient were immunostained under identical conditions with poly-GA antibody. DAPI was used as a nuclear marker. (A) Scale bar depicts 20 µM. The in vitro system shows more poly-GA-positive cells compared to the patient sample. (B) The size of the individual poly-GA aggregates is comparable in patient sample and lentiviral system, whereas the intensity of the poly-GA staining is over two-fold higher in patient material. Poly-GA area and intensity was manually quantified with the imageJ software for 50 inclusions in each condition. Mean ± SD; student-t-test; ***p<0,001.

Following poly-GA immunostaining, I compared fluorescence intensity and inclusion size. Whereas transduced primary neurons, showed more cells with poly-GA aggregates, aggregate size was comparable with the patient material (Figure 14B). In contrast, the poly-GA fluorescence intensity was 2.5-fold higher in patient material compared to neurons (Figure 14C).

Thus, the lentiviral expression model may even slightly underestimate the patient situation and therefore is a valid tool to investigate the effect of poly-GA expression in neurons.

4.5.2. Poly-GA forms insoluble p62-positive aggregates in primary neurons

Subsequently, I analyzed whether poly-GA also forms the typical p62-positive aggregates seen in patients in the neuron system. Therefore, GA_{149}-GFP was expressed lentivirally in primary hippocampal neurons (DIV 6+15).
Immunofluorescence depicted compact p62-positive inclusions that were most common in the cell soma, but were also present in the dendrites (Figure 15).

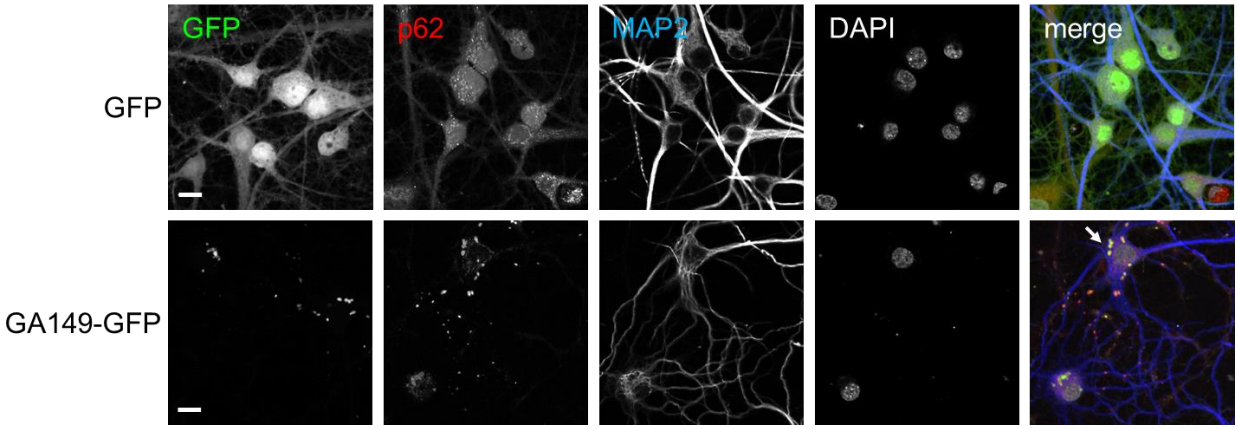

Figure 15: Poly-GA forms p62-positive aggregates in primary neuron culture.
Primary hippocampal neurons were transduced at day 6 *in vitro* with GA_{149}-GFP or GFP as a control. After 15 days in culture, immunostaining for p62 and MAP2 was performed. DAPI was used as a nuclear marker. P62-positive inclusions are formed in cytosol and dendrites (*white arrow*). Scale bar = 15 µM.

In western blots of lentivirally transduced primary cortical rat neurons with GA_{149}-myc or GFP as a control, all poly-GA was detected at the top of the gel, indicating higher molecular weight aggregates (Figure 16A). Consistent with the HEK293 cell results, p62 levels were increased in neurons infected with poly-GA lentivirus compared to control cells (Figure 16A). Protein levels of the synaptic marker PSD-95 and the housekeeping protein β-actin remained unchanged (Figure 16A).

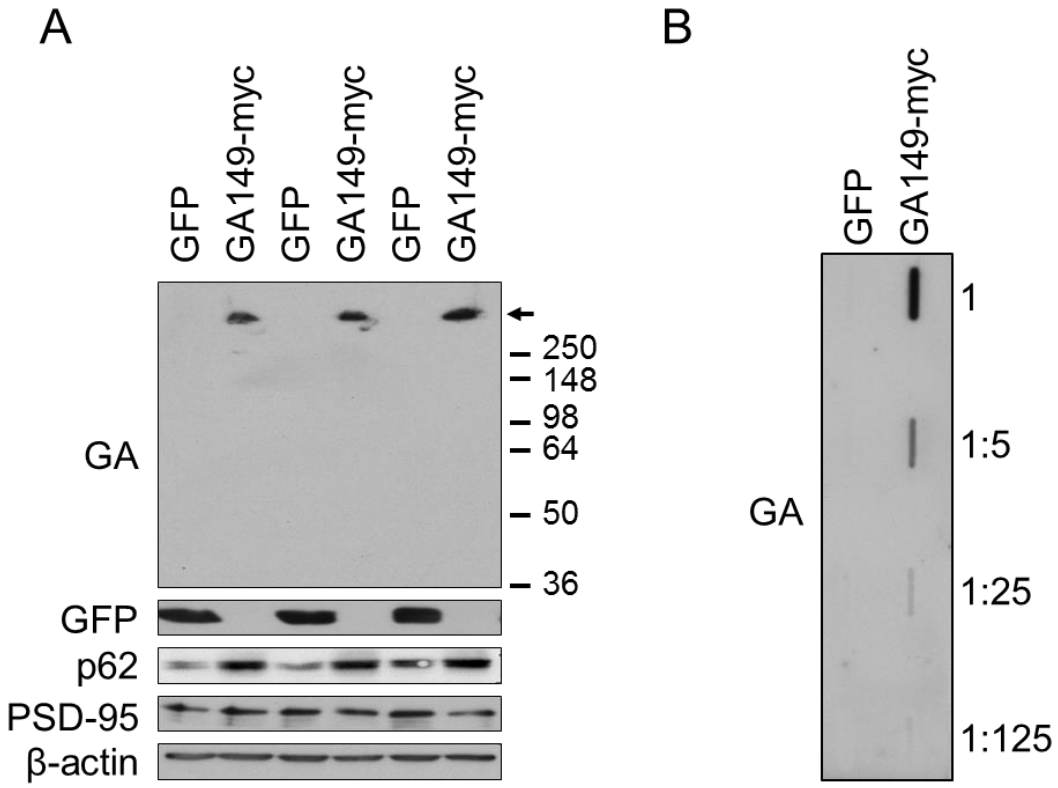

Figure 16: Neuronal p62-positive poly-GA aggregates are insoluble.
Primary cortical neurons transduced with GA_{149}-myc or GFP as a control on day 6 were incubated for 17 days. (A) Immunoblotting with indicated antibodies. Poly-GA is detected at the top of the Gel and p62 levels are increased in GA_{149}-myc expressing neurons. PSD-95 and β-Actin levels remain unchanged. (B) Insoluble aggregates of poly-GA can be detected in the filter trap assay with 2 % SDS concentration.

To further elucidate solubility of poly-GA aggregates in neurons a filter trap assay was performed, indicating the formation of 2 % SDS-resistant poly-GA aggregates (Figure 16B).

4.6. Poly-GA aggregates cause dendrite loss and toxicity in primary neurons

4.6.1. Neuron morphology is impaired in poly-GA expressing cells

Upon poly-GA transduction, I noticed a reduced density of surviving neurons and neurites, visualized by MAP2 staining, seemed to be less complex (Figure 15). To quantify the effect of poly-GA on neuron morphology, I used Sholl analysis which measures neuron complexity by counting the number of dendrites crossing

concentric circles around the cell. Upon transfection of primary cortical neurons (DIV 7+4) with GA_{149}-myc or an empty vector control, together with GFP to visualize neuron morphology, poly-GA expressing neurons showed less and shorter dendrites than the control (Figure 17A).

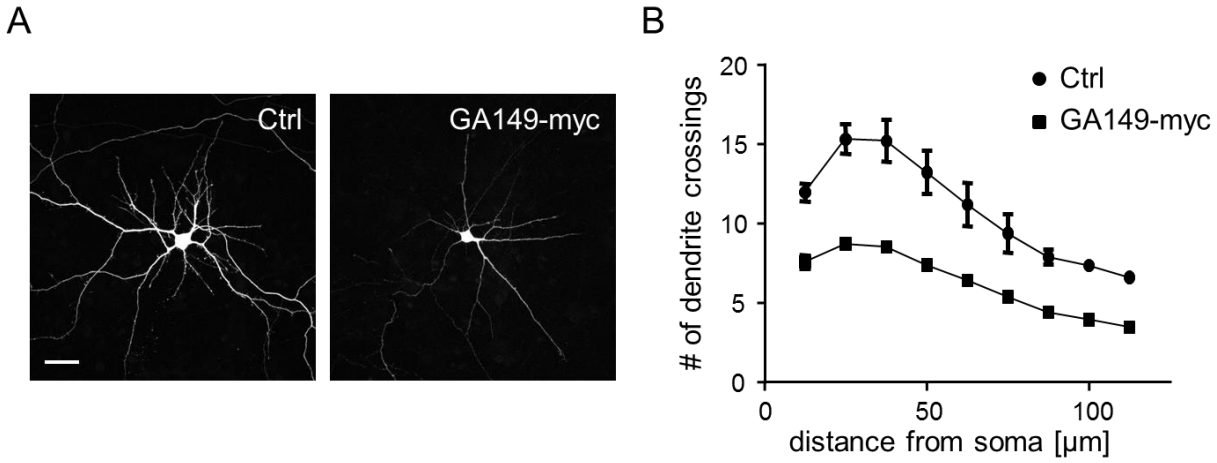

Figure 17: Poly-GA causes dendrite loss in primary neurons.
Cortical neurons were transfected with empty vector or GA_{149}-myc and GFP to visualize the morphology of the neurons (DIV 7+4). (A) Poly-GA neurons show reduced dendrite number and branching. Scale bar = 40 µm (B) Sholl analysis was performed to measure dendrite complexity by manually counting the number of dendrites crossing concentric circles around the cell body. Poly-GA expression leads to decreased dendrite complexity. N = 3 with 40 neurons counted in each experiment. Mean ± SEM, $p<0.001$ for 12.5 µm radius, $p<0.0001$ for 25 to 50 µm radius, $p<0.001$ for 62.5 µm radius, $p<0.01$ for 75 µm radius and $p<0.05$ from 87.5 to 112.5 µm radius (two-way ANOVA).

Sholl analysis revealed a dramatic loss of neuron complexity in poly-GA expressing neurons based on Two-way ANOVA (Figure 17B). These results raised the question, if poly-GA not only influences morphology but is in general toxic to neurons.

4.6.2. Poly-GA induces apoptosis in primary neurons

To comprehensively investigate, if poly-GA induces toxicity in primary rat neurons, I carried out four different toxicity assays, based on different cellular features. Whereas TUNEL and Caspase 3/7 activity assay both measure the induction of apoptosis, XTT and SRB assay are a general measure for cell density. TUNEL staining detects DNA double strand breaks, occurring in apoptotic cells. Compared to empty vector transduced control cells (DIV 6+17), primary rat hippocampal

neurons transduced with GA_{149}-myc show an increased number of apoptotic cells (Figure 18A).

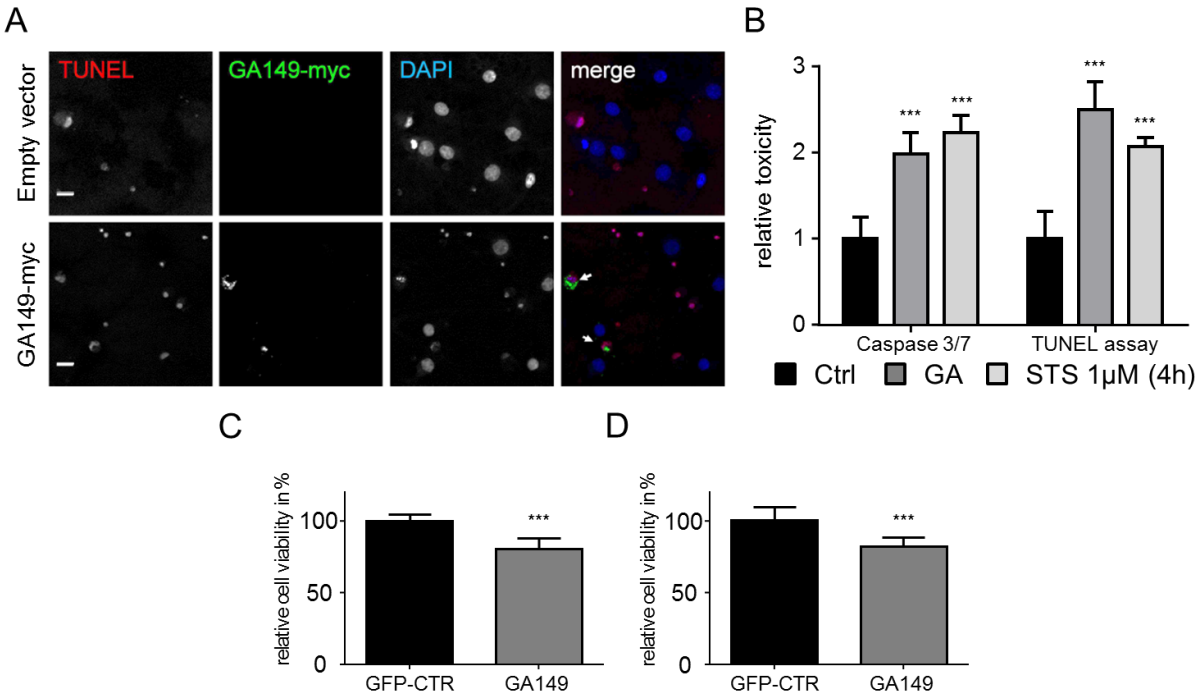

Figure 18: Poly-GA expression induces apoptosis in neurons.
Primary cortical neurons were infected with GA_{149}-myc or a control (DIV 6+17). (A) TUNEL assay reveals apoptotic DNA fragmentation. Co-staining for poly-GA and nuclei. GA_{149}-myc transduces neurons show ~2.5 fold increased apoptosis (arrow). (B) Apoptosis in transduced neurons was analyzed using a fluorogenic assay to detect caspase 3/7 activation and a TUNEL assay to detect apoptotic DNA fragmentation (DIV 6+17). Caspase 3/7 activity was increased 2.0-fold in GA_{149}-myc transduced cortical neurons. TUNEL-positive apoptotic cells (manually counted using the Fiji cell count plug-in) were increased by 2.5-fold in GA_{149}-myc transduced hippocampal neurons compared to control cells. n = 3 experiments with 6 replicates each; mean ± SD, Student's t-test ***p<0,001. (C) XTT assay provides additional evidence for toxicity of GA_{149}-myc. Cell viability is significantly decreased by 25 %. N=3 with 6 replicates each; mean ± SD, Student's t-test ***p<0,001. (D) SRB whole protein assay detects a 20 % reduced cell viability of poly-GA expressing cells compared to GFP control cells. N=3 with 6 replicates each; mean ± SD, Student's t-test ***p<0,001.

The quantification showed a 2.5-fold increase in apoptotic neurons, compared to control cells (Figure 18B). The additional Caspase-3/7 activity assay further confirmed this finding after lentivirus transduction of primary rat cortical neurons with either GA_{149}-myc or GFP control. Here, a 2-fold increase in Caspase 3/7 activity, two crucial enzymes in the apoptosis cascade, could be measured. As a further proof for poly-GA toxicity, I could detect a significant decrease in cell viability by an XTT assay. Upon infection of primary cortical rat neurons with

GA_{149}-myc or GFP control lentivirus (DIV 6+17), I measured a reduction in cell viability of 20 % in poly-GA expressing neurons, compared to control neurons (Figure 18C). Additionally, a SRB assay, performed with primary cortical neurons transduced with either GA_{149}-myc or GFP (DIV 6+17), confirmed this result as poly-GA expression decreased viability to 82 % (Figure 18C).
Thus, poly-GA expression induces apoptosis in primary rat neurons.

4.6.3. Toxicity of poly-GA expression in primary rat neurons is protein dependent

Following the discovery of the toxicity in neurons, I was interested in whether the occurring toxicity is indeed an effect of the poly-GA protein alone or if the RNA, although not the original GGGGCC repeat sequence, may contribute to toxicity. To this end, I used a construct, where the poly-GA start codon was replaced with a stop codon (TAG-GA_{149}) to abolish translation of poly-GA (Figure 8).
To demonstrate that the TAG-GA_{149} does not produce any poly-GA protein, I lentivirally transduced primary cortical neurons with TAG-GA_{149}, ATG-GA_{149} or GFP as a control.

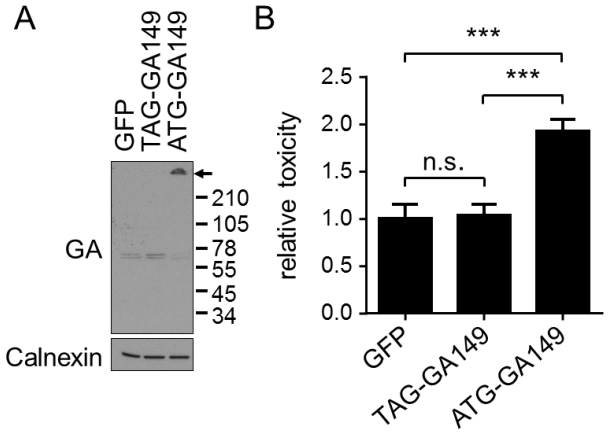

Figure 19: Poly-GA toxicity is protein dependent.
Primary cortical neurons transduced with ATG-GA_{149}-myc, TAG-GA149-myc or GFP as a control. (A) Immunoblots of cortical neurons transduced with GA_{149}-myc constructs with or without start codon (DIV 8+10). Replacing the ATG start codon in the synthetic GA_{149}-myc gene with a TAG stop codon prevents poly-GA expression and aggregation. *Arrow* indicates top of the gel. (B) LDH release assay detected neurotoxicity of GA_{149}-myc only in the presence of an ATG start codon in transduced cortical neurons (DIV 8+14). Mean ± SD; One-way ANOVA with Tukey's post-test. ***$p < 0.001$, $n = 3$ with six replicates in each experiment.

Immunoblotting with a poly-GA antibody detected only poly-GA aggregates in ATG-GA_{149} transduced neurons but not in TAG-GA_{149} or GFP control transduced neurons (Figure 19A), suggesting that the synthetic gene sequence does not support RAN translation. Thus, the TAG-GA_{149} construct can be used to discriminate if the toxicity in poly-GA expressing neurons is exclusively protein dependent. Toxicity in primary cortical rat neurons was assessed with an LDH assay 14 days after transduction. Whereas ATG-GA_{149} expressing neurons showed a 2-fold increase in LDH activity, confirming poly-GA toxicity, no change in LDH activity could be detected for the TAG-GA_{149} expressing neurons, compared to GFP control neurons (Figure 19B). These results demonstrate that, the toxicity observed in primary neuron culture is only dependent on the expression of the poly-GA protein and not the ATG-GA_{149} RNA.

4.7. Other DPR proteins in neurons

4.7.1. No DPR protein apart from poly-GA shows typical insoluble cytoplasmic inclusions

Since I could detect toxicity of poly-GA in neurons, the question arose, if the other four DPR proteins could also affect neuron viability and if their expression in neurons better resembles the patient situation, compared to the observations in the HEK293 cell system. Therefore, primary hippocampal neurons (DIV 8) were transduced with GA_{175}-GFP, GFP-GR_{149}, GP_{80}-V5, PA_{175}-GFP, PR_{175}-GFP or GFP control lentivirus. Immunostaining was performed after 5 days in culture. However, neither poly-GR nor poly-GP, poly-PA or poly-PR showed the patient typical cytoplasmic inclusions, which were seen for poly-GA. As in HEK293 cells poly-GP and poly-PA are distributed diffusely throughout the cytosol and some dendrites and poly-PR shows mainly nuclear inclusions (Figure 20).

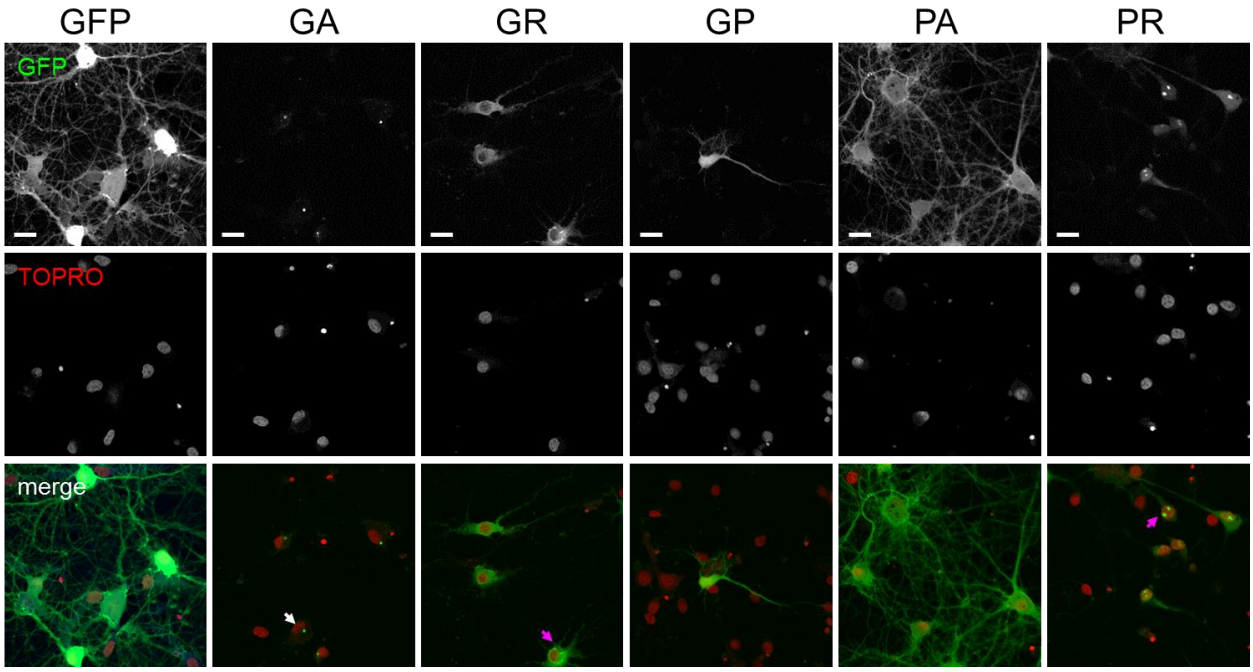

Figure 20: DPR proteins aggregate differently in primary neurons.
Primary hippocampal neurons were infected with GA_{175}-GFP, GFP-GR_{149}, GP_{80}-V5, PR_{175}-GFP, PA_{175}-GFP as well as a GFP as a control. 5 days after transduction cells were analyzed by GFP fluorescence or V5 antibody in the case of GP_{80}. TOPRO was used as a nuclear marker. Only GA_{175}-GFP transfected cells show cytosolic aggregates. GFP-GR_{149} mainly shows a cytosolic halo around the nucleus and some nuclear aggregates. No aggregation could be detected for GP_{80}-V5. PR_{175}-GFP mainly showed nuclear aggregates, whereas no aggregation could be detected for PA_{175}-myc. *White arrows* indicate cytosolic aggregates and *magenta arrows* nuclear aggregates. Scale bar 15 µm.

Poly-GR, however, rather forms a halo around the nucleus and very few cells show intranuclear aggregates (Figure 20).

Moreover, immunoblotting of primary cortical neurons infected with GA_{175}-GFP, GFP-GR_{149}, GP_{80}-V5, PA_{175}-GFP, PR_{175}-GFP or GFP control lentivirus (DIV 8+5) reveals similar results compared to the HEK293 cell system. Whereas poly-GA, poly-GR and poly-PR are detected at the top of the gel, poly-PA runs higher than its expected height, suggesting higher molecular weight species. In contrast to HEK293 results, poly-GP runs higher than its expected height of 20 kDa (Figure 21A).

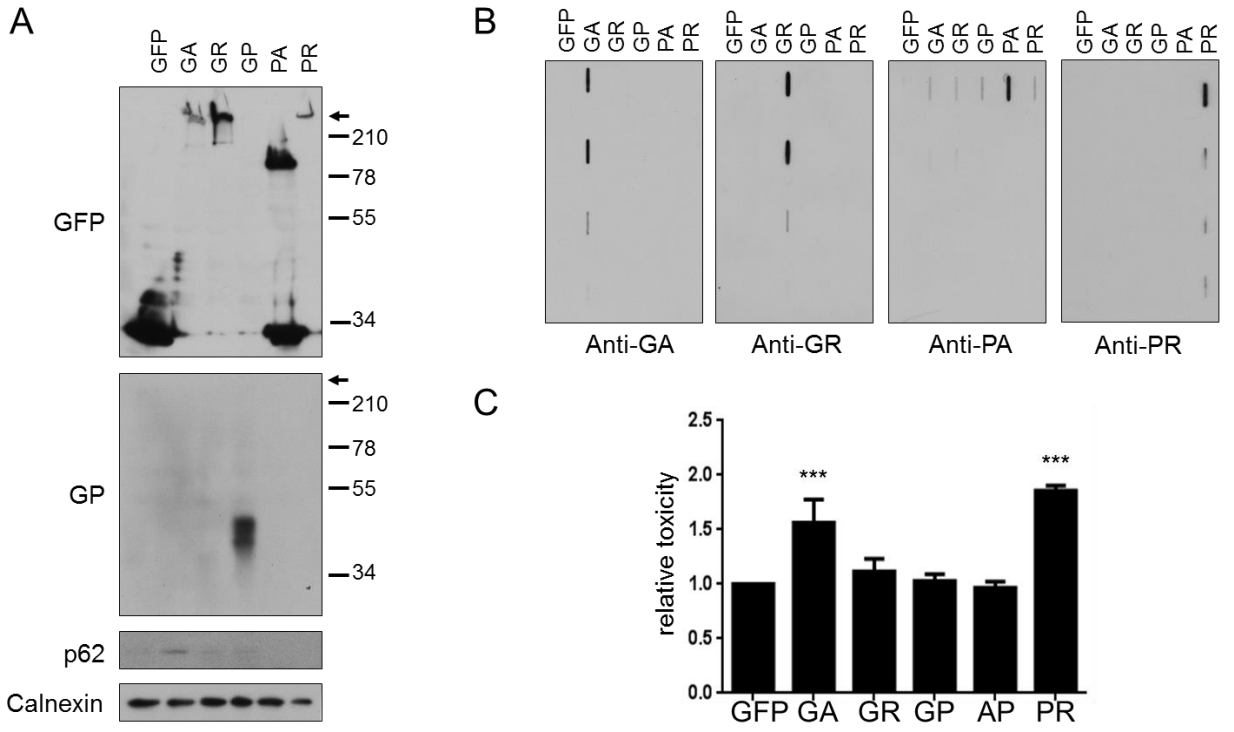

Figure 21: DPR proteins show differential biochemical properties and toxicity in primary neurons.
Primary cortical neurons were transduced with with GA_{175}-GFP, GFP-GR_{149}, GP_{80}-V5, PA_{175}-GFP, PR_{175}-GFP or GFP as a control. After 5 days, cells were harvested for analysis. (A) Immunoblotting with indicated antibodies shows expression of DPR proteins and GFP control. GA_{175}-GFP, GFP-GR_{149}, PA_{175}-GFP and PR_{175}-GFP are detected at the top of the gel (arrow), whereas GP_{80}-V5 runs higher than the expected height of 20 kDa. P62 levels are only elevated in GA_{175}-GFP transfected cells. (B) Filter trap assay for insoluble proteins. GA_{175}-GFP, GFP-GR_{149}, PA-GFP and PR_{175}-GFP form insoluble aggregates. Immunoblotting was carried out with respective antibodies. Immunoblotting with anti-V5 for poly-GP showed no insoluble aggregates (Data not shown). (C) LDH release assay in primary cortical neurons (DIV 8+14) detects 1.6-fold increase in toxicity in poly-GA expressing cells and 2-fold increase in poly-PR expressing cells. All other DPR proteins did not show toxicity. Mean ± SD, one-way ANOVA with Tukey's posttest. N=3 with 6 replicates each, ***p<0,001.

To further elucidate the solubility of the different DPR proteins, a filter trap assay was performed. Thus, primary cortical neurons (DIV 8) were transduced with the above mentioned lentiviruses and the filter trap assay was conducted 10 days after transduction. As can be seen in Figure 21B, poly-GA, poly-GR, Poly-PR and poly-AP could be detected in the filter. Poly-GP could not be detected (data not shown), leading to the conclusion that it does not form 2 % SDS resistant aggregates.

4.7.2. Poly-PR is toxic to neurons

To analyze, whether the remaining four DPR proteins might also contribute to neurotoxicity, I transduced primary cortical neurons on DIV 6 with GA_{175}-GFP, GFP-GR_{149}, GP_{80}-V5, PA-$_{175}$-GFP, PR_{175}-GFP or GFP alone as a control. An LDH assay was performed 14 days after transduction. Apart from poly-GA expressing neurons, showing an increase in toxicity of 1.6 fold, only poly-PR resulted in a significant increase of 2-fold (Figure 21C). For the other DPR proteins poly-GR, poly-GP and poly-PA no significant effect could be detected compared to GFP expressing cells (Figure 21C).
Although the majority of the other DPR species form insoluble aggregates and poly-PR even confers toxicity to the neurons, the detected inclusions do not resemble the inclusions seen in patients.

Thus, the poly-GA model is the most comparable to the patient situation and was focus for my further experiments.

4.8. Identification of the poly-GA interactome

4.8.1. Proteasome components are enriched in the poly-GA interactome

To assess the mechanisms of toxicity of this unusual protein, I wanted to analyze whether important neuronal proteins are sequestered in the aggregates. A first approach to understand how poly-GA is causing neurotoxicity was to identify poly-GA interacting proteins that could contribute to a better understanding of the underlying mechanism. In this approach, I collaborated with Daniel Hornburg and Felix Meissner from the Lab of Matthias Mann at the MPI for Neurobiology in Martinsried. We set up a label-free quantitative proteomics approach using a LC-MS/MS based experiment with immunoprecipitation of the GFP tagged poly-GA from primary cortical neuron culture, transduced with either GA_{149}-GFP or GFP alone (DIV 6+17) and identified proteins attached to the poly-GA aggregates. Immunoblotting of 1 % input and the final Immunoprecipitation sample showed that

poly-GA could be enriched in the IP sample (Figure 22A) used for LC-MS/MS analysis.

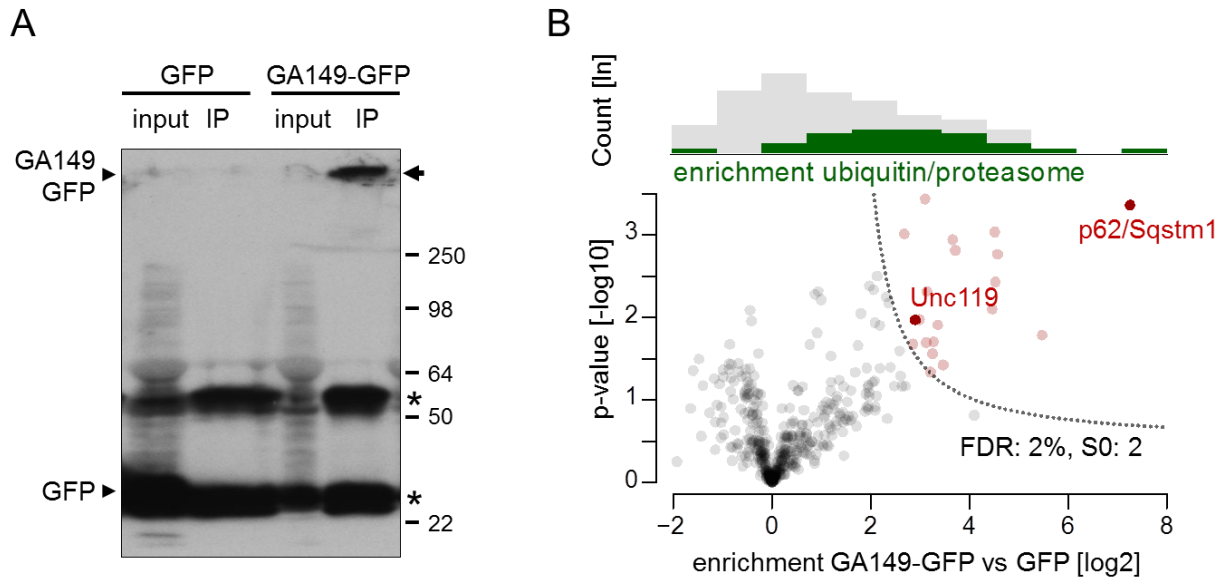

Figure 22: The poly-GA interactome is enriched for the ubiquitin-proteasome system and Unc119.
Primary cortical neurons (DIV 6+17) transduced with either GFP or GA_{149}-GFP lentivirus and subjected to anti-GFP immunoprecipitation. Samples were used for quantitative mass spectrometry analysis (A) Immunoblotting with anti-GFP confirms immunoprecipitation of GFP and GA_{149}-GFP (arrowheads). Asterisks indicate immunoglobulin heavy and light chain. Arrow indicates top of gel. (B) Quantitative proteomics of GFP immunoprecipitations. p62/Sqstm1 shows highest enrichment and statistical significance. Unc119 was identified by two unique peptides (GGGGTGPGAEPVPGASNR and LGPLQGK) and one peptide (YQFTPAFLR) shared with its homolog Unc119b. Full protein names are listed in Table 1. *Upper panel* illustrates distribution of quantified protein abundances binned for enrichment factors (*x*-axis below). Enrichment of ubiquitin-related and proteasomal proteins in the poly-GA interactome is highlighted in green. *Lower panel* depicts volcano plot showing poly-GA interacting proteins. False discovery rate (FDR) controlled statistical analysis identified 20 poly-GA interacting proteins compared to control (*red dots*). *Dotted line* depicts threshold for statistical significance.

We could quantify the relative protein abundances of 450 proteins in the GA_{149}-GFP and the GFP samples, 20 proteins were significantly enriched in IPs from poly-GA expressing neurons (Figure 22B and Table 1). Strikingly, p62 showed the highest enrichment and thus confirmed the validity of affinity purification and the neuron culture system (Figure 15 and Figure 16). Furthermore, proteasomal subunits (e.g. PSMB6) and ubiquitin-related proteins (e.g. Ubiquilin 1 and 2) were 5.7-fold enriched in the IPs of the poly-GA expressing cells ($p = 8.7 \times 10^{-11}$) (Figure 22B and Table 1), suggesting that poly-GA might interfere with proteasome activity and consequently causes toxicity.

Table 1: Proteins interacting with poly-GA identified by mass spectrometry.
Enrichement of proteins in GA_{149}-GFP immunoprecipitates compared to GFP control measured by LC-MS/MS. NCBI gene names, Uniprot identifier, logarithmic p-value and enrichment are listed. Statistical analysis was performed using a t-test with a false discovery rate of 2 % and S0 of 2 (Tusher et al., 2001).

Gene names	Protein IDs	$-\log_{10}(p)$	$\log_2(GA/ctrl)$	Protein names
Sqstm1	O08623-2; O08623; O08623-3	3.37	7.25	p62/Sequestosome-1
Rad23a; Rad23b	Q4KMA2; Q5XFX7	1.79	5.47	UV excision repair protein RAD23 homolog A and B
Ubqln2; Ubqln4	D4AA63; D4A3P1	2.77	4.57	Ubiquilin 2; Ubiquilin 4
Sdcbp	Q9JI92	2.43	4.52	Syntenin-1
Ubb; Ubc; Uba52; Rps27a; LOC100360645	G3V9Z2; P0CG51; Q63429; F1LML2; Q6P7R7; P62986; Q6PED0; P62982; F1M516	3.04	4.51	Polyubiquitin-B; Ubiquitin; Polyubiquitin-C; Ubiquitin; Ubiquitin-related; Ubiquitin-60S ribosomal protein L40; Ubiquitin; 60S ribosomal protein L40; Ubiquitin-40S ribosomal protein S27a; Ubiquitin; 40S ribosomal protein S27a
Klhdc10	Q5U3Y0; *D3ZUK9*	2.10	4.46	Kelch domain-containing protein 10
Bag6	Q6MG49; Q6MG49-2	2.81	3.71	Large proline-rich protein BAG6
Psmb6	P28073	2.95	3.65	Proteasome subunit beta type-6
Ubqln1	*F1M971*; Q9JJP9	1.42	3.47	Ubiquilin 1
Dbn1	Q07266; Q07266-2; C6L8E0	1.91	3.36	Drebrin
Myh10; Myh14	Q9JLT0; G3V9Y1; F1LNF0	1.70	3.28	Myosin-10; Myosin-14
Efhd1; Efhd2	Q4FZY0; D4A9T5	1.56	3.25	EF-hand domain-containing protein D1; EF-hand domain-containing protein D1
Acat2	Q5XI22; F1LS48	1.34	3.21	Acetyl-CoA acetyltransferase, cytosolic
Mlf2	D3ZPN3	2.32	3.13	Myeloid leukemia factor 2
Psmc6	G3V6W6	1.70	3.12	Proteasome (prosome, macropain) 26S subunit, ATPase, 6
Psmb4	*D4A640*; P34067; G3V8U9	3.44	3.10	Proteasome subunit beta type-4
Psmb5	G3V7Q6; P28075	1.97	2.98	proteasome (prosome, macropain) subunit, beta type, 5
Unc119; Unc119b	Q62885; *F1LZN2*; D3ZY58	1.97	2.90	Protein unc-119 homolog A and B
Myo5b; Myo5c	F1M111; F1M3R4; P70569	1.68	2.85	Myosin VB/C
Psmd13	B0BN93	3.01	2.68	26S proteasome non-ATPase regulatory subunit 13

Trypsin-like, Chymotrypsin-like and Caspase-like proteasome activity, however, was not affected in poly-GA expressing HEK293 cells, whereas proteasome inhibitor epoxomycin (8 µM, 2 h) abolished proteasome activity (Figure 23A).

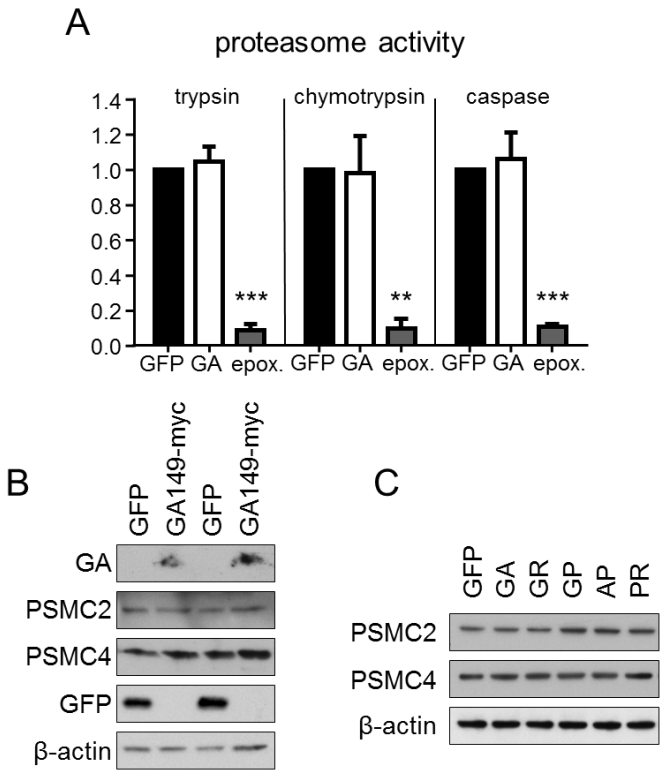

Figure 23: Proteasome activity is unaffected by poly-GA expression in HEK293 cells.
(A) Expression of poly-GA did not affect chymotrypsin-like, trypsin-like and caspase-like protease activity of the proteasome in HEK293 cells compared to GFP control (n=3 experiments with 6 replicates each, mean ± SD, no significant change in one-way ANOVA). The proteasome inhibitor epoxomycine (8 µM, 2 h) significantly blocks proteasome activity in GFP transfected cells (one-way ANOVA with Tukey's post-test, *** $p<0.001$; ** $p<0.01$). (B) Expression of proteasomal subunits (PSMC2, PSMC4) was not affected by expression of DPRs in HEK293 cells (GA_{175}-GFP, GFP-GR_{149}, GP_{80}-V5, PA_{175}-myc and PR_{175}-GFP). (C) Expression of proteasomal subunits (PSMC2; PSMC4) was unchanged in GA_{149}-myc transduced cortical neurons compared to GFP transduced controls. Three separate transductions are shown (DIV 6+17).

Additionally, poly-GA expression did not affect protein levels of the proteasomal subunits PSMC2 and PSMC4 both in HEK293 cells, upon three days of transfection with GA_{175}-GFP, (Figure 23B) and primary cortical neurons after transduction of GA_{175}-GFP lentivirus (DIV 6+17) (Figure 23C). Concluding that changes in the proteasome are presumably not responsible for the poly-GA toxicity seen in neurons.

4.8.2. Poly-GA co-aggregates with the cargo adapter Unc119

Since the proteasome was unaffected in primary neurons, I focused on proteins apart from the proteasome that were significantly enriched in poly-GA expressing neurons. Interestingly, Uncoordinated 119 (Unc119), a cargo adapter of myristoylated proteins (Constantine et al., 2012), was 7.5-fold enriched in poly-GA expressing neurons, compared to control conditions (Figure 22B and Table 1). Unc119 has previously been found in a *C. elegans* screen to impair locomotion and is required for axon development and maintenance in the worm (Knobel et al., 2001; Maduro and Pilgrim, 1995; Maduro et al., 2000), thus being a promising target in the context of ALS and FTD. Furthermore, Unc119 was found to bind to the myristoylated GAGASA motif of Transducin α (GNAT1), which strongly resembles the poly-GA sequence (Zhang et al., 2011).

To validate co-aggregation of Unc119 in cell culture, HEK293 cells were transfected with a HA-Unc119 construct and GA_{175}-GFP for three days. Immunostaining for the HA-tag was performed and immunofluorescence was analyzed revealing profound co-aggregation of poly-GA and Unc119. Additionally, Unc119 partially loses its cytosolic location and is sequestered into poly-GA aggregates (Figure 24). GFP transfected as a control had no effect on Unc119 localization (Figure 24).

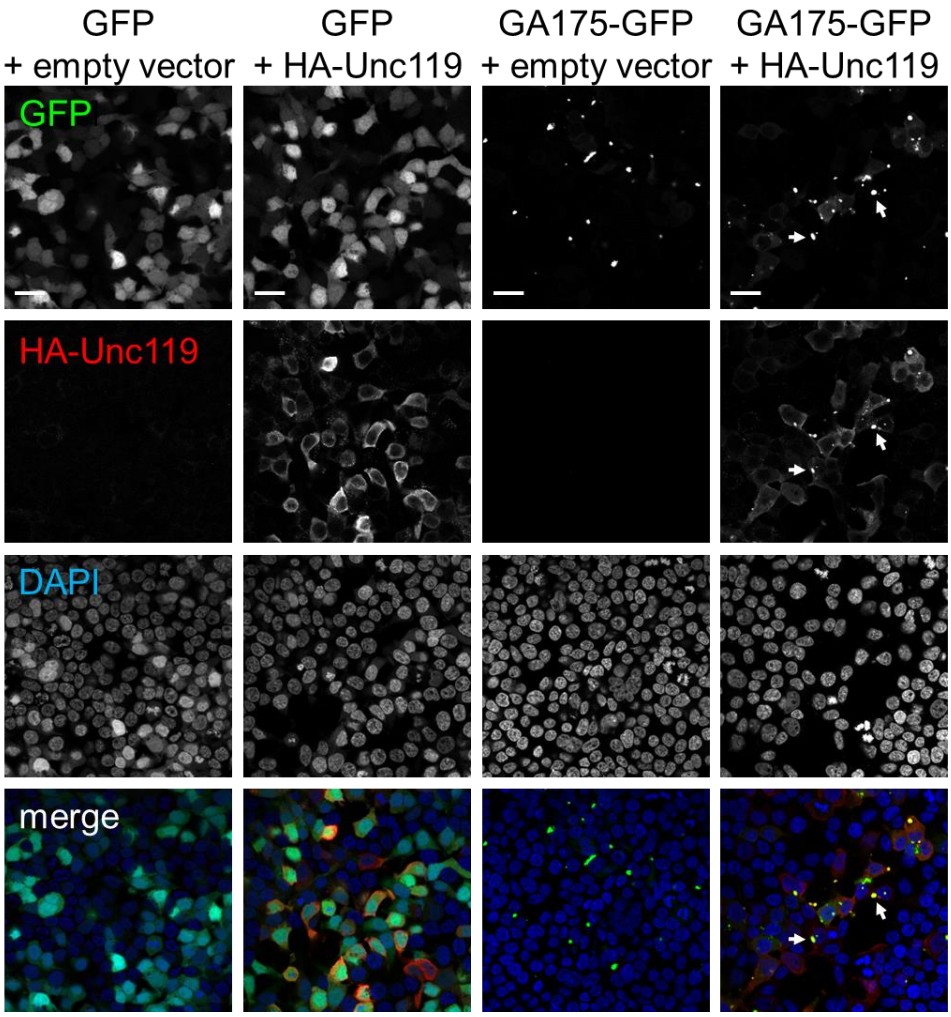

Figure 24: Unc119 co-aggregates with poly-GA in HEK293 cells.
Immunofluorescence of HEK293 cells co-transfected with GFP or GA_{175}-GFP and HA-Unc119 or empty vector. GFP fluorescence, anti-HA immunostaining and DAPI as nuclear marker. Compare the HA-Unc119 localization in column 2 and 4. Many GA_{175}-GFP inclusions show co-aggregation of HA-Unc119 (examples marked with arrows). Scale bar 30 µm.

To further validate Unc119 binding to poly-GA, I performed a co-immunoprecipitation with two different poly-GA constructs, GA_{175}-GFP and GA_{149}-myc, to exclude effects based on the respective tag, and HA-Unc119. HEK293 cells were transfected with the poly-GA constructs or a GFP or myc control and HA-Unc119 for three days. The immunoprecipitation was either performed with a GFP or a myc antibody. In both experiments Unc119 could be detected in the poly-GA IP but not in control conditions, concluding that Unc119 indeed binds to poly-GA (Figure 25).

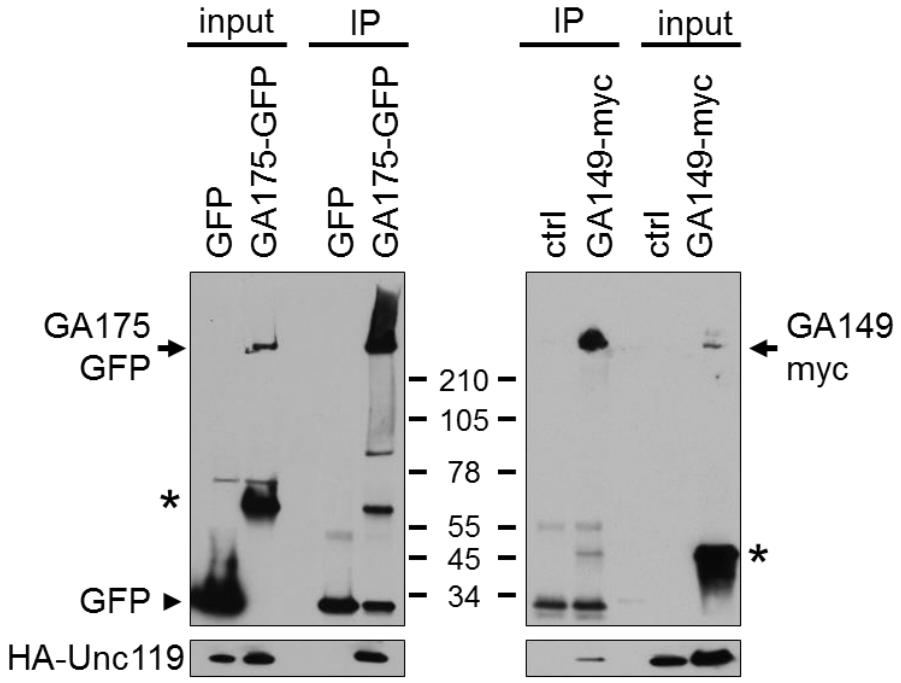

Figure 25: Unc119 directly binds to poly-GA.
Co-immunoprecipitation of Unc119 and poly-GA. HEK293 cells co-transfected with HA-Unc119 and GA_{175}-GFP or GA_{149}-myc for three days. The poly-GA proteins were immunoprecipitated with GFP or myc antibodies. Note that in freshly prepared protein extracts monomeric poly-GA can be resolved when directly loaded (asterisks). Aggregated poly-GA is stuck at the top of the gel (arrow).

4.8.3. Further poly-GA interactors could be confirmed in HEK293 cells

To additionally validate more candidates of the mass spectrometry interactome list, apart from Unc119, the Microtubule-associated Protein RP/EB Family Member 2 (Mapre2) and C-terminal Binding Protein 1 (Ctbp1) were analyzed for co-aggregation in the HEK293 cell expression system via immunostaining. Interestingly, Mapre2 and Ctbp1, although not co-aggregating with poly-GA had an effect on the amount of poly-GA aggregates (Figure 26). Mapre2 expression increased poly-GA aggregate number, whereas expression of Ctbp1 decreased poly-GA aggregate number in HEK293 cells after three days transfection (Figure 26). However, both proteins have no reported link to neurodegeneration so far.

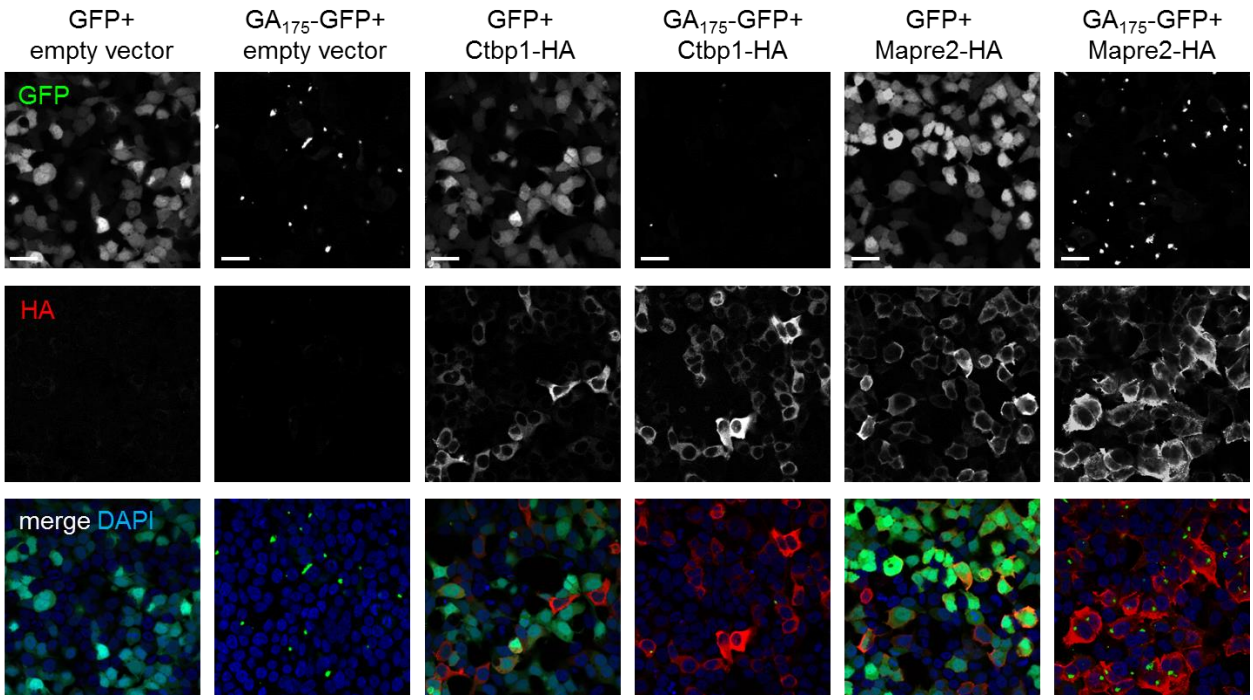

Figure 26: Mapre2 and Ctbp1 influence poly-GA aggregation in HEK293 cells.
HEK293 cells were transfected with GA_{175}-GFP or GFP as a control as well as Ctbp1-HA, Mapre2-HA or an empty vector as control. GFP immunofluorescence and HA antibody immunostaining was analyzed three days after transfection. DAPI was used as a nuclear marker. Although neither Ctbp1 nor Mapre2 co-aggregate with poly-GA they influence poly-GA expression. Ctbp1 decreases the amount of aggregates compared to GFP control whereas Mapre2 increases aggregate number. Scale bar depicts 30 µm.

After these promising results, I validated further candidates of the target list. Ribosomal Protein S5 (Rps5), Fatty Acid Binding Protein 5 (Fabp5), Ribosomal Protein L31 (RPL31), Bcl-2 Associated Athanogene 6 (Bag6), Ependymrelated Protein 1 (Epdr1), Hydroxysteroid-17-beta-dehydrogenase 4 (Hsd17b4) and Transmembraneprotein 160 (Tmem160) were analyzed regarding co-aggregation with poly-GA. Immunofluorescence analysis of these proteins via their HA-tag revealed no co-aggregation or change in localization upon poly-GA co-expression in HEK293 cells for Rps5, Fabp5 or L31 (Figure 27A). However, Bag6, Epdr1, Hsd17b4 and TMEM160 showed profound co-localization with poly-GA aggregates and thus, validate the proteomic poly-GA interactome analysis (Figure 27B).

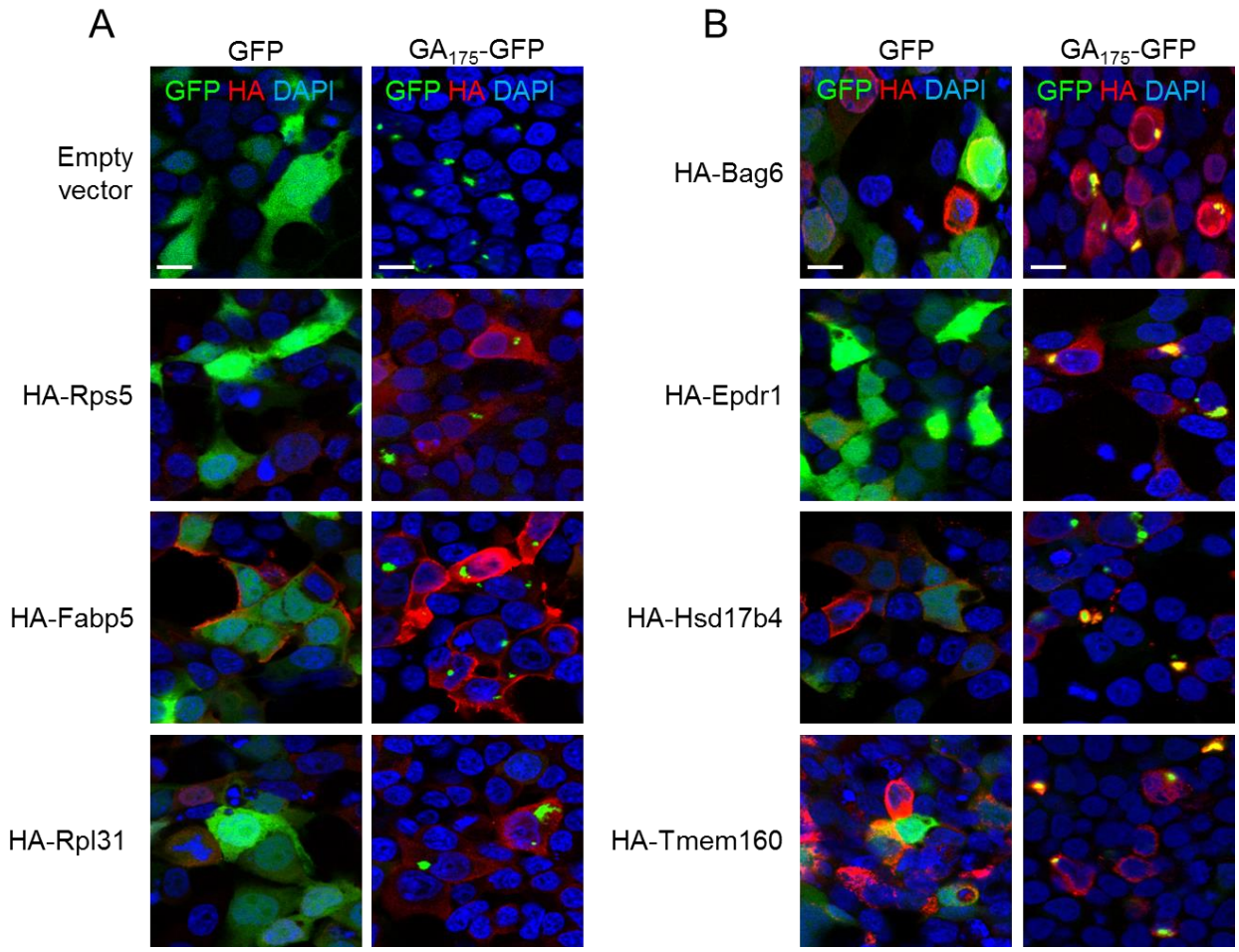

Figure 27: Bag6, Epdr1, Hsd17b4 and Tmem160 co-aggregate with poly-GA in HEK293 cells.
HEK293 cells were transfected with GA_{175}-GFP or GFP as well as the above mentioned GA interactors identified in the mass-spectrometry screen. After three days of transfection, GFP immnuofluorescence was analyzed as well as HA antibody staining. Bag6, Epdr1, Hsd17b4 and Tmem160 show profound co-aggregation with poly-GA, whereas the other potential targets do not. Scale bar 15 µm.

To confirm specific binding of Bag6, Epdr1, Hsd17b4 and TMEM160, I performed a co-immunoprecipitation of GA_{175}-GFP with the aforementioned potential interactors. As can be seen in Figure 28, I was able to confirm the binding of Hsd17b4 and Bag6 to poly-GA. In contrast, no binding was observed for TMEM160 and Epdr1. This might either suggest no binding to poly-GA at all or a technical problem due to low expression of the proteins, since they were also not detectable in the input (Figure 28). Hsd17b4 and Bag6 are interesting candidates to follow up on and to investigate, if and how they contribute to neurotoxicity. Hsd17b4 is involved in the peroxisomal fatty acid beta-oxidation. Notably, mutations in

Hsd17b4 have been linked to the Perrault syndrome, an autosomal recessive disease leading to sensorineural hearing loss with an early childhood onset and in some females developmental delay or intellectual disability, cerebellar ataxia, and motor and sensory peripheral neuropathy (Möller et al., 1999). Bag6 is an anti-apoptotic protein that has been linked to autophagy and various other cellular processes (Sebti et al., 2014). It may also play a role in autoimmunity though a connection to neurodegeneration has not yet been made (Binici and Koch, 2014).

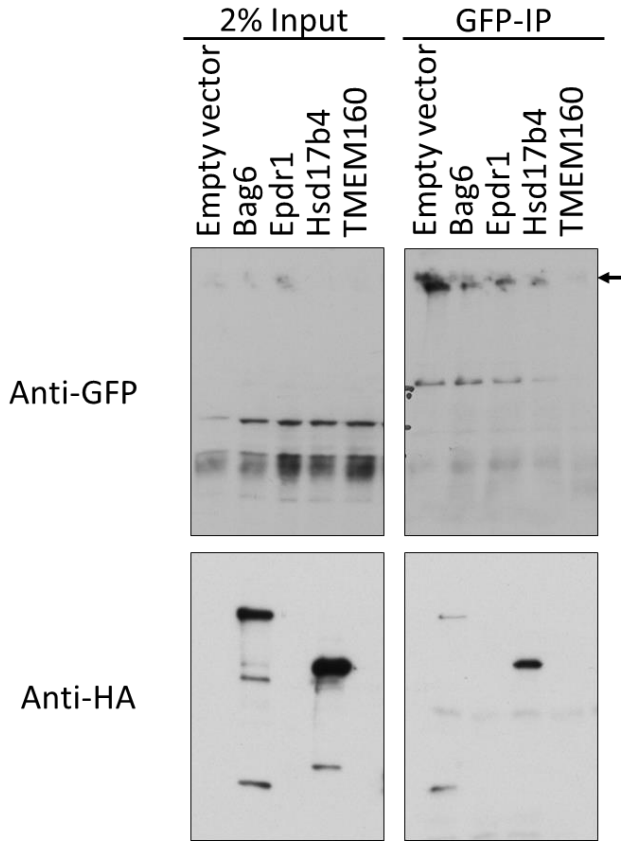

Figure 28: Bag6 and Hsd17b4 bind poly-GA.
Coimmunoprecipitation of novel poly-GA interactors and poly-GA. HEK293 cells cotransfected with HA-Bag6, HA-Epdr1, HA-Hsd17b4, HA-Tmem160 as well as GA_{175}-GFP for three days. The poly-GA proteins were immunoprecipitated with GFP. Aggregated poly-GA is stuck at the top of the gel (arrow).

In summary, I could validate co-aggregation of Bag6, Hsd17b4, Epdr1, and Tmem160, found in the mass spectrometry interactome analysis of poly-GA. Furthermore, I identified Bag6, Hsd17b4, Mapre2 and Ctbp1 as additional targets apart from Unc119 that might play a role in the mechanisms of poly-GA toxicity.

4.9. Unc119 co-aggregates with poly-GA in rat neurons and the co-aggregation is poly-GA specific

Due to the initial results in HEK293 cells, I investigated, if Unc119 also co-aggregates with poly-GA in neurons. Therefore, I transduced primary rat cortical neurons (DIV 6+15) with GA_{149}-GFP or GFP as a control and HA-Unc119. Immunostaining with HA antibody showed co-localization of poly-GA aggregates with Unc119 (Figure 29).

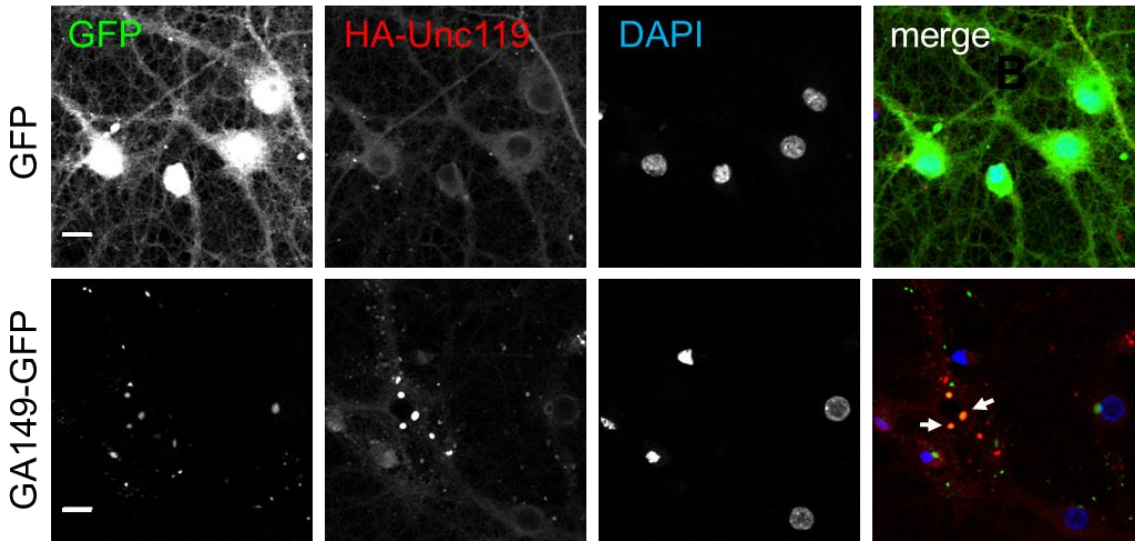

Figure 29: Unc119 co-aggregates with poly-GA in primary neurons.
Immunofluorescence of primary hippocampal neurons co-transduced with HA-Unc119 and either GFP or GA_{149}-GFP (DIV 6+17). *Arrows* indicate examples of poly-GA inclusions showing co-aggregation of HA-Unc119. *Scale bar* 15 µm.

To clarify, if this interaction was poly-GA specific or rather an unspecific aggregate dependent effect, I transfected HEK293 cells with HA-Unc119 combined with GA_{175}-GFP, GFP-GR_{149}, GP_{80}-V5, PA_{175}-myc, PR_{175}-GFP or Q_{102}-GFP as an unrelated aggregate control. As seen in Figure 30, only poly-GA co-aggregates with Unc119 but none of the other DPR species or polyQ, suggesting that the interaction of Unc119 and poly-GA is specific.

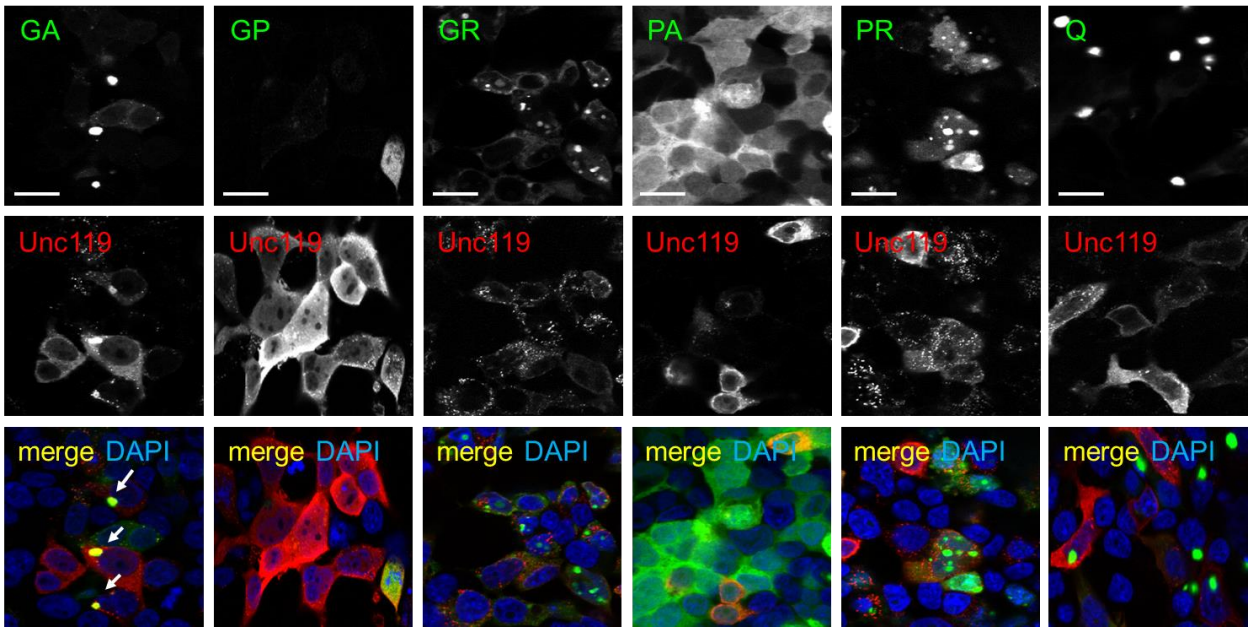

Figure 30: Unc119 specifically co-aggregates with poly-GA.
HEK293 cells were transfected with the five different poly-DPR constructs (GA_{175}-GFP, GFP-GR_{149}, PR_{175}-GFP, PA_{175}-myc and GP_{80}-V5) or Q_{102}-GFP and analyzed using GFP fluorescence and immunostaining of HA-Unc119, PA_{175}-myc and GP_{80}-V5 using specific antibodies 2 days later. HA-Unc119 co-aggregates only with GA_{175}-GFP (*white arrows*). DAPI (*in blue*) was used as a nuclear marker. *Scale bar* 20 µm.

4.10. Unc119 knockdown and antibody validation

Understanding the underlying mechanisms of how poly-GA causes neurotoxicity will help to identify potential therapeutic strategies. Therefore, it is of utmost importance to clarify if and how Unc119 may contribute to poly-GA based neurotoxicity. In this regard, a shRNA based knockdown system specific for Unc119 was established. To test whether the designed shRNA is functional, primary cortical neurons (DIV 8+10) were lentivirally transduced to express either shUnc or a control shRNA. In cortical neurons, shUnc specifically downregulates Unc119 mRNA levels to 7 %, compared to the control shRNA (Figure 31A), hence proving the efficient knockdown.

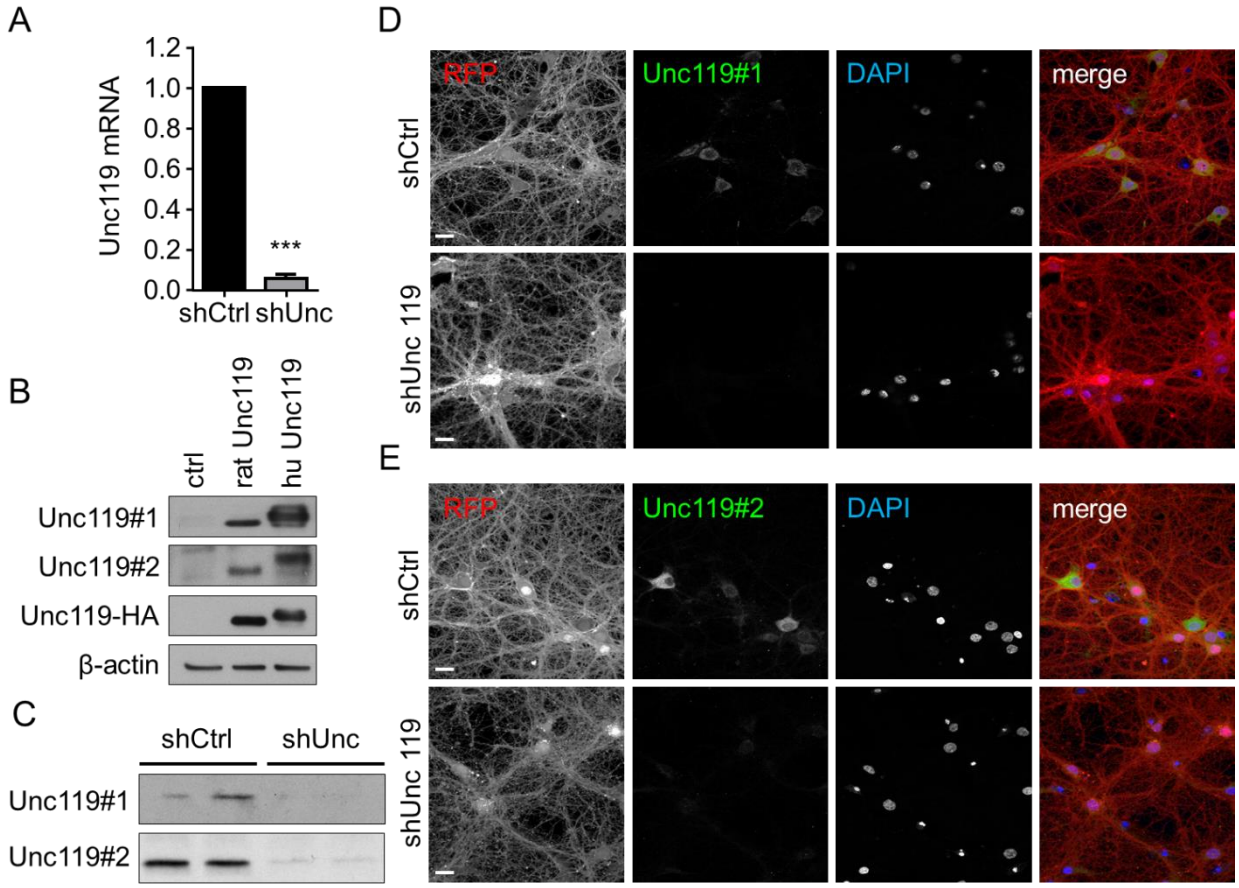

Figure 31: Unc119 antibodies #1 and #2 are specific for human and rat Unc119.
(A) Primary cortical neurons were transduced with an shRNA targeting Unc119 and a control shRNA. RT-qPCR shows efficient reduction of Unc119 mRNA normalized to the reference gene GAPDH. mean ± SEM. N=3. $p<0.001$ in Student's t-test (B) Unc119 antibodies #1 and #2 detect rat and human HA-Unc119 overexpressed in HEK293 cells. Note that HEK293 cells show very little endogenous Unc119. (C-E) Primary cortical neurons were transduced with a shRNA targeting Unc119 or a control shRNA (DIV 7+10). (C) Two Unc119 antibodies (#1 and #2) show reduced Unc119 protein levels upon Unc119 shRNA transduction compared to controls in immunoblots. Two separate transductions are loaded. (D, E) Both antibodies detect reduced Unc119 protein levels by immunostaining. tagRFP co-expressed from the shRNA lentivirus shows high transduction efficiency. Scale bars represent 20 µm.

To analyze the endogenous Unc119 levels, two antibodies were tested; one self-made (Unc119#1) and one commercial one (Unc119#2). HEK293 cells were transfected with HA-ratUnc119, HA-hUnc119 or an empty vector as a control. Both antibodies were able to specifically detect overexpressed human as well as rat Unc119 in western blot analysis (Figure 31B).

Next, the antibodies were tested on endogenous levels of rat Unc119. Therefore, primary cortical neurons (DIV 7+10) were transduced with shUnc and shCtrl. Both antibodies detect Unc119 in cells expressing shCtrl (Figure 31C). As expected, the

Unc119 signal cannot be detected anymore upon shUnc expression, further confirming the knockdown quality and validating the antibodies in immunoblotting (Figure 31C). Following, the antibodies were also validated in immunofluorescence by infecting primary cortical neurons (DIV 7+10) with shUnc and shCtrl as control shRNA. Immunostainings were performed for both antibodies (Figure 31D+E). Unc119#1, as well as Unc119#2, specifically detect Unc119 that is localized in the cytosol of the primary neurons (Figure 31D+E). Thus, both antibodies can be used for further studies to elucidate the role of Unc119 in poly-GA induced neuronal toxicity and the relevance for FTD and ALS.

4.11. Unc119 sequestration contributes to poly-GA toxicity in primary neurons

To assess the effect of poly-GA on Unc119 in neuron culture I transduced cortical neurons at day 6 in culture with GA_{175}-GFP or GFP as a control. Although Unc119 has been found 7.5 fold enriched in the poly-GA interactome, Unc119 was undetectable at the expected size (27 kDa) by immunoblot (Figure 32A).

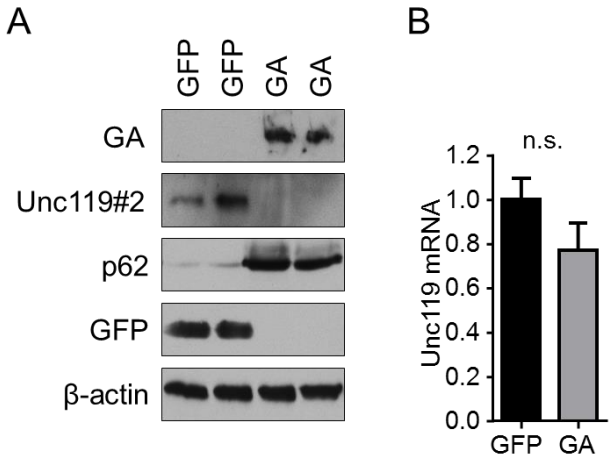

Figure 32: Unc119 is sequestered in poly-GA aggregates in neurons.
(A) Immunoblot with the indicated antibodies in GFP or GA_{149}-myc transduced cortical neurons shows decreased levels of soluble Unc119 running at 27 kDa. Two separate transductions are shown (DIV 6+17). (B) qPCR analysis of neurons transduced as in (A) shows no significant changes in Unc119 mRNA levels (mean ± SD, Student's *t* test, DIV 7+10)

However, the mRNA levels of Unc119 are unaffected (Figure 32B), indicating that Unc119 is translated normally but is then sequestered into insoluble poly-GA aggregates, thus preventing western blot detection. This suggests a loss of function mechanism. To elucidate whether Unc119 loss of function contributes to poly-GA toxicity, I first compared phenotypes of poly-GA expression and Unc119 knockdown. Thus, I analyzed dendrite morphology as I could previously show that GA expression diminishes dendrite outgrowth. For this purpose, primary hippocampal neurons were transfected with shUnc or shCtrl as a control and GFP to visualize morphology. Unc119 knockdown leads to a loss in dendrite complexity similar to the defect seen in poly-GA expressing cells (Figure 33A+B).

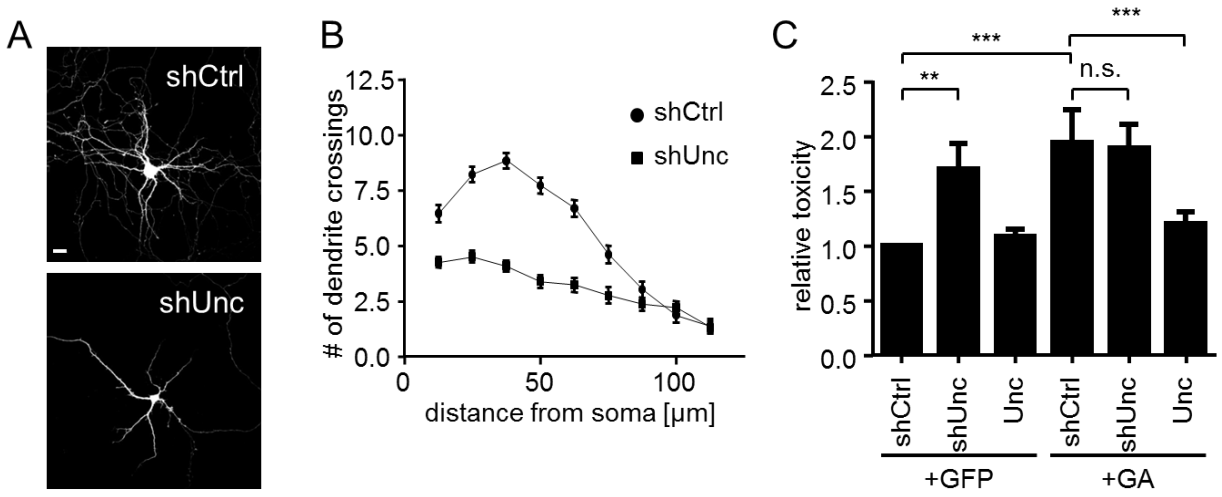

Figure 33: Unc119 loss of function contributes to poly-GA toxicity.
(A, B) Hippocampal neurons transfected with shRNA targeting Unc119 (shUnc) or a non-targeting control (shCtrl) together with GFP to outline cell morphology (DIV 7+5). Dendritic branching was quantified by Sholl analysis. Unc119 knockdown reduced dendrite complexity significantly ($p < 0.0001$ for 12.5–62.5 µm radius and $p < 0.001$ for 75 µm radius, two-way ANOVA, $n = 40$ neurons per condition). *Scale bar* depicts 40 µm. (C) LDH release assay from cortical neurons co-transduced with either GFP or GA_{149}-GFP (GA) together with HA-Unc119 (Unc), shRNA targeting Unc119 (shUnc) or non-targeting shRNA (shCtrl) (DIV 6+17). Note that Unc119 knockdown causes toxicity in GFP-transduced neurons, but does not increase poly-GA toxicity further. HA-Unc119 expression rescues GA_{149}-GFP toxicity. One-way ANOVA with Tukey's post-test. $^{**}p < 0.01$, $^{***}p < 0.001$, $n = 3$ with six replicates in each experiment

Moreover, lentiviral knockdown of Unc119 in cortical neurons induced toxicity in an LDH-release assay 1.8-fold compared to the control shCtrl (Figure 33C). Overexpression of Unc119 alone showed no effect on cell viability. In contrast, the overexpression of Unc119 in GA_{149}-myc expressing neurons could rescue the toxic

phenotype suggesting that Unc119 loss of function indeed contributes to the poly-GA toxicity in neurons (Figure 33C). Additionally, knockdown of Unc119 in GA_{149}-myc expressing cells did not deteriorate viability further, indicating that Unc119 loss of function is important in the mechanisms of poly-GA induced toxicity.

In summary, poly-GA aggregates may cause loss of Unc119 function by sequestration and could thereby contribute to poly-GA mediated neurotoxicity and finally to FTD/ALS pathogenesis.

4.12. Unc119 is detected in *C9orf72* patient poly-GA aggregates

As the previous results suggested a participation of Unc119 in the pathomechanism of ALS and FTD, it was important to analyze whether Unc119 can be detected in *C9orf72* patient aggregates. Before investigating this, both Unc119 antibodies were validated thoroughly in patient material. Therefore competition experiments with GST-Unc119 using immunoblotting (Figure 34A) and immunohistochemistry (Figure 34B) were performed. Upon pre-incubation with denatured as well as native GST-Unc119 the signal intensity of overexpressed human as well as rat Unc119 protein was strongly reduced in immunoblots of HEK293 cells transfected with either HA-hUnc119 or HA-rUnc119 (Figure 34A).

This is also true for pre-incubation with native-GST-Unc119 and Unc119#1 antibody in immunohistochemistry of frontal cortex (SFG) region and dentate gyrus of a *C9orf72* mutation carrier. Aggregate as well as cytosolic staining of Unc119 in both regions is almost completely abolished (Figure 34B) upon pre-incubation, thus validating both antibodies for use in human tissue.

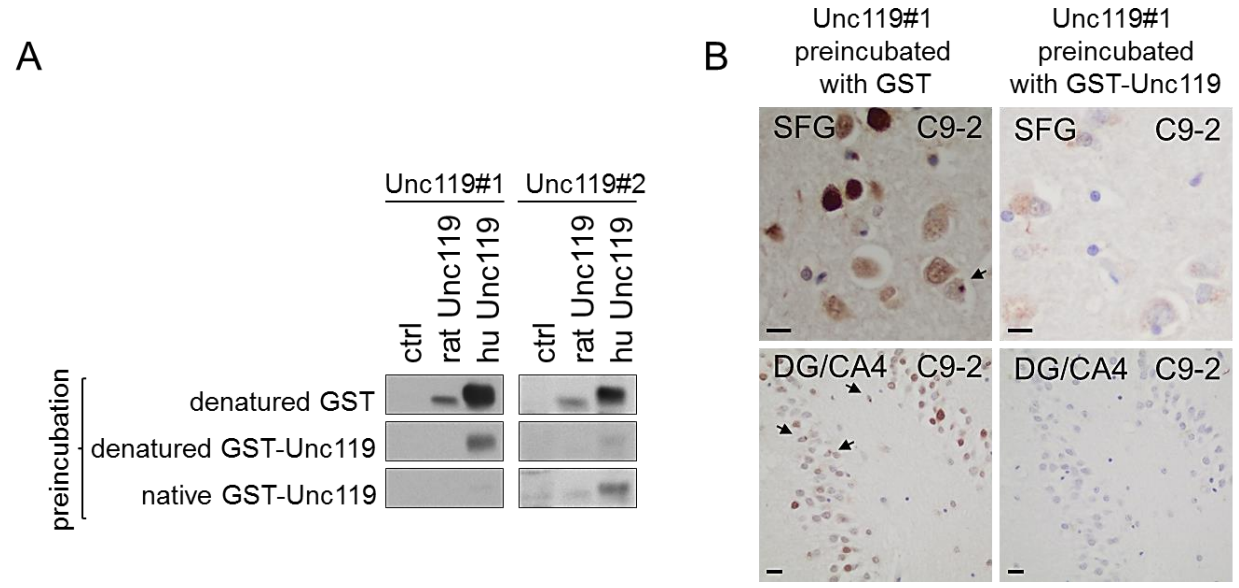

Figure 34: Antigen pre-incubation confirms specificity of Unc119 staining in patient material.
(A) Immunoblots of HEK293 cells transfected with rat and human HA-Unc119 using antibodies Unc119#1 and #2. To confirm specificity Unc119 antibodies were preincubated with 25 µg/ml native or denatured GST-Unc119 or denatured GST as a control. While specific Unc119#2 signal is best blocked with denatured GST-Unc119, the Unc119#1 antibody is best blocked with native GST-Unc119, which may explain the better sensitivity of Unc119#1 for immunohistochemistry. (B) Using the Unc119#1 antibody preincubated with GST-Unc119 but not with GST alone abolishes the staining of cells and inclusions strongly indicating antibody specificity for immunohistochemistry as shown for the superior frontal gyrus (SFG) and the hippocampal dentate gyrus/cornu ammonis region 4 (DG/CA4) of a *C9orf72* mutation carrier. Scale bars depict 10 µm for SFG and 30 µm for DG/CA4.

To investigate if Unc119 forms intracellular inclusions in *C9orf72* patients, immunohistochemistry staining of a *C9orf72* mutation carrier and a healthy control in the CA3/4 region of the hippocampus was carried out by Martin Schludi. Intracellular Unc119 inclusions resembling poly-GA aggregates could only be detected in *C9orf72* mutation carriers but not in healthy controls (Figure 35A).

Furthermore, I performed a filter trap assay to confirm that Unc119 is sequestered into poly-GA aggregates and is therefore insoluble. In the frontal cortex of two *C9orf72* patients but not in two aged matched healthy controls, insoluble Unc119 could be detected in the filter (Figure 35B).

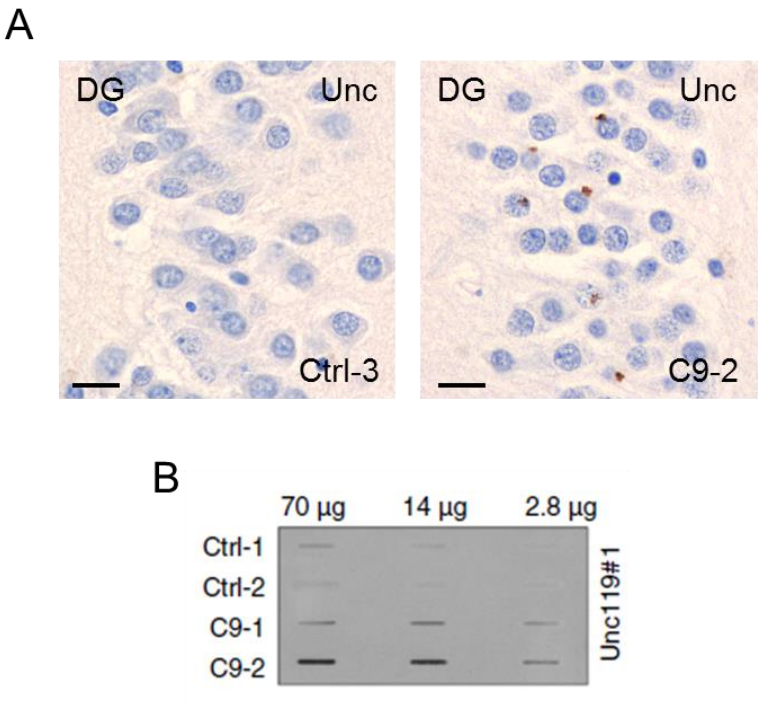

Figure 35: Unc119 forms neuronal cytoplasmic inclusions in *C9orf72* patients.
(A) Immnuohistochemistry analysis of Unc119 in the frontal cortex of a *C9orf72* mutation carrier and a healthy control. *C9orf72* mutation carriers, but not controls, show cytoplasmic inclusions resembling poly-GA inclusions in their shape. Scale bar 20 µm. (B) Filter trap assay detects insoluble Unc119 in 1 % SDS in *C9orf72* mutation carriers but not healthy controls.

To examine if Unc119 co-aggregates with poly-GA in *C9orf72* patients I performed double immunofluorescence stainings together with Martin Schludi using both Unc119 antibodies. Co-localization of Unc119 and poly-GA could be confirmed in the cortex and cerebellum of *C9orf72* cases (Figure 36A+B, Figure 37A). However, no aggregates could be detected in control cases (Figure 36C and Figure 37B). Importantly, in a fraction of neurons nearly all Unc119 was sequestered into aggregates and no residual cytosolic staining could be detected (Figure 36A).

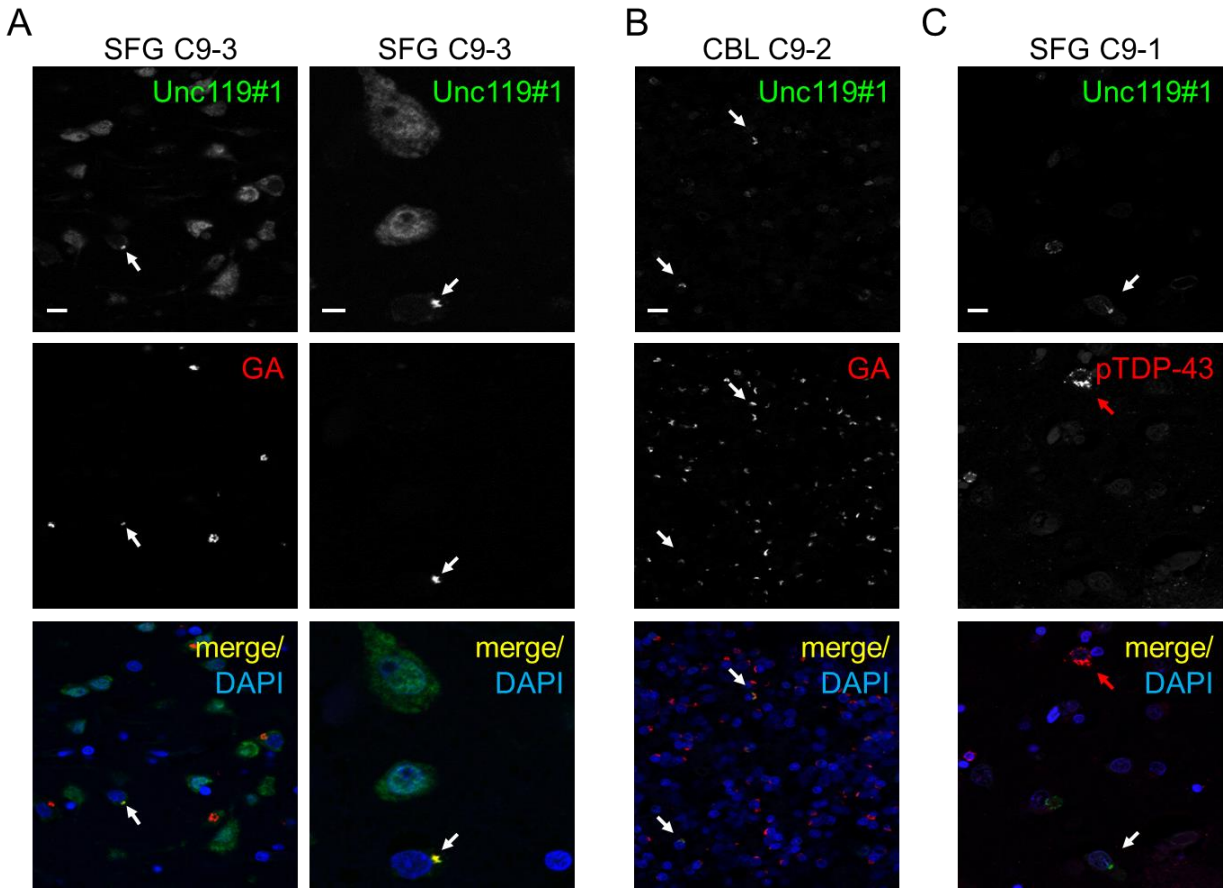

Figure 36: Poly-GA but not TDP-43 co-aggregates with Unc119 in patients with *C9orf72* mutation.
Double immunofluorescence analysis of Unc119 with poly-GA or phosphorylated TDP-43 (p-TDP-43) in *C9orf72* mutation cases C9-1, C9-2 and C9-3. (A) In the superior frontal gyrus (SFG), a subset of poly-GA-positive neuronal cytoplasmic inclusions also contains Unc119. Redistribution of Unc119 compared to poly-GA-negative cells can be seen in a fraction of co-aggregating cells (*white arrows*). (B) In the cerebellar granular cell layer (CBL) abundant cytoplasmic poly-GA inclusions are only rarely positive for Unc119 (*white arrows*). (C) As shown for the superior frontal gyrus, Unc119 (*white arrow*) and p-TDP-43 (*red arrow*) are not co-localized in the same cytoplasmic inclusions. *Scale bars* represent 10 µm for overviews and 5 µm for the close-up in the second column of (A)

Strikingly, all Unc119 inclusions were found to be poly-GA positive indicating that DPR proteins drive inclusion formation. Moreover, despite abundant poly-GA and phospho-TDP-43 (p-TDP-43) pathology in the frontal cortex, Unc119 only co-localized with poly-GA but not p-TDP-43 inclusions. This further validates poly-GA specific co-aggregation of Unc119 (Figure 36C and Figure 37B).

Taken together, Unc119 specifically co-aggregates with poly-GA inclusions in *C9orf72* patients.

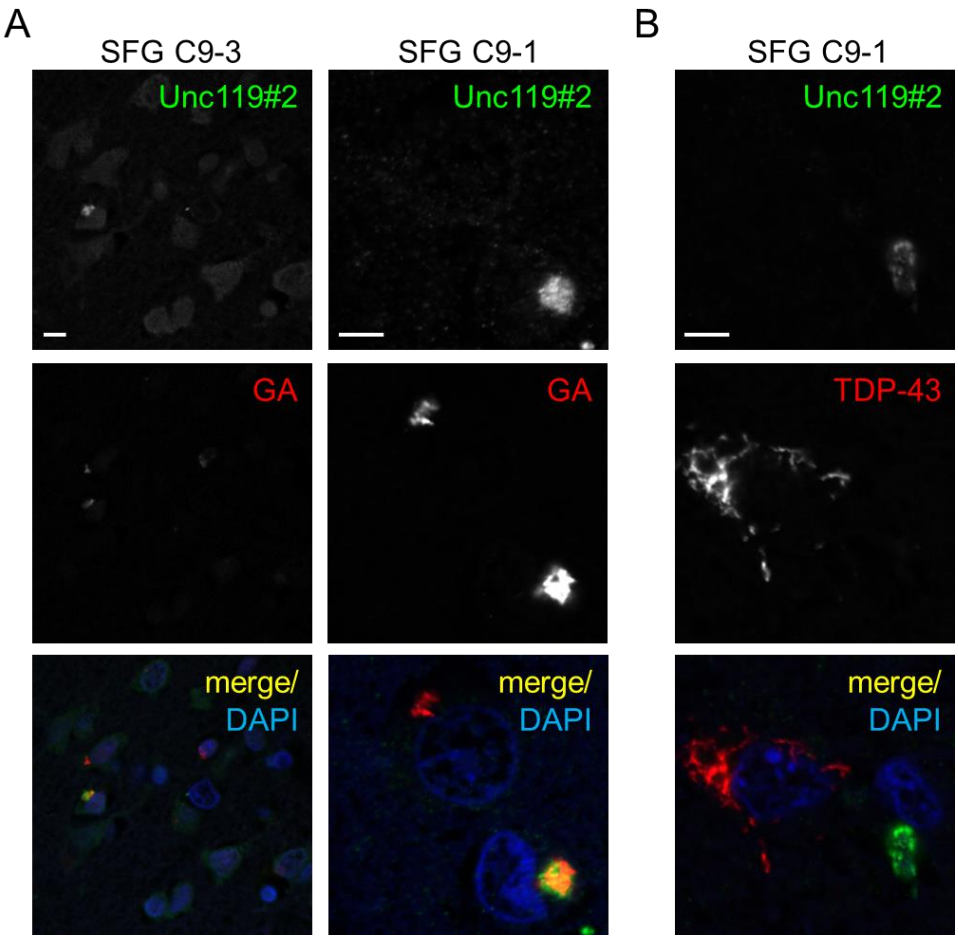

Figure 37: Second antibody Unc119 #2 confirmes co-aggregation of Unc119 and poly-GA.
Double immunofluorescence analysis of Unc119 with poly-GA or p-TDP-43 in *C9orf72* mutation cases C9-1 and C9-3. (A) In the superior frontal gyrus (SFG), a subset of poly-GA positive NCI also contains Unc119. (B) There is no co-localization of poly-GA and p-TDP-43 in the frontal cortex. Scale bars represent 10 µm in overviews and 5 µm in close ups.

4.13.Poly-GA may induce TDP-43 pathology in primary neurons

Although the data I have presented in this thesis strongly suggest an important contribution of DPR proteins to neurodegeneration in *C9orf72* mutation carriers, it is still unclear if and how DPR proteins can induce the p-TDP-43 pathology that is seen in most *C9orf72* patients. It is still under discussion whether DPR pathology precedes TDP-43 pathology. Reports of a few patients with abundant DPR pathology but no detectable p-TDP-43 inclusions support this hypothesis (Proudfoot et al., 2014).

To investigate if poly-GA might be involved in the development of TDP-43 pathology I transduced primary cortical rat neurons (DIV 6+15) with either GA_{149}-myc or GFP as a control. Immunoblotting for TDP-43 revealed no differences in TDP-43 expression on the expected height of 43 kDa and furthermore I could not detect any pTDP-43 (Figure 38A and data not shown). Upon longer exposure, however, I could detect TDP-43 at the top of the gel specifically in poly-GA expressing neurons (Figure 38A). As this alone does not implicate poly-GA in the development of TDP-43 pathology, I performed immunofluorescence analysis of GA_{149}-myc transduced hippocampal neurons (DIV 6+15) and GFP control neurons. Whereas TDP-43 in control neurons was strictly restricted to the nucleus, a portion of poly-GA expressing neurons also showed TDP-43 outside of the nucleus. The distribution seemed to be diffuse with small aggregates in the cytosol (Figure 38B). A quantification of this phenotype in at least 250 cells per condition in three experiments revealed a significant shift of TDP-43 from the nucleus to cytosol in poly-GA expressing neurons.

Whereas 95 % of control cells showed TDP-43 expression exclusively in the nucleus, in poly GA expressing neurons, more than 50 % of tranduced cells showed additional TDP-43 in the cytosol forming the aforementioned tiny aggregates (Figure 38C). Additionally, only 46 % of the neurons showed TDP-43 to be exclusively located in the nucleus. Moreover, 5 % of control and poly-GA cells showed a partial mislocalization of TDP-43 even though no poly-GA aggregate was present which is depicted in basal misloc.

Thus, a first hint that poly-GA might be involved in the induction of TDP-43 pathology is provided. However, more detailed analyzes are necessary to understand which type of aggregate is formed and if these initial aggregates can further develop into the pTDP-43 pathology seen in patients.

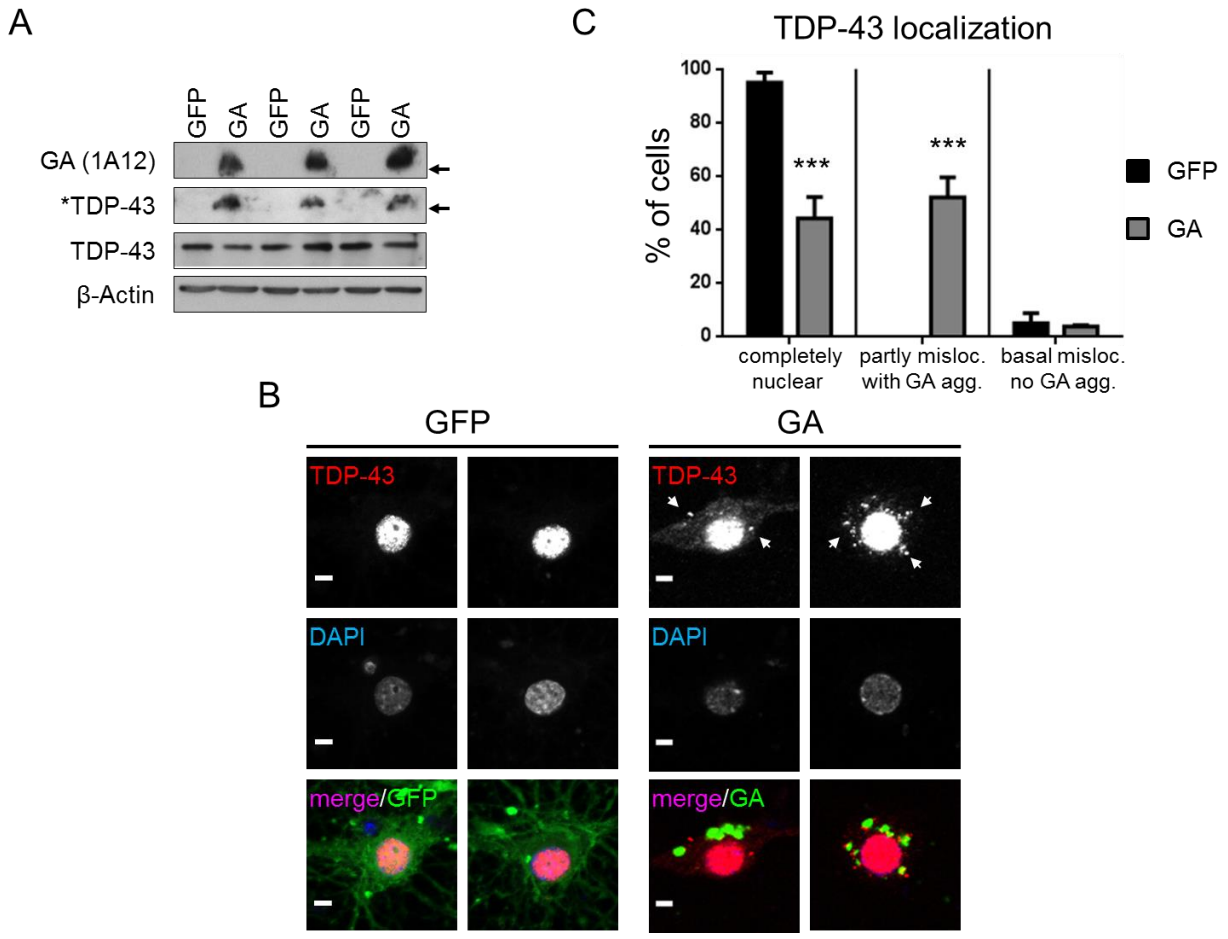

Figure 38: Poly-GA induces cytoplasmic mislocalization of TDP-43.
(A) Cortical neurons infected with GFP or GA_{149}-myc lentivirus (DIV 6+15). Immunoblots with the indicated antibodies. TDP-43* depicts TDP-43 found in the stacking gel with a longer exposure time. *Arrows* depict top of the gel. (B) Hippocampal neurons transduced with GFP or GA_{149}-myc lentivirus. Immunostaining with TDP-43 and DAPI as nuclear marker (DIV 6+15). Arrows mark the formation of dot-like TDP-43 structures. Scale bar, 5 µm. (C) Quantification of TDP-43 mislocalization. 250 cells counted per condition and experiment. A significant increase in mislocalized TDP-43 of 52% compared to control cells could be detected (n=3; paired student t-test $p<0.001$)

In summary, I could establish a cell culture system to investigate DPR protein contribution to the pathogenesis of *C9orf72* FTD/ALS. The cell culture system replicates important key features found in *C9orf72* patients, such as p62-positive cytosolic inclusions as well as neurodegeneration. Strikingly, with my cell culture model I could detect Unc119 in the poly-GA interactome of primary neurons and identified this protein as a novel component of poly-GA aggregates in patients.

Moreover, I could demonstrate a direct role of Unc119 in the poly-GA mediated neurotoxicity.

Finally and most importantly, I could establish a first link between DPR proteins and TDP-43, the protein whose aggregates correlate best with neurodegeneration in *C9orf72* FTD/ALS.

5. Discussion

5.1. Translation of the *C9orf72* hexanucleotide repeat expansion

The discovery of the hexanucleotide repeat expansion in *C9orf72* as a major cause for FTD/ALS, 10 years after initial implication of this locus, has been an important breakthrough (DeJesus-Hernandez et al., 2011; Renton et al., 2011). Understanding how the mutation causes disease is crucial in order to develop therapeutic approaches. Therefore, appropriate cell culture models are valuable tools to elucidate underlying molecular mechanisms. Three (not mutually exclusive) theories exist, how the *C9orf72* repeat expansion could lead to neurodegeneration. First, loss of C9orf72 protein expression and thereby function. Second, RNA mediated toxicity through sequestration of important RNA-binding proteins and third, toxic protein gain of function through translation of the repeat into DPR proteins. All of these mechanisms need to be addressed to get a clear picture on their contribution to *C9orf72* related FTD/ALS.

In 2013, our lab and others could show that the intronic hexanucleotide repeat expansion is indeed translated and sense proteins poly-GA, poly-GR and poly-GP are detected in p62-positive star-shaped inclusions of *C9orf72* patients. As part of this study, I was the first to show that the repeat RNA is stabilized and transcripts in sense and antisense direction are produced. Thus, I offered the first hint that antisense proteins might also be a part of the whole picture. A few months afterwards, this result was confirmed by the detection of antisense proteins poly-PA, poly-PR and poly-GP in FTD/ALS patients (Gendron et al., 2013; Mori et al., 2013a; Zu et al., 2013).

To follow up on these initial results, my thesis focused on the contribution of all five DPR proteins to disease. For this purpose, I established a primary neuron cell culture system lacking the original repeat sequence to exclude RNA repeat based mechanisms. Poly-GA expression recapitulates the main features seen in patients such as p62 accumulation and neurotoxicity, thus directly links *C9orf72* repeat translation to neurodegeneration. Furthermore, my model was able to predict new

pathologic features such as Unc119 co-aggregation, thus is a valuable tool to analyze underlying disease mechanisms.

5.2. DPR aggregation and toxicity

The approach in my thesis was to express all five DPR proteins from almost GGGGCC-free constructs containing an ATG start codon in a cell culture system to understand if and how DPR proteins contribute to the disease. Through that approach, I mainly excluded RNA-based toxicity and in comparison to previous GGGGCC-based constructs, my model showed higher expression levels of the DPR proteins. Furthermore, it was the first model to show aggregation of DPR proteins *in vitro*. Together, this presumably accelerates the disease mechanisms that take years to build up in patients.

The sense and antisense DPR proteins surprisingly showed very different aggregation patterns in cell culture. Only poly-GA formed the typical compact p62-positive inclusions, suggesting that it possibly is the main driving force for aggregation. This is consistent with the observation that poly-GA is present in nearly all TDP-43 negative inclusions, whereas the other DPR proteins are only detected in 10-50 % of these inclusions (Mori et al., 2013a; Mori et al., 2013c). Strikingly, the charged DPR proteins poly-GR and poly-PR showed mainly nuclear inclusions, similar to poly-GA aggregates rarely identified in patients (Mackenzie et al., 2013; Schludi et al., 2015). It is possible, that they are actively transported into the nucleus as positively charged arginines are a typical feature of nuclear localization signals (Palmeri and Malim, 1999; Truant and Cullen, 1999). The difference in aggregation pattern in my model, compared to patients, may be a result of the different length of the proteins, as the repeat number in my system is much shorter than in patients. Additionally, the lack of other DPR proteins may cause the differences, since in patients a combination of DPR proteins can often be found in one aggregate. Overall, my findings on DPR localization are in line with results from other groups also showing comparable aggregation patterns in primary neuron culture, drosophila and mice (Chew et al., 2015; Yamakawa et al., 2015; Yang et al., 2015; Zhang et al., 2014).

Despite robust DPR expression in transfected HEK293 cells, I could not find evidence for cell death due to protein toxicity of the five DPR species. Furthermore, I could not detect any toxicity of the GGGGCC expression constructs without ATG start codon and the GGGGCC repeat based ATG-driven poly-GP construct, suggesting HEK293 cells are not susceptible to either *C9orf72* repeat RNA or protein toxicity under these conditions, however, another study could detect toxicity of poly-PR and poly-GP in HEK293 cells in an LDH activity assay. This discrepancy may be a result of different expression levels or DPR protein length.

In contrast to HEK293 cells, caspase activation, DNA fragmentation and increased LDH release in primary neurons suggest that p62-positive poly-GA inclusions lead to apoptosis in primary hippocampal and cortical neurons. Nuclear poly-PR inclusions also induce cell death in primary neurons in an LDH release assay. As the synthetic genes largely lack GGGGCC repeats and, as can be seen for the poly-GA construct, require ATG-initiated protein expression to cause toxicity, DPR proteins themselves are neurotoxic. Nonetheless, my results do not rule out an additional or synergistic effect of GGGGCC repeat-RNA or *C9orf72* haploinsufficiency in the pathogenesis of *C9orf72* FTLD/ALS.

Apart from my work, a lot of studies accumulated during the last year showing toxicity for different DPR proteins in several culture models (Kwon et al., 2014; Mizielinska et al., 2014; Wen et al., 2014; Yamakawa et al., 2015; Zhang et al., 2014), thus, of DPR proteins in the disease. All of these studies used almost GGGGCC-free expression constructs in various length (50 to 175 repeats) to focus on DPR protein effects. However, in most studies only poly-GA showed an aggregation pattern and p62 co-aggregation comparable to what is seen in patients (May et al., 2014; Wen et al., 2014; Yamakawa et al., 2015; Zhang et al., 2014). The arginine-rich proteins poly-GR and poly-PR formed aggregates in the nucleus and especially in the nucleolus that could not be detected in patients so far (Schludi et al., 2015). This, however, may be due to a rapid death of neurons harboring these toxic aggregates during the course of disease (Cooper-Knock et al., 2015). Therefore, it will be very hard to confirm or dismiss this hypothesis completely. Poly-GP and poly-PA did not show any aggregation and were mostly distributed

throughout the whole cell (May et al., 2014; Wen et al., 2014; Yamakawa et al., 2015; Zhang et al., 2014).

Overall, studies favor poly-GA, poly-PR and poly-GR as the potential toxic species. Whereas Zhang, Yamakawa and May mainly saw toxicity of poly-GA in primary neurons and N2a cells, Mizielinska, Wen and Kwon saw strong toxicity for poly-PR and poly-GR in Drosophila, primary neurons and other cell lines. However, Mizielinska and colleagues also saw mild toxicity for poly-GA in their study. The differences seen in toxicity of these three proteins in the individual studies may occur due to different construct design or cell culture models and further studies are needed to elucidate the individual contribution to neurodegeneration seen in patients. A detailed description of all available models on DPR protein toxicity can be found in Table 2 under 5.6 *C9orf72* disease models. The toxic mechanisms of poly-PR and poly-GR are presumably due to unspecific RNA and DNA binding that may lead to transcriptional dysregulation and nucleolar stress (Kwon et al., 2014; Mizielinska et al., 2014; Wen et al., 2014). Yet, nucleolar stress could not be detected in patient samples (Schludi et al., 2015) and thus questions if these mechanisms are important in patients or rather a cell culture artefact. In contrast, poly-GA may interfere with cellular proteostasis by inhibiting protein degradation (Yamakawa et al., 2015; Zhang et al., 2014). Toxicity might also be mediated through sequestering important cellular proteins such as Unc119. Unfortunately, Unc119 function outside sensory neurons is so far poorly understood. Interestingly, I could identify p62, an important protein in the ubiquitin-proteasome system and autophagy, as the top-hit in our mass spectrometry approach. Apart from p62, proteins of the ubiquitin-proteasome system were found to be enriched, however, proteasome activity was not impaired in the assays I used. Interestingly, two other groups could show in their cell culture systems, show that poly-GA may indeed decrease proteasome activity and cause toxicity (Yamakawa et al., 2015; Zhang et al., 2014). This difference may occur due to different expression levels of the poly-GA protein, different cellular systems or the assays used to assess UPS activity. In contrast to the UPS activity assay I used that assessed the activity of chymotrypsin-like, trypsin-like and caspase-like activity with specific substrates, Yamakawa and

colleagues used an Ub-G76V-GFP reporter to assess UPS activity and Zhang and colleagues focused only on chymotrypsin-like activity. Overall, the ubiquitin-proteasome system is clearly linked to repeat expansion disorders such as *C9orf72* FTD/ALS or Huntington's disease (Schipper-Krom et al., 2012), however, the contribution to neurodegeneration is still under discussion. Additionally, autophagy might also be altered, as p62 is an important protein in the autophagy mechanisms (Pankiv et al., 2007).

After the discovery of DPR proteins in *C9orf72* FTD/ALS, a debate arose whether these proteins contribute to disease progression or are just innocent bystanders. Studies by Mackenzie, Schludi and others showed that none of the DPR proteins correlate with neurodegeneration in the patient brain questioning their involvement (Davidson et al., 2014; Gomez-Deza et al., 2015; Mackenzie et al., 2013; Schludi et al., 2015). The only correlations found in patients so far, are all related to the repeat length of the hexanucleotide repeat expansion. Repeat length inversely correlates with disease duration in FTD patients and age of onset (Benussi et al., 2013; Suh et al., 2015; van Blitterswijk et al., 2013).

Interestingly, living *C9orf72* patients also show atrophy of the thalamus and cerebellum, areas with high DPR load, in imaging approaches, a phenotype that is highly associated with *C9orf72* FTD/ALS (Mahoney et al., 2012b). furthermore cerebellar atrophy can be detected in an MRI 10 years before the expected onset, further strengthening the specific involvement of the cerebellum in *C9orf72* FTD/ALS (Rohrer et al., 2015b).

Overall, multiple potential explanations exist, how DPR proteins contribute to ALS/FTD without showing a spatial correlation to neurodegeneration. For example, formation of cytosolic aggregates might be a protective mechanism and soluble species are the cause of neuronal loss. Additionally, a combination of DPR proteins and/or RNA toxicity might be responsible for neurodegeneration in the patients and therefore focusing on a specific DPR aggregate type might not yield a correlation. The recent publication of an AAV-mouse model by Chew and colleagues could show that a combination of DPR proteins and repeat RNA is toxic in this model.

Taken together, there is a lot of evidence from cellular and animal models for a crucial role of DPR proteins in *C9orf72* FTD/ALS.

5.3. Poly-GA interactome and its disease relevance

To understand the underlying mechanism of poly-GA toxicity, it is important to identify its interacting partners. Interactomics have yielded interesting insights into aggregate toxicity mechanisms of other neurodegenerative diseases by identifying sequestered proteins that allow conclusions on cellular pathways involved and additionally have helped to discover new modulators of toxicity (Hipp et al., 2014; Olzscha et al., 2011; Ripaud et al., 2014).

Using a quantitative proteomics approach, I discovered several interacting proteins upon GA_{149}-GFP transduction of primary cortical neurons.

P62, the main component of DPR inclusions was identified as the top hit in this experiment and thus, also validated the experimental approach and the feasibility of mass spectrometry analysis in analyzing aggregate interactomics. Apart from p62 and the ubiquitin-proteasome system mentioned above, the screen yielded some other interesting interacting partners such as Unc119, a cargo adapter of myristoylated proteins, the cytosolic chaperone Bag6 or Hsd17b4, an important enzyme in the peroxisomal fatty acid beta-oxidation (Binici and Koch, 2014; Constantine et al., 2012; Möller et al., 1999). Co-aggregation of many interaction partners, found in the mass spectrometry analysis, could be also validated in immunofluorescence. I focused on Unc119, because it had been linked to neuromuscular function in *C. elegans* previously (see below). Additional experiments are needed to elucidate if Bag6 and Hsd17b4 can also be found in patient aggregates and how their loss of function through sequestration might contribute to neurotoxicity. Interestingly, Bag6 is an important modulator of autophagy and loss of Bag6 leads to inhibition of autophagy, which would fit to the increase in p62 seen in poly-GA expressing cells and patients (Sebti et al., 2014). Additionally, it is also known that Bag6 is involved in the degradation of mislocalized proteins, explaining why binding to poly-GA is occurring (Hessa et al., 2011).

Hsd17b4, also known as Mfp2, is a peroxisomal matrix protein in the mitochondrium. Strikingly, Mfp2 knockout mice show a neurodegenerative phenotype characterized through motor deficits such as poor balance and coordination, ataxia and cerebellar atrophy (Verheijden et al., 2014).

In conclusion, the mass spectrometry results validated important key findings of *C9orf72* FTD/ALS such as p62 co-aggregation and accumulation of the ubiquitin-proteasome system. Additionally, it yielded an important and novel poly-GA interaction partner Unc119 that is potentially relevant for the pathogenesis. Furthermore, the other validated co-aggregation proteins, Bag6 and Hsd17b4 may provide further insights into poly-GA induced toxicity in patients.

5.4. The role of Unc119 in neurodegeneration

Up to this time, the novel poly-GA interacting protein Unc119, a cargo adapter of myristoylated proteins, has mainly been investigated in *C. elegans* and the mammalian retina. In my thesis, I discovered that it also has a function in cortical neurons, as knockdown lead to loss of dendrite complexity and toxicity in these neurons. Importantly, Unc119 knockout in *C. elegans* almost completely paralyzes the worms and disturbs axonal development and maintenance (Knobel et al., 2001; Maduro and Pilgrim, 1995; Maduro et al., 2000). As Unc119 is sequestered into poly-GA aggregates in *C9orf72* FTD/ALS, Unc119 loss of function may have an important role in underlying disease mechanisms.

Unfortunately, not much is known about Unc119 function in mammals outside the retina. As a trafficking factor for myristoylated proteins it specifically binds myristate residues through a hydrophobic pocket composed of β-sheets (Constantine et al., 2012). Most intriguingly, the binding motif to Transducin α, a photoreceptor protein in the retina, has been mapped to the myristoylated N-terminal GAGASA sequence which strongly supports the interaction data with poly-GA (Zhang et al., 2011). Apart from Transducin α, the only other known cargos in the nervous system are Gα proteins in the *C. elegans* olfactory system (Constantine et al., 2012). Unfortunately, none of those can directly explain the underlying disease mechanisms of *C9orf72* FTD/ALS. Therefore it will be important to investigate how

Unc119 sequestration affects neuronal function in *C9orf72* patients. It is possible, that poly-GA enters and clogs the hydrophobic cavity of Unc119 and thus, inhibits transport of so far unidentified myristoylated Unc119 cargos in cortical neurons. This may contribute to neurotoxicity observed upon Unc119 knockdown or poly-GA expression. Interestingly, an Unc119 nonsense mutation was found in a patient with cone rod dystrophy and Unc119 knockout, as well as truncation mutations, cause retinal degeneration in mice (Ishiba et al., 2007; Kobayashi et al., 2000; Mori et al., 2006; Zhang et al., 2011). Thus, fitting perfectly to the observed toxicity upon Unc119 knockdown in cortical and hippocampal neurons. Strikingly, Unc119 overexpression partially rescues poly-GA toxicity in primary neurons, while Unc119 knockdown does not further increase poly-GA toxicity. Together, this indicates that Unc119 sequestration is a major contributor to poly-GA toxicity in *C9orf72* FTD/ALS.

5.5. The relationship between TDP-43 and DPR proteins

A very important feature of *C9orf72* FTD/ALS is accumulation of another protein, TDP-43, whose abundance correlates with neurodegeneration and disease progression, whereas DPR pathology does not (Mackenzie et al., 2013; Schludi et al., 2015). TDP-43 rarely co-aggregates with DPR proteins and the link between *C9orf72* repeat expansion and TDP-43 pathology is not known so far. GGGGCC repeat expressing fly models and loss of function models in zebrafish failed to recapitulate TDP-43 pathology (Lee et al., 2013; Xu et al., 2013) seen in patients. Importantly, my poly-GA neuronal cell culture expression model induces cytoplasmic TDP-43 mislocalization into small aggregates suggesting a direct link between DPR and TDP-43 pathology. These small aggregates are already insoluble as they cannot enter the 4 % stacking gel and are retained at the top of the gel. Thus, suggesting that they may be a precursor of p-TDP-43 inclusions seen in patients. However, I could not detect any p-TDP-43 in the neuronal expression system. Overall, these findings are in contrast to the poor correlation of DPR and p-TDP-43 inclusions in patient brains. Still, there is evidence that DPR inclusions occur earlier than TDP-43 pathology and may serve as a trigger. In patients for

example, p-TDP-43 occasionally surrounds a DPR core, but never vice versa (Mackenzie et al., 2013; Mori et al., 2013c). Additionally, there are patients that show FTD/ALS like symptoms and abundant DPR pathology, but lack TDP-43 pathology (Proudfoot et al., 2014). This strongly suggests that DPR pathology precedes TDP-43 pathology and may cause initial symptoms. This would be comparable to Alzheimer's disease, where Aβ pathology occurs 10-15 years earlier than Tau pathology in a distinct regional distribution (Musiek and Holtzman, 2015; Perrin et al., 2009). Apart from my initial experiments, there is also evidence for a connection from another group, showing that RNA and DPR expression triggers pronounced TDP-43 pathology in an AAV mouse model (Chew et al., 2015). However, they also did not identify the underlying mechanisms. There are several possibilities how these aggregates may occur. First, poly-GA aggregates may induce stress response in the cell leading to the formation of stress granules and the recruitment of TDP-43 into those stress granules as can be seen after oxidative stress in primary neurons (Colombrita et al., 2009). Second, poly-GA may interfere with the proteasome and/or autophagy and dysfunction of these important cellular processes may causes TDP-43 mislocalization. This is in line with a conditional knockout mouse of the proteasome subunit Rpt3 showing mislocalization of TDP-43 (Tashiro et al., 2012). Third, TDP-43 is a DNA/RNA binding protein which shuttles between cytosol and nucleus although its main function lies in the nucleus, poly-GA may interfere with this shuttling process and, for example, inhibit importin-dependent transport into the nucleus and thus may keep TDP-43 in the cytosol (Ayala et al., 2008; Dormann and Haass, 2011; Miyamoto et al., 2004).

In general, multiple explanations for the discrepancy between TDP pathology occurring in model systems or in the patient are conceivable. These explanations need to be addressed in future studies, particularly in animal models. First, end-stage pathology may not accurately depict the early steps of pathogenesis. Second, DPR proteins may trigger TDP-43 aggregation through non-cell autonomous effects, similar to spreading and seeding of a-syn and tau pathology (Holmes and Diamond, 2012). Third, soluble DPR species may be more toxic than the inclusions itself as it has been observed for poly-Q and Tau (Ferreira et al., 2007; Takahashi et al., 2008).

Nevertheless, the data presented here provide the first link between *C9orf72* repeat expansion and TDP-43 pathology, which undoubtedly plays an important role in the pathogenesis of FTD/ALS.

5.6. *C9orf72* disease models

Over the last few years, a large amount of studies has accumulated trying to decipher the underlying mechanisms of *C9orf72* FTD/ALS. *In vitro* and *in vivo* models have been designed to mimic the patient situation and to investigate the disease causing mechanisms. All models with brief description of the key results are listed in table 2 with the disease mechanisms investigated and the obtained findings.

Table 2: Summary of *C9orf72 in vitro* and *in vivo* models to investigate underlying disease mechanisms

mechanism targeted	model organism	effect	citation
C9orf72 loss of function	knockdown in N2a cells and primary cortical neurons	defects in endocytosis and autophagy	(Farg et al., 2014)
C9orf72 loss of function	knockdown in zebrafish	axonopathy and motordysfunction	(Ciura et al., 2013)
C9orf72 loss of function	knockout in *C. elegans*	motor neuron degeneration and motordysfunction	(Therrien et al., 2013)
C9orf72 loss of function	conditional knockout mice	only weight loss without neuropathological abnormalities	(Koppers et al., 2015)
repeat RNA toxic gain of function *C9orf72* loss of function	iPS cells from ALS patients differentiated into motor neurons	no reduced *C9orf72* levels, knockdown showed no toxicity RNA foci and sequestration of RNA-binding proteins hnRNPA1 and Pur α	(Sareen et al., 2013)
repeat RNA toxic gain of function	human patient fibroblasts	RNA foci	(Lagier-Tourenne et al., 2013)
repeat RNA toxic gain of function	intronic repeat sequence in drosophila	RNA foci and neurodegeneration	(Xu et al., 2013)
repeat RNA toxic gain of function	intronic repeat sequence in zebrafish and neuronal cell lines	RNA foci, sequestration of RNA-binding proteins (RBPs) SF2, SC35 and hnRNPH and neurodegeneration	(Lee et al., 2013)

DPR protein toxic gain of function	expression of DPR proteins from synthetic genes lacking GGGGCC repeats in HEK293 cell and primary neurons	p62-positive cytoplasmic poly-GA inclusions neurotoxicity for poly-GA dendrite loss for poly-GA and sequestration of Unc119 mislocalization of TDP-43 (unpublished)	(May et al., 2014)
DPR protein toxic gain of function	expression of DPR proteins from synthetic genes lacking GGGGCC repeats in HEK293 cell and primary neurons	ubiquitin-positive poly-GA cytoplasmic inclusions; neurotoxicity for poly-GA; dendrite loss for poly-GA and ER stress	(Zhang et al., 2014)
DPR protein toxic gain of function	expression of DPR proteins from synthetic genes lacking GGGGCC repeats in primary neurons	p62-positive cytoplasmic poly-GA inclusions inhibition of UPS function by poly-GA and poly-GR neurotoxicity of poly-GA and poly-GR	(Yamakawa et al., 2015)
DPR protein toxic gain of function	addition of short peptides n=20 to U2OS cells	toxicity of poly-GR and poly-PR nucleolar localization	(Kwon et al., 2014)
DPR protein toxic gain of function	expression of DPR proteins from synthetic genes lacking GGGGCC repeats in NSC-34 and HEK293 cells	toxicity of poly-GR and poly-PR no aggregation seen for all DPR proteins	(Tao et al., 2015)
DPR protein toxic gain of function	expression of DPR proteins from synthetic genes lacking GGGGCC repeats in drosophila	toxicity of poly-GR and poly-PR, mild toxicity for poly-GA	(Mizielinska et al., 2014)
DPR protein toxic gain of function	expression of DPR proteins from synthetic genes lacking GGGGCC repeats in drosophila, Hela cells and iPS cell derived human neurons	toxicity of poly-GR and poly-PR in drosophila recruitment of poly-GR into poly-GA cytoplasmic inclusions in cell lines	(Yang et al., 2015)

DPR protein and RNA toxic gain of function	intronic repeat sequence in HEK293 and SY5Y cells	RNA foci, toxicity in cell models of antisense RNA and protein (poly-GP and poly-PR)	(Zu et al., 2013)
DPR protein and RNA toxic gain of function	human iPS cells from 2 FTD patients differentiated into neurons	RNA foci, poly-GP expression, increased p62 levels and increased sensitivity to cellular stress through inhibition of autophagy	(Almeida et al., 2013)
DPR proteins and repeat RNA toxic gain of function	human fibroblasts from 3 *C9orf72* patients differentiated into neurons	RNA foci DPR expression (poly-GP)	(Su et al., 2014)
DPR proteins and repeat RNA toxic gain of function	expression of DPR proteins from synthetic genes lacking GGGGCC repeats and repeat RNA in drosophila, Nsc-34 cells and primary neurons	poly-PR nuclear aggregates are toxic, combination of RNA and protein has synergistic effect on toxicity	(Wen et al., 2014)
DPR protein and RNA toxic gain of function	AAV mouse model for sense repeat and proteins	RNA foci, p62-positive cytoplasmic inclusions, neurodegeneration, TDP-43 mislocalization	(Chew et al., 2015)
all three mechanisms	human iPS cells from patients differentiated into neurons	*C9orf72* downregulation, RNA foci, sequestration of RBP ADARB2, diffuse poly-GP expression and high sensitivity to glutamate-induced excitotoxicity	(Donnelly et al., 2013)

So far, few reports focused on *C9orf72* loss of function. Although initially some results from *C. elegans* and zebrafish showed motor deficits and motor neuron degeneration (Ciura et al., 2013; Therrien et al., 2013) thus, pointed to a role of *C9orf72* loss of function in the disease, results in mice showing no obvious phenotype even after long periods of time (Koppers et al., 2015) question this involvement. Therefore, further work is needed to elucidate the exact contribution.

In contrast, a lot of evidence is accumulating for the toxic gain of function hypothesis for both RNA and protein toxicity. Patient-derived pluripotent stem cells (iPS cells) differentiated into motor neurons could recapitulate RNA foci and sequestration of RNA-binding proteins. In addition, transcriptomic analyses showed a similar gene regulation pattern as in *C9orf72* patients (Donnelly et al., 2013; Sareen et al., 2013; Stepto et al., 2014; Zu et al., 2013). However, neurotoxicity in these models needs to be further confirmed and results from iPS cells are highly variable at the moment. Additionally, several important features seen in patients such as TDP-43 mislocalization and aggregation as well as p62-positive inclusions are missing in these models. As already mentioned above, DPR protein overexpression models and specifically poly-GA based models recapitulate several important features seen in patients such as p62-positive cytoplasmic inclusions, TDP-43 mislocalization (unpublished) and most importantly, neurodegeneration. Thus, models combining DPR protein and RNA expression such as the AAV mouse model by Chew and colleagues may have the biggest potential in reproducing important key features of *C9orf72* patients. However, in the future also mice expressing specific DPR proteins or only high levels of repeat RNA without DPR expression (intermitting stop codons) will be necessary to determine the relative role of these entities in *C9orf72* ALS/FTD.

5.7. Implications for FTD/ALS

The *C9orf72* hexanucleotide repeat expansion is the first autosomal dominant mutation that equally often causes ALS and FTD, which tightened the connection between these diseases even further.

My work and the work of several other groups have demonstrated that DPR proteins may play an important role in *C9orf72* FTD/ALS. Most notably, DPR proteins can cause toxicity in different cellular models by several mechanisms (Chew et al., 2015; Mizielinska et al., 2014; Wen et al., 2014; Yamakawa et al., 2015; Yang et al., 2015; Zhang et al., 2014). If and how these mechanisms are connected and if one or the other is more important in the patient needs further investigations. It is also possible that a combination of several DPR species and sense and antisense

repeat RNA causes the massive neuronal loss seen in patients (Yang et al., 2015). Furthermore, it is still unclear if aggregates, soluble or intermediate DPR protein species are responsible for the neuronal loss. Since the distribution of DPR aggregates of neither species strongly correlates with neurodegeneration (Schludi et al., 2015), toxicity may not be caused by the prominent cytosolic aggregates. However, additional studies are needed for a reliable conclusion. Nonetheless, the discovery of the hexanucleotide repeat expansion leading to toxic RNA transcripts and protein aggregates may offer a highly specific treatment option for patients (including gene therapy), because the repeat stretch does not occur in a healthy individual and has no physiological function. Thus, a repeat directed therapy may have little side effects.

5.8. Summary and future perspectives

Taken together, I established a cell culture model to investigate the role of DPR proteins in *C9orf72* FTD/ALS. This model reproduces important features seen in patients such as cytosolic p62-positive poly-GA inclusions. Poly-GA causes neurotoxicity and dendritic loss in primary neuronal culture. Additionally, I was able to identify the novel DPR co-aggregating protein Unc119 *in vitro* that is partially sequestered in DPR aggregates in patients and may have an important role in poly-GA toxicity. Furthermore, I provided first evidence for a link between DPR and TDP-43 pathology *in vitro*. Thus, DPR proteins likely have an important function in *C9orf72* FTD/ALS.

Nonetheless, several questions remain that need further investigation:

1. As Unc119 is a cargo adapter for myristoylated proteins the loss of function may influence the localization and function of several myristoylated target proteins. Thus, identifying the neuronal Unc119 cargos will be a crucial step to uncover underlying disease mechanisms.

2. Another important question is how TDP-43 aggregate formation is connected to DPR pathology. As I could show, poly-GA leads to partial re-localization

of TDP-43. Since TDP-43 pathology is a common factor in most forms of FTD/ALS, there may be a common mechanism by which TDP-43 becomes mislocalized in genetic and sporadic cases. For example, deficits in nuclear transport may cause cytoplasmic TDP-43 accumulation. A second hypothesis could be dysfunctional autophagy as induction of autophagy enhances TDP-43 turnover in an ALS mouse model (Barmada et al., 2014) and several ALS/FTD associated genes are known to be related to autophagy suggesting a general disease relevant mechanism (Ching and Weihl, 2013; Shen et al., 2015).

3. Transgenic animal models are crucial for further mechanistic studies and preclinical tests. So far, the only published mouse model for *C9orf72* gain of function mechanisms relies on AAV injection and although it does recapitulate important disease features, genetic mouse models to dissect the role of DPR and RNA-based mechanisms will be very important tools in the future.

4. More studies are needed to dissect the contribution of DPR protein, RNA toxicity and haploinsufficiency. Do all three mechanisms contribute to the disease equally or is the gain of toxic RNA and/or protein function the main mechanism? Thus, cell culture models overexpressing repeat RNA and DPR proteins at the same time are needed to understand the individual contributions of both, sense and antisense RNA as well as all five different DPR proteins.

5. In the end the most important question is how to transform the knowledge acquired in cell culture and animal experiments into a valid therapeutic strategy to improve the life of patients. Based on the toxic-gain of function hypothesis, there is already a very interesting approach using antisense oligonucleotides (ASOs) that bind to mRNA or pre-mRNA and lead to their silencing or degradation. This approach would prevent both RNA and protein toxicity mechanisms. There are already ASO therapies in clinical trials for

other diseases (Fernandes et al., 2013) and a group of researchers lead by C. Lagier-Tourenne and D. Cleveland is already testing the potential in *C9orf72* FTD/ALS (Lagier-Tourenne et al., 2013).

In the end, combining the data from animal models, cell culture and patients will help to decipher the specific role of DPR proteins and the other proposed disease mechanisms, RNA-mediated toxicity and *C9orf72* loss function. Taking into account the progress that has been made over the past two years alone, there is a unique potential to find a feasible therapy for these severe neurodegenerative diseases in the near future.

6. References

Al-Sarraj, S., King, A., Troakes, C., Smith, B., Maekawa, S., Bodi, I., Rogelj, B., Al-Chalabi, A., Hortobagyi, T., and Shaw, C.E. (2011). p62 positive, TDP-43 negative, neuronal cytoplasmic and intranuclear inclusions in the cerebellum and hippocampus define the pathology of C9orf72-linked FTLD and MND/ALS. Acta Neuropathologica 122, 691-702.

Almeida, S., Gascon, E., Tran, H., Chou, H.J., Gendron, T.F., DeGroot, S., Tapper, A.R., Sellier, C., Charlet-Berguerand, N., and Karydas, A. (2013). Modeling key pathological features of frontotemporal dementia with C9ORF72 repeat expansion in iPSC-derived human neurons. Acta Neuropathologica 126, 385-399.

Andersen, P.M., and Al-Chalabi, A. (2011). Clinical genetics of amyotrophic lateral sclerosis: what do we really know? Nature Reviews Neurology 7, 603-615.

Ash, P.E., Bieniek, K.F., Gendron, T.F., Caulfield, T., Lin, W.L., Dejesus-Hernandez, M., van Blitterswijk, M.M., Jansen-West, K., Paul, J.W., 3rd, Rademakers, R., *et al.* (2013). Unconventional Translation of C9ORF72 GGGGCC Expansion Generates Insoluble Polypeptides Specific to c9FTD/ALS. Neuron.

Ayala, Y.M., Zago, P., D'Ambrogio, A., Xu, Y.-F., Petrucelli, L., Buratti, E., and Baralle, F.E. (2008). Structural determinants of the cellular localization and shuttling of TDP-43. Journal of cell science 121, 3778-3785.

Baloh, R.H. (2011). TDP-43: the relationship between protein aggregation and neurodegeneration in amyotrophic lateral sclerosis and frontotemporal lobar degeneration. FEBS Journal 278, 3539-3549.

Barmada, S.J., Serio, A., Arjun, A., Bilican, B., Daub, A., Ando, D.M., Tsvetkov, A., Pleiss, M., Li, X., and Peisach, D. (2014). Autophagy induction enhances TDP43 turnover and survival in neuronal ALS models. Nature chemical biology 10, 677-685.

Barmada, S.J., Skibinski, G., Korb, E., Rao, E.J., Wu, J.Y., and Finkbeiner, S. (2010). Cytoplasmic mislocalization of TDP-43 is toxic to neurons and enhanced by a mutation associated with familial amyotrophic lateral sclerosis. The Journal of Neuroscience 30, 639-649.

Basso, M., Samengo, G., Nardo, G., Massignan, T., D'Alessandro, G., Tartari, S., Cantoni, L., Marino, M., Cheroni, C., and De Biasi, S. (2009). Characterization of detergent-insoluble proteins in ALS indicates a causal link between nitrative stress and aggregation in pathogenesis. PloS one 4, e8130.

Belzil, V.V., Bauer, P.O., Gendron, T.F., Murray, M.E., Dickson, D., and Petrucelli, L. (2014). Characterization of DNA hypermethylation in the cerebellum of c9FTD/ALS patients. Brain research 1584, 15-21.

Belzil, V.V., Bauer, P.O., Prudencio, M., Gendron, T.F., Stetler, C.T., Yan, I.K., Pregent, L., Daughrity, L., Baker, M.C., and Rademakers, R. (2013a). Reduced C9orf72 gene expression in

c9FTD/ALS is caused by histone trimethylation, an epigenetic event detectable in blood. Acta Neuropathologica 126, 895-905.

Belzil, V.V., Gendron, T.F., and Petrucelli, L. (2013b). RNA-mediated toxicity in neurodegenerative disease. Molecular and Cellular Neuroscience 56, 406-419.

Bennion Callister, J., and Pickering-Brown, S.M. (2014). Pathogenesis/genetics of frontotemporal dementia and how it relates to ALS. Experimental Neurology 262, 84-90.

Benussi, L., Rossi, G., Glionna, M., Tonoli, E., Piccoli, E., Fostinelli, S., Paterlini, A., Flocco, R., Albani, D., and Pantieri, R. (2013). C9ORF72 hexanucleotide repeat number in frontotemporal lobar degeneration: a genotype-phenotype correlation study. Journal of Alzheimer's disease: JAD 38, 799-808.

Binici, J., and Koch, J. (2014). BAG-6, a jack of all trades in health and disease. Cellular and Molecular Life Sciences 71, 1829-1837.

Blokhuis, A.M., Groen, E.J.N., Koppers, M., van den Berg, L.H., and Pasterkamp, R.J. (2013). Protein aggregation in amyotrophic lateral sclerosis. Acta Neuropathologica 125, 777-794.

Borroni, B., Bonvicini, C., Alberici, A., Buratti, E., Agosti, C., Archetti, S., Papetti, A., Stuani, C., Di Luca, M., and Gennarelli, M. (2009). Mutation within TARDBP leads to frontotemporal dementia without motor neuron disease. Human mutation 30, E974-E983.

Braak, H., and Braak, E. (1991). Neuropathological stageing of Alzheimer-related changes. Acta Neuropathol (Berl) 82, 239-259.

Braak, H., Del Tredici, K., Rüb, U., de Vos, R.A., Steur, E.N.J., and Braak, E. (2003). Staging of brain pathology related to sporadic Parkinson's disease. Neurobiology of aging 24, 197-211.

Browne, S.E., Bowling, A.C., Macgarvey, U., Baik, M.J., Berger, S.C., Muquit, M.M., Bird, E.D., and Beal, M.F. (1997). Oxidative damage and metabolic dysfunction in Huntington's disease: selective vulnerability of the basal ganglia. Annals of neurology 41, 646-653.

Bucciantini, M., Giannoni, E., Chiti, F., Baroni, F., Formigli, L., Zurdo, J., Taddei, N., Ramponi, G., Dobson, C.M., and Stefani, M. (2002). Inherent toxicity of aggregates implies a common mechanism for protein misfolding diseases. Nature 416, 507-511.

Byrne, S., Elamin, M., Bede, P., Shatunov, A., Walsh, C., Corr, B., Heverin, M., Jordan, N., Kenna, K., Lynch, C., *et al.* (2012). Cognitive and clinical characteristics of patients with amyotrophic lateral sclerosis carrying a C9orf72 repeat expansion: a population-based cohort study. Lancet Neurol 11, 232-240.

Caccamo, A., Majumder, S., Richardson, A., Strong, R., and Oddo, S. (2010). Molecular Interplay between Mammalian Target of Rapamycin (mTOR), Amyloid-β, and Tau EFFECTS ON COGNITIVE IMPAIRMENTS. Journal of Biological Chemistry 285, 13107-13120.

Caspersen, C., Wang, N., Yao, J., Sosunov, A., Chen, X., Lustbader, J.W., Xu, H.W., Stern, D., McKhann, G., and Yan, S.D. (2005). Mitochondrial Abeta: a potential focal point for neuronal

metabolic dysfunction in Alzheimer's disease. FASEB journal: official publication of the Federation of American Societies for Experimental Biology 19, 2040-2041.

Chan, N.C., Salazar, A.M., Pham, A.H., Sweredoski, M.J., Kolawa, N.J., Graham, R.L., Hess, S., and Chan, D.C. (2011). Broad activation of the ubiquitin-proteasome system by Parkin is critical for mitophagy. Human molecular genetics, ddr048.

Chen-Plotkin, A.S., Lee, V.M.Y., and Trojanowski, J.Q. (2010). TAR DNA-binding protein 43 in neurodegenerative disease. Nat Rev Neurol 6, 211-220.

Chen, L., Thiruchelvam, M.J., Madura, K., and Richfield, E.K. (2006). Proteasome dysfunction in aged human α-synuclein transgenic mice. Neurobiology of disease 23, 120-126.

Cheroni, C., Marino, M., Tortarolo, M., Veglianese, P., De Biasi, S., Fontana, E., Zuccarello, L.V., Maynard, C.J., Dantuma, N.P., and Bendotti, C. (2009). Functional alterations of the ubiquitin-proteasome system in motor neurons of a mouse model of familial amyotrophic lateral sclerosis†. Human molecular genetics 18, 82-96.

Chew, J., Gendron, T.F., Prudencio, M., Sasaguri, H., Zhang, Y.-J., Castanedes-Casey, M., Lee, C.W., Jansen-West, K., Kurti, A., and Murray, M.E. (2015). C9ORF72 repeat expansions in mice cause TDP-43 pathology, neuronal loss, and behavioral deficits. Science, aaa9344.

Chhangani, D., and Mishra, A. (2013). Protein Quality Control System in Neurodegeneration: A Healing Company Hard to Beat but Failure is Fatal. Mol Neurobiol 48, 141-156.

Ching, J.K., and Weihl, C.C. (2013). Rapamycin-induced autophagy aggravates pathology and weakness in a mouse model of VCP-associated myopathy. Autophagy 9, 799-800.

Chiti, F., and Dobson, C.M. (2006). Protein misfolding, functional amyloid, and human disease. Annu Rev Biochem 75, 333-366.

Ciura, S., Lattante, S., Le Ber, I., Latouche, M., Tostivint, H., Brice, A., and Kabashi, E. (2013). Loss of function of C9orf72 causes motor deficits in a zebrafish model of Amyotrophic Lateral Sclerosis. Annals of neurology 74, 180-187.

Cleary, J.D., and Ranum, L.P. (2013). Repeat-associated non-ATG (RAN) translation in neurological disease. Hum Mol Genet.

Colombrita, C., Zennaro, E., Fallini, C., Weber, M., Sommacal, A., Buratti, E., Silani, V., and Ratti, A. (2009). TDP-43 is recruited to stress granules in conditions of oxidative insult. Journal of neurochemistry 111, 1051-1061.

Constantine, R., Zhang, H., Gerstner, C.D., Frederick, J.M., and Baehr, W. (2012). Uncoordinated (UNC)119: coordinating the trafficking of myristoylated proteins. Vision Res 75, 26-32.

Cooper-Knock, J., Hewitt, C., Highley, J.R., Brockington, A., Milano, A., Man, S., Martindale, J., Hartley, J., Walsh, T., Gelsthorpe, C., *et al.* (2012). Clinico-pathological features in amyotrophic lateral sclerosis with expansions in C9ORF72. Brain 135, 751-764.

Cooper-Knock, J., Kirby, J., Highley, R., and Shaw, P.J. (2015). The spectrum of C9orf72-mediated neurodegeneration and amyotrophic lateral sclerosis. Neurotherapeutics 12, 326-339.

Crouch, P.J., Blake, R., Duce, J.A., Ciccotosto, G.D., Li, Q.-X., Barnham, K.J., Curtain, C.C., Cherny, R.A., Cappai, R., and Dyrks, T. (2005). Copper-dependent inhibition of human cytochrome c oxidase by a dimeric conformer of amyloid-β1-42. The Journal of neuroscience 25, 672-679.

Cummings, C.J., Mancini, M.A., Antalffy, B., DeFranco, D.B., Orr, H.T., and Zoghbi, H.Y. (1998). Chaperone suppression of aggregation and altered subcellular proteasome localization imply protein misfolding in SCA1. Nature genetics 19, 148-154.

Dantuma, N.P., and Bott, L.C. (2014). The ubiquitin-proteasome system in neurodegenerative diseases: precipitating factor, yet part of the solution. Frontiers in Molecular Neuroscience 7, 70.

Dantuma, N.P., Lindsten, K., Glas, R., Jellne, M., and Masucci, M.G. (2000). Short-lived green fluorescent proteins for quantifying ubiquitin/proteasome-dependent proteolysis in living cells. Nature biotechnology 18, 538-543.

Davidson, Y.S., Barker, H., Robinson, A.C., Thompson, J.C., Harris, J., Troakes, C., Smith, B., Al-Saraj, S., Shaw, C., and Rollinson, S. (2014). Brain distribution of dipeptide repeat proteins in frontotemporal lobar degeneration and motor neurone disease associated with expansions in C9ORF72. Acta Neuropathol Commun 2, 70.

DeJesus-Hernandez, M., Mackenzie, I.R., Boeve, B.F., Boxer, A.L., Baker, M., Rutherford, N.J., Nicholson, A.M., Finch, N.A., Flynn, H., Adamson, J., *et al.* (2011). Expanded GGGGCC hexanucleotide repeat in noncoding region of C9ORF72 causes chromosome 9p-linked FTD and ALS. Neuron 72, 245-256.

Deng, H.-X., Chen, W., Hong, S.-T., Boycott, K.M., Gorrie, G.H., Siddique, N., Yang, Y., Fecto, F., Shi, Y., and Zhai, H. (2011). Mutations in UBQLN2 cause dominant X-linked juvenile and adult-onset ALS and ALS/dementia. Nature 477, 211-215.

Deng, Y., Albin, R., Penney, J., Young, A., Anderson, K., and Reiner, A. (2004). Differential loss of striatal projection systems in Huntington's disease: a quantitative immunohistochemical study. Journal of chemical neuroanatomy 27, 143-164.

Dols-Icardo, O., García-Redondo, A., Rojas-García, R., Sánchez-Valle, R., Noguera, A., Gómez-Tortosa, E., Pastor, P., Hernández, I., Esteban-Pérez, J., and Suárez-Calvet, M. (2014). Characterization of the repeat expansion size in C9orf72 in amyotrophic lateral sclerosis and frontotemporal dementia. Human molecular genetics 23, 749-754.

Donnelly, C.J., Zhang, P.-W., Pham, J.T., Haeusler, A.R., Mistry, N.A., Vidensky, S., Daley, E.L., Poth, E.M., Hoover, B., and Fines, D.M. (2013). RNA toxicity from the ALS/FTD C9ORF72 expansion is mitigated by antisense intervention. Neuron 80, 415-428.

Dormann, D., and Haass, C. (2011). TDP-43 and FUS: a nuclear affair. Trends in neurosciences 34, 339-348.

Ebrahimi-Fakhari, D., Cantuti-Castelvetri, I., Fan, Z., Rockenstein, E., Masliah, E., Hyman, B.T., McLean, P.J., and Unni, V.K. (2011). Distinct roles in vivo for the ubiquitin–proteasome system and the autophagy–lysosomal pathway in the degradation of α-synuclein. The Journal of Neuroscience 31, 14508-14520.

Eisele, Y.S., Obermüller, U., Heilbronner, G., Baumann, F., Kaeser, S.A., Wolburg, H., Walker, L.C., Staufenbiel, M., Heikenwalder, M., and Jucker, M. (2010). Peripherally applied Aβ-containing inoculates induce cerebral β-amyloidosis. Science 330, 980-982.

Fallini, C., Bassell, G.J., and Rossoll, W. (2012). The ALS disease protein TDP-43 is actively transported in motor neuron axons and regulates axon outgrowth. Human molecular genetics 21, 3703-3718.

Farg, M.A., Sundaramoorthy, V., Sultana, J.M., Yang, S., Atkinson, R.A., Levina, V., Halloran, M.A., Gleeson, P.A., Blair, I.P., and Soo, K.Y. (2014). C9ORF72, implicated in amytrophic lateral sclerosis and frontotemporal dementia, regulates endosomal trafficking. Human molecular genetics, ddu068.

Feiguin, F., Godena, V.K., Romano, G., D'Ambrogio, A., Klima, R., and Baralle, F.E. (2009). Depletion of TDP-43 affects Drosophila motoneurons terminal synapsis and locomotive behavior. FEBS letters 583, 1586-1592.

Fernandes, S.A., Douglas, A.G., Varela, M.A., Wood, M.J., and Aoki, Y. (2013). Oligonucleotide-based therapy for FTD/ALS caused by the C9orf72 repeat expansion: a perspective. Journal of nucleic acids 2013.

Ferrari, R., Kapogiannis, D., Huey, E.D., and Momeni, P. (2011). FTD and ALS: a tale of two diseases. Current Alzheimer research 8, 273-294.

Ferreira, S.T., Vieira, M.N., and De Felice, F.G. (2007). Soluble protein oligomers as emerging toxins in Alzheimer's and other amyloid diseases. IUBMB life 59, 332-345.

Fortun, J., Dunn, W.A., Joy, S., Li, J., and Notterpek, L. (2003). Emerging role for autophagy in the removal of aggresomes in Schwann cells. The Journal of neuroscience 23, 10672-10680.

Fratta, P., Polke, J.M., Newcombe, J., Mizielinska, S., Lashley, T., Poulter, M., Beck, J., Preza, E., Devoy, A., and Sidle, K. (2015). Screening a UK amyotrophic lateral sclerosis cohort provides evidence of multiple origins of the C9orf72 expansion. Neurobiology of aging 36, 546. e541-546. e547.

Frost, B., Jacks, R.L., and Diamond, M.I. (2009). Propagation of tau misfolding from the outside to the inside of a cell. Journal of Biological Chemistry 284, 12845-12852.

Galimberti, D., Reif, A., Dell'Osso, B., Kittel-Schneider, S., Leonhard, C., Herr, A., Palazzo, C., Villa, C., Fenoglio, C., and Serpente, M. (2014). The C9ORF72 hexanucleotide repeat expansion is a rare cause of schizophrenia. Neurobiology of aging 35, 1214. e1217-1214. e1210.

García-Redondo, A., Dols-Icardo, O., Rojas-García, R., Esteban-Pérez, J., Cordero-Vázquez, P., Muñoz-Blanco, J.L., Catalina, I., González-Muñoz, M., Varona, L., and Sarasola, E. (2013).

Analysis of the C9orf72 gene in patients with amyotrophic lateral sclerosis in Spain and different populations worldwide. Human mutation 34, 79-82.

Gellera, C., Tiloca, C., Del Bo, R., Corrado, L., Pensato, V., Agostini, J., Cereda, C., Ratti, A., Castellotti, B., and Corti, S. (2012). Ubiquilin 2 mutations in Italian patients with amyotrophic lateral sclerosis and frontotemporal dementia. Journal of Neurology, Neurosurgery & Psychiatry, jnnp-2012-303433.

Gendron, T.F., Bieniek, K.F., Zhang, Y.J., Jansen-West, K., Ash, P.E., Caulfield, T., Daughrity, L., Dunmore, J.H., Castanedes-Casey, M., Chew, J., *et al.* (2013). Antisense transcripts of the expanded C9ORF72 hexanucleotide repeat form nuclear RNA foci and undergo repeat-associated non-ATG translation in c9FTD/ALS. Acta Neuropathologica 126, 829-844.

Gomez-Deza, J., Lee, Y.-b., Troakes, C., Nolan, M., Al-Sarraj, S., Gallo, J.-M., and Shaw, C.E. (2015). Dipeptide repeat protein inclusions are rare in the spinal cord and almost absent from motor neurons in C9ORF72 mutant amyotrophic lateral sclerosis and are unlikely to cause their degeneration. Acta neuropathologica communications 3, 1-7.

Gu, M., Gash, M., Mann, V., Javoy-Agid, F., Cooper, J., and Schapira, A. (1996). Mitochondrial defect in Huntington's disease caudate nucleus. Annals of neurology 39, 385-389.

Guela, C., Wu, C.-K., Saroff, D., Lorenzo, A., Yuan, M., and Yankner, B.A. (1998). Aging renders the brain vulnerable to amyloid β-protein neurotoxicity. Nature medicine 4, 827-831.

Guerreiro, R., Brás, J., and Hardy, J. (2015). SnapShot: Genetics of ALS and FTD. Cell 160, 798-798. e791.

Guo, J.L., and Lee, V.M. (2014). Cell-to-cell transmission of pathogenic proteins in neurodegenerative diseases. Nature medicine 20, 130-138.

Guo, W., Chen, Y., Zhou, X., Kar, A., Ray, P., Chen, X., Rao, E.J., Yang, M., Ye, H., and Zhu, L. (2011). An ALS-associated mutation affecting TDP-43 enhances protein aggregation, fibril formation and neurotoxicity. Nature structural & molecular biology 18, 822-830.

Hara, T., Nakamura, K., Matsui, M., Yamamoto, A., Nakahara, Y., Suzuki-Migishima, R., Yokoyama, M., Mishima, K., Saito, I., and Okano, H. (2006). Suppression of basal autophagy in neural cells causes neurodegenerative disease in mice. Nature 441, 885-889.

Hardy, J., and Rogaeva, E. (2014). Motor neuron disease and frontotemporal dementia: sometimes related, sometimes not. Experimental Neurology 262, 75-83.

Harper, J.D., and Lansbury Jr, P.T. (1997). Models of amyloid seeding in Alzheimer's disease and scrapie: mechanistic truths and physiological consequences of the time-dependent solubility of amyloid proteins. Annual review of biochemistry 66, 385-407.

Hessa, T., Sharma, A., Mariappan, M., Eshleman, H.D., Gutierrez, E., and Hegde, R.S. (2011). Protein targeting and degradation are coupled for elimination of mislocalized proteins. Nature 475, 394-397.

Hipp, M.S., Park, S.-H., and Hartl, F.U. (2014). Proteostasis impairment in protein-misfolding and-aggregation diseases. Trends in cell biology 24, 506-514.

Hipp, M.S., Patel, C.N., Bersuker, K., Riley, B.E., Kaiser, S.E., Shaler, T.A., Brandeis, M., and Kopito, R.R. (2012). Indirect inhibition of 26S proteasome activity in a cellular model of Huntington's disease. The Journal of cell biology 196, 573-587.

Holm, I., Isaacs, A., and Mackenzie, I.A. (2009). Absence of FUS-immunoreactive pathology in frontotemporal dementia linked to chromosome 3 (FTD-3) caused by mutation in the CHMP2B gene. Acta Neuropathologica 118, 719-720.

Holmes, B.B., and Diamond, M.I. (2012). Cellular mechanisms of protein aggregate propagation. Current opinion in neurology 25, 721.

Hosler, B.A., Siddique, T., Sapp, P.C., Sailor, W., Huang, M.C., Hossain, A., Daube, J.R., Nance, M., Fan, C., Kaplan, J., *et al.* (2000). Linkage of familial amyotrophic lateral sclerosis with frontotemporal dementia to chromosome 9q21-q22. Jama 284, 1664-1669.

Ii, K., Ito, H., Tanaka, K., and Hirano, A. (1997). Immunocytochemical co-localization of the proteasome in ubiquitinated structures in neurodegenerative diseases and the elderly. Journal of Neuropathology & Experimental Neurology 56, 125-131.

Ishiba, Y., Higashide, T., Mori, N., Kobayashi, A., Kubota, S., McLaren, M.J., Satoh, H., Wong, F., and Inana, G. (2007). Targeted inactivation of synaptic HRG4 (UNC119) causes dysfunction in the distal photoreceptor and slow retinal degeneration, revealing a new function. Experimental eye research 84, 473-485.

Ishihara, N., and Mizushima, N. (2009). A receptor for eating mitochondria. Developmental cell 17, 1-2.

Ivanov, I.P., Firth, A.E., Michel, A.M., Atkins, J.F., and Baranov, P.V. (2011). Identification of evolutionarily conserved non-AUG-initiated N-terminal extensions in human coding sequences. Nucleic Acids Res 39, 4220-4234.

Iwata, A., Christianson, J.C., Bucci, M., Ellerby, L.M., Nukina, N., Forno, L.S., and Kopito, R.R. (2005). Increased susceptibility of cytoplasmic over nuclear polyglutamine aggregates to autophagic degradation. Proceedings of the National Academy of Sciences of the United States of America 102, 13135-13140.

Jana, N.R., Zemskov, E.A., Wang, G.-h., and Nukina, N. (2001). Altered proteasomal function due to the expression of polyglutamine-expanded truncated N-terminal huntingtin induces apoptosis by caspase activation through mitochondrial cytochrome c release. Human molecular genetics 10, 1049-1059.

Jarrett, J.T., and Lansbury, P.T. (1993). Seeding "one-dimensional crystallization" of amyloid: a pathogenic mechanism in Alzheimer's disease and scrapie? Cell 73, 1055-1058.

Josephs, K., Knopman, D., Whitwell, J., Boeve, B., Parisi, J., Petersen, R., and Dickson, D. (2005). Survival in two variants of tau-negative frontotemporal lobar degeneration: FTLD-U vs FTLD-MND. Neurology 65, 645-647.

Josephs, K.A. (2008). Frontotemporal dementia and related disorders: deciphering the enigma. Annals of neurology 64, 4-14.

Josephs, K.A. (2010). Caudate atrophy on MRI is a characteristic feature of FTLD-FUS. 17, 969-975.

Josephs, K.A., Hodges, J.R., Snowden, J.S., Mackenzie, I.R., Neumann, M., Mann, D.M., and Dickson, D.W. (2011). Neuropathological background of phenotypical variability in frontotemporal dementia. Acta Neuropathologica 122, 137-153.

Ju, J.-S., and Weihl, C.C. (2010). p97/VCP at the intersection of the autophagy and the ubiquitin proteasome system. Autophagy 6, 283-285.

Jucker, M., and Walker, L.C. (2013). Self-propagation of pathogenic protein aggregates in neurodegenerative diseases. Nature 501, 45-51.

Kabashi, E., Lin, L., Tradewell, M.L., Dion, P.A., Bercier, V., Bourgouin, P., Rochefort, D., Hadj, S.B., Durham, H.D., and Velde, C.V. (2010). Gain and loss of function of ALS-related mutations of TARDBP (TDP-43) cause motor deficits in vivo. Human molecular genetics 19, 671-683.

Kawaguchi, Y., Kovacs, J.J., McLaurin, A., Vance, J.M., Ito, A., and Yao, T.-P. (2003). The deacetylase HDAC6 regulates aggresome formation and cell viability in response to misfolded protein stress. Cell 115, 727-738.

Keck, S., Nitsch, R., Grune, T., and Ullrich, O. (2003). Proteasome inhibition by paired helical filament-tau in brains of patients with Alzheimer's disease. Journal of neurochemistry 85, 115-122.

Keller, J.N., Hanni, K.B., and Markesbery, W.R. (2000). Impaired proteasome function in Alzheimer's disease. Journal of neurochemistry 75, 436-439.

Kiernan, M.C., Vucic, S., Cheah, B.C., Turner, M.R., Eisen, A., Hardiman, O., Burrell, J.R., and Zoing, M.C. (2011). Amyotrophic lateral sclerosis. Lancet 377, 942-955.

Kirkin, V., McEwan, D.G., Novak, I., and Dikic, I. (2009). A role for ubiquitin in selective autophagy. Molecular cell 34, 259-269.

Knobel, K.M., Davis, W.S., Jorgensen, E.M., and Bastiani, M.J. (2001). UNC-119 suppresses axon branching in C. elegans. Development 128, 4079-4092.

Kobayashi, A., Higashide, T., Hamasaki, D., Kubota, S., Sakuma, H., An, W., Fujimaki, T., McLaren, M.J., Weleber, R.G., and Inana, G. (2000). HRG4 (UNC119) mutation found in cone-rod dystrophy causes retinal degeneration in a transgenic model. Invest Ophthalmol Vis Sci 41, 3268-3277.

Komatsu, M., Waguri, S., Chiba, T., Murata, S., Iwata, J.-i., Tanida, I., Ueno, T., Koike, M., Uchiyama, Y., and Kominami, E. (2006). Loss of autophagy in the central nervous system causes neurodegeneration in mice. Nature 441, 880-884.

Koppers, M., Blokhuis, A.M., Westeneng, H.-J., Terpstra, M.L., Zundel, C.A.C., Vieira de Sá, R., Schellevis, R.D., Waite, A.J., Blake, D.J., Veldink, J.H., *et al.* (2015). C9orf72 ablation in mice does not cause motor neuron degeneration or motor deficits. Annals of Neurology, n/a-n/a.

Kordower, J.H., Chu, Y., Hauser, R.A., Freeman, T.B., and Olanow, C.W. (2008). Lewy body–like pathology in long-term embryonic nigral transplants in Parkinson's disease. Nature medicine 14, 504-506.

Korolchuk, V.I., Mansilla, A., Menzies, F.M., and Rubinsztein, D.C. (2009). Autophagy inhibition compromises degradation of ubiquitin-proteasome pathway substrates. Molecular cell 33, 517-527.

Kristiansen, M., Deriziotis, P., Dimcheff, D.E., Jackson, G.S., Ovaa, H., Naumann, H., Clarke, A.R., van Leeuwen, F.W., Menéndez-Benito, V., and Dantuma, N.P. (2007). Disease-associated prion protein oligomers inhibit the 26S proteasome. Molecular cell 26, 175-188.

Kuhn, P.H., Wang, H., Dislich, B., Colombo, A., Zeitschel, U., Ellwart, J.W., Kremmer, E., Roßner, S., and Lichtenthaler, S.F. (2010). ADAM10 is the physiologically relevant, constitutive α-secretase of the amyloid precursor protein in primary neurons. The EMBO journal 29, 3020-3032.

Kwon, I., Xiang, S., Kato, M., Wu, L., Theodoropoulos, P., Wang, T., Kim, J., Yun, J., Xie, Y., and McKnight, S.L. (2014). Poly-dipeptides encoded by the C9orf72 repeats bind nucleoli, impede RNA biogenesis, and kill cells. Science 345, 1139-1145.

Lagier-Tourenne, C., Baughn, M., Rigo, F., Sun, S., Liu, P., Li, H.-R., Jiang, J., Watt, A.T., Chun, S., and Katz, M. (2013). Targeted degradation of sense and antisense C9orf72 RNA foci as therapy for ALS and frontotemporal degeneration. Proceedings of the National Academy of Sciences 110, E4530-E4539.

Le Ber, I., Camuzat, A., Guerreiro, R., Bouya-Ahmed, K., Bras, J., Nicolas, G., Gabelle, A., Didic, M., De Septenville, A., and Millecamps, S. (2013). SQSTM1 mutations in French patients with frontotemporal dementia or frontotemporal dementia with amyotrophic lateral sclerosis. JAMA neurology 70, 1403-1410.

Lee, D.Y., and Brown, E.J. (2012). Ubiquilins in the crosstalk among proteolytic pathways.

Lee, Y.B., Chen, H.J., Peres, J.N., Gomez-Deza, J., Attig, J., Stalekar, M., Troakes, C., Nishimura, A.L., Scotter, E.L., Vance, C., *et al.* (2013). Hexanucleotide repeats in ALS/FTD form length-dependent RNA foci, sequester RNA binding proteins, and are neurotoxic. Cell Rep 5, 1178-1186.

Lesage, S., Le Ber, I., Condroyer, C., Broussolle, E., Gabelle, A., Thobois, S., Pasquier, F., Mondon, K., Dion, P.A., Rochefort, D., *et al.* (2013). C9orf72 repeat expansions are a rare genetic cause of parkinsonism. Brain 136, 385-391.

Levine, T.P., Daniels, R.D., Gatta, A.T., Wong, L.H., and Hayes, M.J. (2013). The product of C9orf72, a gene strongly implicated in neurodegeneration, is structurally related to DENN Rab-GEFs. Bioinformatics 29, 499-503.

Li, J.-Y., Englund, E., Holton, J.L., Soulet, D., Hagell, P., Lees, A.J., Lashley, T., Quinn, N.P., Rehncrona, S., and Björklund, A. (2008). Lewy bodies in grafted neurons in subjects with Parkinson's disease suggest host-to-graft disease propagation. Nature medicine 14, 501-503.

Li, J., Uversky, V.N., and Fink, A.L. (2001). Effect of familial Parkinson's disease point mutations A30P and A53T on the structural properties, aggregation, and fibrillation of human α-synuclein. Biochemistry 40, 11604-11613.

Lim, J., and Yue, Z. (2015). Neuronal Aggregates: Formation, Clearance, and Spreading. Developmental Cell 32, 491-501.

Lin, M.-J., Cheng, C.-W., and Shen, C.-K.J. (2011). Neuronal function and dysfunction of Drosophila dTDP. PLoS One 6.

Lindersson, E., Beedholm, R., Højrup, P., Moos, T., Gai, W., Hendil, K.B., and Jensen, P.H. (2004). Proteasomal inhibition by α-synuclein filaments and oligomers. Journal of Biological Chemistry 279, 12924-12934.

Liu, E.Y., Russ, J., Wu, K., Neal, D., Suh, E., McNally, A.G., Irwin, D.J., Van Deerlin, V.M., and Lee, E.B. (2014). C9orf72 hypermethylation protects against repeat expansion-associated pathology in ALS/FTD. Acta Neuropathologica 128, 525-541.

Lomen-Hoerth, C., Anderson, T., and Miller, B. (2002). The overlap of amyotrophic lateral sclerosis and frontotemporal dementia. Neurology 59, 1077-1079.

Mackenzie, I.R., Arzberger, T., Kremmer, E., Troost, D., Lorenzl, S., Mori, K., Weng, S.M., Haass, C., Kretzschmar, H.A., Edbauer, D., and Neumann, M. (2013). Dipeptide repeat protein pathology in C9ORF72 mutation cases: clinico-pathological correlations. Acta Neuropathologica 126, 859-879.

Mackenzie, I.R., Bigio, E.H., Ince, P.G., Geser, F., Neumann, M., Cairns, N.J., Kwong, L.K., Forman, M.S., Ravits, J., and Stewart, H. (2007). Pathological TDP-43 distinguishes sporadic amyotrophic lateral sclerosis from amyotrophic lateral sclerosis with SOD1 mutations. Annals of neurology 61, 427-434.

Mackenzie, I.R.A., Neumann, M., Baborie, A., Sampathu, D.M., Plessis, D.D., Jaros, E., Perry, R.H., Trojanowski, J.Q., Mann, D.M.A., and Lee, V.M.Y. (2011). A harmonized classification system for FTLD-TDP pathology. Acta Neuropathologica 122, 111-113.

Mackenzie, I.R.A., Neumann, M., Bigio, E.H., Cairns, N.J., Alafuzoff, I., Kril, J., Kovacs, G.G., Ghetti, B., Halliday, G., Holm, I.E., *et al*. (2010). Nomenclature and nosology for neuropathologic subtypes of frontotemporal lobar degeneration: an update. Acta Neuropathologica 119, 1-4.

Maduro, M., and Pilgrim, D. (1995). Identification and cloning of unc-119, a gene expressed in the Caenorhabditis elegans nervous system. Genetics 141, 977-988.

Maduro, M.F., Gordon, M., Jacobs, R., and Pilgrim, D.B. (2000). The UNC-119 family of neural proteins is functionally conserved between humans, Drosophila and C. elegans. J Neurogenet 13, 191-212.

Maekawa, S., Leigh, P.N., King, A., Jones, E., Steele, J.C., Bodi, I., Shaw, C.E., Hortobagyi, T., and Al-Sarraj, S. (2009). TDP-43 is consistently co-localized with ubiquitinated inclusions in sporadic and Guam amyotrophic lateral sclerosis but not in familial amyotrophic lateral sclerosis with and without SOD1 mutations. Neuropathology 29, 672-683.

Mahoney, C.J., Beck, J., Rohrer, J.D., Lashley, T., Mok, K., Shakespeare, T., Yeatman, T., Warrington, E.K., Schott, J.M., Fox, N.C., *et al.* (2012a). Frontotemporal dementia with the C9ORF72 hexanucleotide repeat expansion: clinical, neuroanatomical and neuropathological features. Brain 135, 736-750.

Mahoney, C.J., Downey, L.E., Ridgway, G.R., Beck, J., Clegg, S., Blair, M., Finnegan, S., Leung, K.K., Yeatman, T., and Golden, H. (2012b). Longitudinal neuroimaging and neuropsychological profiles of frontotemporal dementia with C9ORF72 expansions. Alzheimers Res Ther 4, 41.

Majounie, E., Renton, A.E., Mok, K., Dopper, E.G., Waite, A., Rollinson, S., Chio, A., Restagno, G., Nicolaou, N., Simon-Sanchez, J., *et al.* (2012). Frequency of the C9orf72 hexanucleotide repeat expansion in patients with amyotrophic lateral sclerosis and frontotemporal dementia: a cross-sectional study. Lancet Neurol 11, 323-330.

Manczak, M., Anekonda, T.S., Henson, E., Park, B.S., Quinn, J., and Reddy, P.H. (2006). Mitochondria are a direct site of Aβ accumulation in Alzheimer's disease neurons: implications for free radical generation and oxidative damage in disease progression. Human molecular genetics 15, 1437-1449.

Martin, L.J., Pan, Y., Price, A.C., Sterling, W., Copeland, N.G., Jenkins, N.A., Price, D.L., and Lee, M.K. (2006). Parkinson's disease α-synuclein transgenic mice develop neuronal mitochondrial degeneration and cell death. The Journal of neuroscience 26, 41-50.

May, S., Hornburg, D., Schludi, M.H., Arzberger, T., Rentzsch, K., Schwenk, B.M., Grässer, F.A., Mori, K., Kremmer, E., and Banzhaf-Strathmann, J. (2014). C9orf72 FTLD/ALS-associated Gly-Ala dipeptide repeat proteins cause neuronal toxicity and Unc119 sequestration. Acta Neuropathologica 128, 485-503.

McCampbell, A., Taylor, J.P., Taye, A.A., Robitschek, J., Li, M., Walcott, J., Merry, D., Chai, Y., Paulson, H., Sobue, G., and Fischbeck, K.H. (2000). CREB-binding protein sequestration by expanded polyglutamine. Human Molecular Genetics 9, 2197-2202.

McNaught, K.S.P., and Jenner, P. (2001). Proteasomal function is impaired in substantia nigra in Parkinson's disease. Neuroscience letters 297, 191-194.

Meisler, M.H., Grant, A.E., Jones, J.M., Lenk, G.M., He, F., Todd, P.K., Kamali, M., Albin, R.L., Lieberman, A.P., and Langenecker, S.A. (2013). C9ORF72 expansion in a family with bipolar disorder. Bipolar disorders 15, 326-332.

Meyer-Luehmann, M., Coomaraswamy, J., Bolmont, T., Kaeser, S., Schaefer, C., Kilger, E., Neuenschwander, A., Abramowski, D., Frey, P., and Jaton, A.L. (2006). Exogenous induction of cerebral ß-amyloidogenesis is governed by agent and host. Science 313, 1781-1784.

Millecamps, S., Boillee, S., Le Ber, I., Seilhean, D., Teyssou, E., Giraudeau, M., Moigneu, C., Vandenberghe, N., Danel-Brunaud, V., Corcia, P., *et al.* (2012). Phenotype difference between ALS patients with expanded repeats in C9ORF72 and patients with mutations in other ALS-related genes. J Med Genet 49, 258-263.

Miller, R.G., Mitchell, J., Lyon, M., and Moore, D.H. (2007). Riluzole for amyotrophic lateral sclerosis (ALS)/motor neuron disease (MND). The Cochrane Library.

Mitra, S., Tsvetkov, A.S., and Finkbeiner, S. (2009). Single neuron ubiquitin-proteasome dynamics accompanying inclusion body formation in huntington disease. Journal of Biological Chemistry 284, 4398-4403.

Miyamoto, Y., Saiwaki, T., Yamashita, J., Yasuda, Y., Kotera, I., Shibata, S., Shigeta, M., Hiraoka, Y., Haraguchi, T., and Yoneda, Y. (2004). Cellular stresses induce the nuclear accumulation of importin α and cause a conventional nuclear import block. The Journal of cell biology 165, 617-623.

Mizielinska, S., Grönke, S., Niccoli, T., Ridler, C.E., Clayton, E.L., Devoy, A., Moens, T., Norona, F.E., Woollacott, I.O., and Pietrzyk, J. (2014). C9orf72 repeat expansions cause neurodegeneration in Drosophila through arginine-rich proteins. Science 345, 1192-1194.

Mizielinska, S., Lashley, T., Norona, F.E., Clayton, E.L., Ridler, C.E., Fratta, P., and Isaacs, A.M. (2013). C9orf72 frontotemporal lobar degeneration is characterised by frequent neuronal sense and antisense RNA foci. Acta Neuropathologica 126, 845-857.

Möller, G., Leenders, F., van Grunsven, E.G., Dolez, V., Qualmann, B., Kessels, M.M., Markus, M., Krazeisen, A., Husen, B., and Wanders, R.J. (1999). Characterization of the HSD17B4 gene: D-specific multifunctional protein 2/17β-hydroxysteroid dehydrogenase IV. The Journal of steroid biochemistry and molecular biology 69, 441-446.

Montuschi, A., Iazzolino, B., Calvo, A., Moglia, C., Lopiano, L., Restagno, G., Brunetti, M., Ossola, I., Presti, A.L., and Cammarosano, S. (2015). Cognitive correlates in amyotrophic lateral sclerosis: a population-based study in Italy. Journal of Neurology, Neurosurgery & Psychiatry 86, 168-173.

Mori, K., Arzberger, T., Grasser, F.A., Gijselinck, I., May, S., Rentzsch, K., Weng, S.M., Schludi, M.H., van der Zee, J., Cruts, M., *et al.* (2013a). Bidirectional transcripts of the expanded C9orf72 hexanucleotide repeat are translated into aggregating dipeptide repeat proteins. Acta Neuropathologica 126, 881-893.

Mori, K., Lammich, S., Mackenzie, I.R., Forne, I., Zilow, S., Kretzschmar, H., Edbauer, D., Janssens, J., Kleinberger, G., Cruts, M., *et al.* (2013b). hnRNP A3 binds to GGGGCC repeats and is a constituent of p62-positive/TDP43-negative inclusions in the hippocampus of patients with C9orf72 mutations. Acta Neuropathologica.

Mori, K., Weng, S.M., Arzberger, T., May, S., Rentzsch, K., Kremmer, E., Schmid, B., Kretzschmar, H.A., Cruts, M., Van Broeckhoven, C., *et al.* (2013c). The C9orf72 GGGGCC Repeat Is Translated into Aggregating Dipeptide-Repeat Proteins in FTLD/ALS. Science.

Mori, N., Ishiba, Y., Kubota, S., Kobayashi, A., Higashide, T., McLaren, M.J., and Inana, G. (2006). Truncation Mutation in HRG4 (UNC119) Leads to Mitochondrial ANT-1–Mediated Photoreceptor Synaptic and Retinal Degeneration by Apoptosis. Investigative ophthalmology & visual science 47, 1281-1292.

Morita, M., Al-Chalabi, A., Andersen, P., Hosler, B., Sapp, P., Englund, E., Mitchell, J., Habgood, J., De Belleroche, J., and Xi, J. (2006). A locus on chromosome 9p confers susceptibility to ALS and frontotemporal dementia. Neurology 66, 839-844.

Musiek, E.S., and Holtzman, D.M. (2015). Three dimensions of the amyloid hypothesis: time, space and'wingmen'. Nature neuroscience, 800-806.

Neumann, M., Sampathu, D.M., Kwong, L.K., Truax, A.C., Micsenyi, M.C., Chou, T.T., Bruce, J., Schuck, T., Grossman, M., Clark, C.M., *et al.* (2006). Ubiquitinated TDP-43 in frontotemporal lobar degeneration and amyotrophic lateral sclerosis. Science 314, 130-133.

Ng, A.S.L., Rademakers, R., and Miller, B.L. (2015). Frontotemporal dementia: a bridge between dementia and neuromuscular disease. Annals of the New York Academy of Sciences 1338, 71-93.

Nicklas, W., Vyas, I., and Heikkila, R.E. (1985). Inhibition of NADH-linked oxidation in brain mitochondria by 1-methyl-4-phenyl-pyridine, a metabolite of the neurotoxin, 1-methyl-4-phenyl-1, 2, 5, 6-tetrahydropyridine. Life sciences 36, 2503-2508.

O'Dowd, S., Curtin, D., Waite, A.J., Roberts, K., Pender, N., Reid, V., O'Connell, M., Williams, N.M., Morris, H.R., Traynor, B.J., and Lynch, T. (2012). C9ORF72 expansion in amyotrophic lateral sclerosis/frontotemporal dementia also causes parkinsonism. Mov Disord 27, 1072-1074.

Olzscha, H., Schermann, S.M., Woerner, A.C., Pinkert, S., Hecht, M.H., Tartaglia, G.G., Vendruscolo, M., Hayer-Hartl, M., Hartl, F.U., and Vabulas, R.M. (2011). Amyloid-like aggregates sequester numerous metastable proteins with essential cellular functions. Cell 144, 67-78.

Ortega, Z., Díaz-Hernández, M., Maynard, C.J., Hernández, F., Dantuma, N.P., and Lucas, J.J. (2010). Acute polyglutamine expression in inducible mouse model unravels ubiquitin/proteasome system impairment and permanent recovery attributable to aggregate formation. The Journal of Neuroscience 30, 3675-3688.

Palmeri, D., and Malim, M.H. (1999). Importin β can mediate the nuclear import of an arginine-rich nuclear localization signal in the absence of importin α. Molecular and cellular biology 19, 1218-1225.

Pankiv, S., Clausen, T.H., Lamark, T., Brech, A., Bruun, J.-A., Outzen, H., Øvervatn, A., Bjørkøy, G., and Johansen, T. (2007). p62/SQSTM1 binds directly to Atg8/LC3 to facilitate degradation of ubiquitinated protein aggregates by autophagy. Journal of Biological Chemistry 282, 24131-24145.

Peabody, D.S. (1989). Translation initiation at non-AUG triplets in mammalian cells. J Biol Chem 264, 5031-5035.

Perrin, R.J., Fagan, A.M., and Holtzman, D.M. (2009). Multimodal techniques for diagnosis and prognosis of Alzheimer's disease. Nature 461, 916-922.

Pick, A. (1892). Über die Beziehung der senilen Atrophie zur Aphasie. Prager Medizinische Wochenschrift 17, 165-167.

Price, D.L., Wong, P.C., Markowska, A.L., Lee, M.K., Thinakaren, G., Cleveland, D.W., Sisodia, S.S., and Borchelt, D.R. (2000). The value of transgenic models for the study of neurodegenerative diseases. Annals of the New York Academy of Sciences 920, 179-191.

Project, T.B. (2006). FDG Pet-Scan Dementia Today.

Proudfoot, M., Gutowski, N.J., Edbauer, D., Hilton, D.A., Stephens, M., Rankin, J., and Mackenzie, I.R. (2014). Early dipeptide repeat pathology in a frontotemporal dementia kindred with C9ORF72 mutation and intellectual disability. Acta Neuropathologica 127, 451-458.

Rademakers, R., Neumann, M., and Mackenzie, I.R. (2012). Advances in understanding the molecular basis of frontotemporal dementia. Nat Rev Neurol 8, 423-434.

Ramachandran, P.S., Boudreau, R.L., Schaefer, K.A., La Spada, A.R., and Davidson, B.L. (2014). Nonallele specific silencing of ataxin-7 improves disease phenotypes in a mouse model of SCA7. Molecular Therapy 22, 1635-1642.

Ravikumar, B., Vacher, C., Berger, Z., Davies, J.E., Luo, S., Oroz, L.G., Scaravilli, F., Easton, D.F., Duden, R., and O'Kane, C.J. (2004). Inhibition of mTOR induces autophagy and reduces toxicity of polyglutamine expansions in fly and mouse models of Huntington disease. Nature genetics 36, 585-595.

Ren, P.-H., Lauckner, J.E., Kachirskaia, I., Heuser, J.E., Melki, R., and Kopito, R.R. (2009). Cytoplasmic penetration and persistent infection of mammalian cells by polyglutamine aggregates. Nature cell biology 11, 219-225.

Renton, A.E., Majounie, E., Waite, A., Simon-Sanchez, J., Rollinson, S., Gibbs, J.R., Schymick, J.C., Laaksovirta, H., van Swieten, J.C., Myllykangas, L., *et al.* (2011). A hexanucleotide repeat expansion in C9ORF72 is the cause of chromosome 9p21-linked ALS-FTD. Neuron 72, 257-268.

Rideout, H.J., Lang-Rollin, I., and Stefanis, L. (2004). Involvement of macroautophagy in the dissolution of neuronal inclusions. The international journal of biochemistry & cell biology 36, 2551-2562.

Ripaud, L., Chumakova, V., Antonin, M., Hastie, A.R., Pinkert, S., Körner, R., Ruff, K.M., Pappu, R.V., Hornburg, D., and Mann, M. (2014). Overexpression of Q-rich prion-like proteins suppresses polyQ cytotoxicity and alters the polyQ interactome. Proceedings of the National Academy of Sciences 111, 18219-18224.

Rohrer, J.D., Isaacs, A.M., Mizielinska, S., Mead, S., Lashley, T., Wray, S., Sidle, K., Fratta, P., Orrell, R.W., and Hardy, J. (2015a). C9orf72 expansions in frontotemporal dementia and amyotrophic lateral sclerosis. The Lancet Neurology 14, 291-301.

Rohrer, J.D., Nicholas, J.M., Cash, D.M., van Swieten, J., Dopper, E., Jiskoot, L., van Minkelen, R., Rombouts, S.A., Cardoso, M.J., and Clegg, S. (2015b). Presymptomatic cognitive and neuroanatomical changes in genetic frontotemporal dementia in the Genetic Frontotemporal dementia Initiative (GENFI) study: a cross-sectional analysis. The Lancet Neurology 14, 253-262.

Rosen, H.J., Allison, S.C., Ogar, J.M., Amici, S., Rose, K., Dronkers, N., Miller, B.L., and Gorno-Tempini, M.L. (2006). Behavioral features in semantic dementia vs other forms of progressive aphasias. Neurology 67, 1752-1756.

Rubino, E., Rainero, I., Chiò, A., Rogaeva, E., Galimberti, D., Fenoglio, P., Grinberg, Y., Isaia, G., Calvo, A., and Gentile, S. (2012). SQSTM1 mutations in frontotemporal lobar degeneration and amyotrophic lateral sclerosis. Neurology 79, 1556-1562.

Rubio-Texeira, M., and Kaiser, C.A. (2006). Amino acids regulate retrieval of the yeast general amino acid permease from the vacuolar targeting pathway. Molecular biology of the cell 17, 3031-3050.

Sabatelli, M., Conforti, F.L., Zollino, M., Mora, G., Monsurro, M.R., Volanti, P., Marinou, K., Salvi, F., Corbo, M., Giannini, F., *et al.* (2012). C9ORF72 hexanucleotide repeat expansions in the Italian sporadic ALS population. Neurobiol Aging 33, 1848 e1815-1820.

Salmon, P., and Trono, D. (2007). Production and titration of lentiviral vectors. Current protocols in human genetics, 12.10. 11-12.10. 24.

Sanders, D.W., Kaufman, S.K., DeVos, S.L., Sharma, A.M., Mirbaha, H., Li, A., Barker, S.J., Foley, A.C., Thorpe, J.R., and Serpell, L.C. (2014). Distinct tau prion strains propagate in cells and mice and define different tauopathies. Neuron 82, 1271-1288.

Sareen, D., O'Rourke, J.G., Meera, P., Muhammad, A.K.M.G., Grant, S., Simpkinson, M., Bell, S., Carmona, S., Ornelas, L., Sahabian, A., *et al.* (2013). Targeting RNA Foci in iPSC-Derived Motor Neurons from ALS Patients with a C9ORF72 Repeat Expansion. Science Translational Medicine 5, 208ra149.

Sarkar, S., Davies, J.E., Huang, Z., Tunnacliffe, A., and Rubinsztein, D.C. (2007). Trehalose, a novel mTOR-independent autophagy enhancer, accelerates the clearance of mutant huntingtin and α-synuclein. Journal of Biological Chemistry 282, 5641-5652.

Sasayama, H., Shimamura, M., Tokuda, T., Azuma, Y., Yoshida, T., Mizuno, T., Nakagawa, M., Fujikake, N., Nagai, Y., and Yamaguchi, M. (2012). Knockdown of the Drosophila fused in sarcoma (FUS) homologue causes deficient locomotive behavior and shortening of motoneuron terminal branches.

Saxena, S., and Caroni, P. (2011). Selective neuronal vulnerability in neurodegenerative diseases: from stressor thresholds to degeneration. Neuron 71, 35-48.

Schapira, A., Cooper, J., Dexter, D., Clark, J., Jenner, P., and Marsden, C. (1990). Mitochondrial complex I deficiency in Parkinson's disease. Journal of neurochemistry 54, 823-827.

Schipper-Krom, S., Juenemann, K., Jansen, A.H., Wiemhoefer, A., van den Nieuwendijk, R., Smith, D.L., Hink, M.A., Bates, G.P., Overkleeft, H., and Ovaa, H. (2014). Dynamic recruitment of active proteasomes into polyglutamine initiated inclusion bodies. FEBS letters 588, 151-159.

Schipper-Krom, S., Juenemann, K., and Reits, E.A. (2012). The ubiquitin-proteasome system in Huntington's disease: are proteasomes impaired, initiators of disease, or coming to the rescue? Biochemistry research international 2012.

Schludi, M.H., May, S., Grässer, F.A., Rentzsch, K., Kremmer, E., Küpper, C., Klopstock, T., Arzberger, T., Edbauer, D., and Alliance, B.B.B. (2015). Distribution of dipeptide repeat proteins in cellular models and C9orf72 mutation cases suggests link to transcriptional silencing. Acta Neuropathologica, 1-18.

Sebti, S., Prébois, C., Pérez-Gracia, E., Bauvy, C., Desmots, F., Pirot, N., Gongora, C., Bach, A.-S., Hubberstey, A.V., and Palissot, V. (2014). BAG6/BAT3 modulates autophagy by affecting EP300/p300 intracellular localization. Autophagy 10, 1341-1342.

Seelaar, H., Klijnsma, K.Y., de Koning, I., van der Lugt, A., Chiu, W.Z., Azmani, A., Rozemuller, A.J.M., and van Swieten, J.C. (2010). Frequency of ubiquitin and FUS-positive, TDP-43-negative frontotemporal lobar degeneration. Journal of Neurology 257, 747-753.

Seo, H., Sonntag, K.C., and Isacson, O. (2004). Generalized brain and skin proteasome inhibition in Huntington's disease. Annals of neurology 56, 319-328.

Shen, W.-C., Li, H.-Y., Chen, G.-C., Chern, Y., and Tu, P.-h. (2015). Mutations in the ubiquitin-binding domain of OPTN/optineurin interfere with autophagy-mediated degradation of misfolded proteins by a dominant-negative mechanism. Autophagy 11, 685-700.

Snowden, J.S., Neary, D., and MANN, D.M. (2002). Frontotemporal dementia. The British Journal of Psychiatry 180, 140-143.

Snyder, H., Mensah, K., Theisler, C., Lee, J., Matouschek, A., and Wolozin, B. (2003). Aggregated and monomeric α-synuclein bind to the S6′ proteasomal protein and inhibit proteasomal function. Journal of Biological Chemistry 278, 11753-11759.

Song, D.D., Shults, C.W., Sisk, A., Rockenstein, E., and Masliah, E. (2004). Enhanced substantia nigra mitochondrial pathology in human α-synuclein transgenic mice after treatment with MPTP. Experimental Neurology 186, 158-172.

Stallings, N.R., Puttaparthi, K., Luther, C.M., Burns, D.K., and Elliott, J.L. (2010). Progressive motor weakness in transgenic mice expressing human TDP-43. Neurobiology of disease 40, 404-414.

Stepto, A., Gallo, J.-M., Shaw, C.E., and Hirth, F. (2014). Modelling C9ORF72 hexanucleotide repeat expansion in amyotrophic lateral sclerosis and frontotemporal dementia. Acta Neuropathologica 127, 377-389.

Stewart, H., Rutherford, N.J., Briemberg, H., Krieger, C., Cashman, N., Fabros, M., Baker, M., Fok, A., DeJesus-Hernandez, M., Eisen, A., *et al.* (2012). Clinical and pathological features of amyotrophic lateral sclerosis caused by mutation in the C9ORF72 gene on chromosome 9p. Acta Neuropathologica 123, 409-417.

Strong, M.J. (2008). The syndromes of frontotemporal dysfunction in amyotrophic lateral sclerosis. Amyotrophic Lateral Sclerosis 9, 323-338.

Strong, M.J., Grace, G.M., Freedman, M., Lomen-Hoerth, C., Woolley, S., Goldstein, L.H., Murphy, J., Shoesmith, C., Rosenfeld, J., and Leigh, P.N. (2009). Consensus criteria for the diagnosis of frontotemporal cognitive and behavioural syndromes in amyotrophic lateral sclerosis. Amyotrophic Lateral Sclerosis 10, 131-146.

Su, Z., Zhang, Y., Gendron, T.F., Bauer, P.O., Chew, J., Yang, W.-Y., Fostvedt, E., Jansen-West, K., Belzil, V.V., and Desaro, P. (2014). Discovery of a biomarker and lead small molecules to target r (GGGGCC)-associated defects in c9FTD/ALS. Neuron 83, 1043-1050.

Suh, E., Lee, E.B., Neal, D., Wood, E.M., Toledo, J.B., Rennert, L., Irwin, D.J., McMillan, C.T., Krock, B., and Elman, L.B. (2015). Semi-automated quantification of C9orf72 expansion size reveals inverse correlation between hexanucleotide repeat number and disease duration in frontotemporal degeneration. Acta Neuropathologica, 1-10.

Suzuki, N., Maroof, A.M., Merkle, F.T., Koszka, K., Intoh, A., Armstrong, I., Moccia, R., Davis-Dusenbery, B.N., and Eggan, K. (2013). The mouse C9ORF72 ortholog is enriched in neurons known to degenerate in ALS and FTD. Nature neuroscience 16, 1725-1727.

Swart, C., Haylett, W., Kinnear, C., Johnson, G., Bardien, S., and Loos, B. (2014). Neurodegenerative disorders: Dysregulation of a carefully maintained balance? Experimental Gerontology 58, 279-291.

Synofzik, M., Maetzler, W., Grehl, T., Prudlo, J., vom Hagen, J.M., Haack, T., Rebassoo, P., Munz, M., Schöls, L., and Biskup, S. (2012). Screening in ALS and FTD patients reveals 3 novel UBQLN2 mutations outside the PXX domain and a pure FTD phenotype. Neurobiology of aging 33, 2949. e2913-2949. e2917.

Takahashi, T., Kikuchi, S., Katada, S., Nagai, Y., Nishizawa, M., and Onodera, O. (2008). Soluble polyglutamine oligomers formed prior to inclusion body formation are cytotoxic. Human molecular genetics 17, 345-356.

Tao, Z., Wang, H., Xia, Q., Li, K., Li, K., Jiang, X., Xu, G., Wang, G., and Ying, Z. (2015). Nucleolar stress and impaired stress granule formation contribute to C9orf72 RAN translation-induced cytotoxicity. Human Molecular Genetics 24, 2426-2441.

Tashiro, Y., Urushitani, M., Inoue, H., Koike, M., Uchiyama, Y., Komatsu, M., Tanaka, K., Yamazaki, M., Abe, M., and Misawa, H. (2012). Motor neuron-specific disruption of proteasomes, but not autophagy, replicates amyotrophic lateral sclerosis. Journal of Biological Chemistry 287, 42984-42994.

Therrien, M., Rouleau, G.A., Dion, P.A., and Parker, J.A. (2013). Deletion of C9ORF72 results in motor neuron degeneration and stress sensitivity in C. elegans. PloS one 8, e83450.

Todd, P.K., Oh, S.Y., Krans, A., He, F., Sellier, C., Frazer, M., Renoux, A.J., Chen, K.C., Scaglione, K.M., Basrur, V., *et al.* (2013). CGG repeat-associated translation mediates neurodegeneration in fragile X tremor ataxia syndrome. Neuron 78, 440-455.

Touriol, C., Bornes, S., Bonnal, S., Audigier, S., Prats, H., Prats, A.C., and Vagner, S. (2003). Generation of protein isoform diversity by alternative initiation of translation at non-AUG codons. Biol Cell 95, 169-178.

Truant, R., and Cullen, B.R. (1999). The arginine-rich domains present in human immunodeficiency virus type 1 Tat and Rev function as direct importin β-dependent nuclear localization signals. Molecular and cellular biology 19, 1210-1217.

Tseng, B.P., Green, K.N., Chan, J.L., Blurton-Jones, M., and LaFerla, F.M. (2008). Aβ inhibits the proteasome and enhances amyloid and tau accumulation. Neurobiology of aging 29, 1607-1618.

Tusher, V.G., Tibshirani, R., and Chu, G. (2001). Significance analysis of microarrays applied to the ionizing radiation response. Proc Natl Acad Sci U S A 98, 5116-5121.

van Blitterswijk, M., DeJesus-Hernandez, M., Niemantsverdriet, E., Murray, M.E., Heckman, M.G., Diehl, N.N., Brown, P.H., Baker, M.C., Finch, N.A., and Bauer, P.O. (2013). Association between repeat sizes and clinical and pathological characteristics in carriers of C9ORF72 repeat expansions (Xpansize-72): a cross-sectional cohort study. The Lancet Neurology 12, 978-988.

Van Damme, P., and Robberecht, W. (2009). Recent advances in motor neuron disease. Current opinion in neurology 22, 486-492.

van der Zee, J., Gijselinck, I., Dillen, L., Van Langenhove, T., Theuns, J., Engelborghs, S., Philtjens, S., Vandenbulcke, M., Sleegers, K., Sieben, A., *et al.* (2013). A Pan-European study of the C9orf72 Repeat Associated with FTLD: Geographic Prevalence, Genomic Instability and Intermediate Repeats. Hum Mutat 34, 363-373.

van Welsem, M., Hogenhuis, J., Meininger, V., Metsaars, W., Hauw, J.J., and Seilhean, D. (2002). The relationship between Bunina bodies, skein-like inclusions and neuronal loss in amyotrophic lateral sclerosis. Acta Neuropathologica 103, 583-589.

Vance, C., Al-Chalabi, A., Ruddy, D., Smith, B.N., Hu, X., Sreedharan, J., Siddique, T., Schelhaas, H.J., Kusters, B., and Troost, D. (2006). Familial amyotrophic lateral sclerosis with frontotemporal dementia is linked to a locus on chromosome 9p13. 2–21.3. Brain 129, 868-876.

Vance, C., Rogelj, B., Hortobagyi, T., De Vos, K.J., Nishimura, A.L., Sreedharan, J., Hu, X., Smith, B., Ruddy, D., Wright, P., *et al.* (2009). Mutations in FUS, an RNA processing protein, cause familial amyotrophic lateral sclerosis type 6. Science 323, 1208-1211.

Vengoechea, J., David, M.P., Yaghi, S.R., Carpenter, L., and Rudnicki, S.A. (2013). Clinical variability and female penetrance in X-linked familial FTD/ALS caused by a P506S mutation in UBQLN2. Amyotrophic Lateral Sclerosis and Frontotemporal Degeneration 14, 615-619.

Verheijden, S., Beckers, L., De Munter, S., Van Veldhoven, P.P., and Baes, M. (2014). Central nervous system pathology in MFP2 deficiency: insights from general and conditional knockout mouse models. Biochimie 98, 119-126.

Vichai, V., and Kirtikara, K. (2006). Sulforhodamine B colorimetric assay for cytotoxicity screening. Nat Protocols 1, 1112-1116.

Wang, J.-W., Brent, J.R., Tomlinson, A., Shneider, N.A., and McCabe, B.D. (2011). The ALS-associated proteins FUS and TDP-43 function together to affect Drosophila locomotion and life span. The Journal of clinical investigation 121, 4118.

Watanabe, M., Dykes-Hoberg, M., Culotta, V.C., Price, D.L., Wong, P.C., and Rothstein, J.D. (2001). Histological evidence of protein aggregation in mutant SOD1 transgenic mice and in amyotrophic lateral sclerosis neural tissues. Neurobiology of disease 8, 933-941.

Wen, X., Tan, W., Westergard, T., Krishnamurthy, K., Markandaiah, S.S., Shi, Y., Lin, S., Shneider, N.A., Monaghan, J., and Pandey, U.B. (2014). Antisense proline-arginine RAN dipeptides linked to C9ORF72-ALS/FTD form toxic nuclear aggregates that initiate in vitro and in vivo neuronal death. Neuron 84, 1213-1225.

Xi, Z., Zinman, L., Moreno, D., Schymick, J., Liang, Y., Sato, C., Zheng, Y., Ghani, M., Dib, S., Keith, J., *et al.* (2013). Hypermethylation of the CpG Island Near the GC Repeat in ALS with a C9orf72 Expansion. Am J Hum Genet.

Xu, Y.-F., Gendron, T.F., Zhang, Y.-J., Lin, W.-L., D'Alton, S., Sheng, H., Casey, M.C., Tong, J., Knight, J., and Yu, X. (2010). Wild-type human TDP-43 expression causes TDP-43 phosphorylation, mitochondrial aggregation, motor deficits, and early mortality in transgenic mice. The Journal of Neuroscience 30, 10851-10859.

Xu, Z., Poidevin, M., Li, X., Li, Y., Shu, L., Nelson, D.L., Li, H., Hales, C.M., Gearing, M., Wingo, T.S., and Jin, P. (2013). Expanded GGGGCC repeat RNA associated with amyotrophic lateral sclerosis and frontotemporal dementia causes neurodegeneration. Proc Natl Acad Sci U S A 110, 7778-7783.

Yamakawa, M., Ito, D., Honda, T., Kubo, K.-i., Noda, M., Nakajima, K., and Suzuki, N. (2015). Characterization of the dipeptide repeat protein in the molecular pathogenesis of c9FTD/ALS. Human Molecular Genetics 24, 1630-1645.

Yamamoto, A., Lucas, J.J., and Hen, R. (2000). Reversal of neuropathology and motor dysfunction in a conditional model of Huntington's disease. Cell 101, 57-66.

Yang, D., Abdallah, A., Li, Z., Lu, Y., Almeida, S., and Gao, F.-B. (2015). FTD/ALS-associated poly(GR) protein impairs the Notch pathway and is recruited by poly(GA) into cytoplasmic inclusions. Acta Neuropathologica, 1-11.

Yoshida, M. (2004). Amyotrophic lateral sclerosis with dementia: the clinicopathological spectrum. Neuropathology 24, 87-102.

Zhang, C., and Saunders, A.J. (2009). An emerging role for Ubiquilin 1 in regulating protein quality control system and in disease pathogenesis. Discovery medicine 8, 18.

Zhang, D., Iyer, L.M., He, F., and Aravind, L. (2012). Discovery of novel DENN proteins: implications for the evolution of eukaryotic intracellular membrane structures and human disease. Frontiers in genetics 3.

Zhang, H., Constantine, R., Vorobiev, S., Chen, Y., Seetharaman, J., Huang, Y.J., Xiao, R., Montelione, G.T., Gerstner, C.D., Davis, M.W., *et al.* (2011). UNC119 is required for G protein trafficking in sensory neurons. Nat Neurosci 14, 874-880.

Zhang, Y.-J., Jansen-West, K., Xu, Y.-F., Gendron, T.F., Bieniek, K.F., Lin, W.-L., Sasaguri, H., Caulfield, T., Hubbard, J., and Daughrity, L. (2014). Aggregation-prone c9FTD/ALS poly (GA) RAN-translated proteins cause neurotoxicity by inducing ER stress. Acta Neuropathologica 128, 505-524.

Zu, T., Duvick, L.A., Kaytor, M.D., Berlinger, M.S., Zoghbi, H.Y., Clark, H.B., and Orr, H.T. (2004). Recovery from polyglutamine-induced neurodegeneration in conditional SCA1 transgenic mice. The Journal of neuroscience 24, 8853-8861.

Zu, T., Gibbens, B., Doty, N.S., Gomes-Pereira, M., Huguet, A., Stone, M.D., Margolis, J., Peterson, M., Markowski, T.W., Ingram, M.A., *et al.* (2011). Non-ATG-initiated translation directed by microsatellite expansions. Proc Natl Acad Sci U S A 108, 260-265.

Zu, T., Liu, Y., Banez-Coronel, M., Reid, T., Pletnikova, O., Lewis, J., Miller, T.M., Harms, M.B., Falchook, A.E., Subramony, S.H., *et al.* (2013). RAN proteins and RNA foci from antisense transcripts in C9ORF72 ALS and frontotemporal dementia. Proc Natl Acad Sci U S A 110, E4968-4977.

7. Acknowledgements

At times our light goes out and is rekindled by a spark from another person.
Each of us owes deepest gratitude to those who have rekindled the flame within us.
– Albert Schweitzer

Es gibt viele Menschen, die mich bei der Erstellung dieser Arbeit unterstützt haben und ohne die es mir nicht möglich gewesen wäre sie erfolgreich zu beenden. Aus diesem Grunde möchte ich mich besonders bedanken bei:

Prof. Dr. Dieter Edbauer (Eddie), dass du mir die Chance gegeben hast ein Teil deines Labors zu sein. Danke, für deinen Enthusiasmus für unsere Projekte (Geht da was?), und deine Unterstützung, besonders in den schwierigen Zeiten, mental, an der Bench und mit Schokolade! Es war eine Achterbahnfahrt auf der ich viel gelernt habe und ich war immer gerne Teil deines Teams!

Prof. Dr. Dr. h.c. Christian Haass, als offizieller Doktorvater, speziell für ihr offenes Ohr für uns „Eddies"! Ich habe mich immer auch als Teil des Haass-Labors gefühlt und bin Ihnen sehr dankbar für Ihren wissenschaftlichen Input und für Ihren Enthusiasmus und Ihr Vertrauen in Bezug auf unsere Projekte mit der Alzheimer Gesellschaft München.

Allen Mitgliedern meiner Prüfungskommission, welche zum jetzigen Zeitpunkt noch nicht feststehen.

Meinen **Kollegen im Eddie Lab**. Ich hätte mir keine besseren Kollegen/Freunde wünschen können, mit denen ich diese verrückte Fahrt erlebt habe. Danke für all die vielen schönen Erinnerungen! Danke für all die wissenschaftlichen Diskussionen und Euren Input zu meinen Projekten, und Danke, dass ihr mir in den holprigen Zeiten eine solche Stütze wart!

Martin Schludi, danke dass du in so vielen Projekten mein „partner in crime" warst, und immer an den Erfolg geglaubt hast. **Kristin Rentzsch**, danke für die Berge an Western blots und all die andere Unterstützung, wenn ich sie gebraucht habe! **Carina Lehmer**, es gibt Menschen mit denen braucht man nicht viele Worte und ich bin froh, dass ich dich im letzten Jahr kennen lernen durfte! **Franziska Schreiber**, ich freue mich noch auf viele Gin-Tonics mit langen Gesprächen! **Benjamin Schwenk** dafür dass du großer PhD-Bruder, genauso Fußballverrückter und Party-People bist! **Denise Orozco** dafür, dass du mich immer motiviert hast und mit deinem Enthusiasmus für Wissenschaft angesteckt hast. **Hanne Hartmann**, für deine Fröhlichkeit und deine Hilfsbereitschaft im Labor.
Meinen neuen Kollegen **Qihui Zhou** und **Bahram Khosravi**, es hat mich gefreut euch kennen zu lernen und ich wünsche Euch viel Spaß und Erfolg in dem liebenswerten, chaotischen Haufen! **Johannes Trambauer**, auch wenn du nicht

„offiziell“ Teil des Eddielab bist, gehörst du doch irgendwie dazu und ich werde deine Kommentare beim Mittagessen vermissen.
Meinen ehemaligen Kollegen **Julia Banzhaf** und **Shih-Ming Weng** (Jonas) für die schöne Atmosphäre im Labor, die gemeinsame Zeit und den wissenschaftlichen Input.

Sabine Odoy, dafür dass du mir, immer schnell neue Antikörper, Medien oder sonstiges organisiert hast, wenn ich wieder verzweifelt vor dir stand und ganz dringend etwas gebraucht habe.

Unseren Kooperationspartner **Daniel Hornburg, Felix Meissner, Matthias Mann, Thomas Arzberger und Kohji Mori**, für Ihren wissenschaftlichen Input in den gemeinsamen Projekten.

Den Girls der Schnitzelgruppe **Dr. Teresa Bachhuber**, **Katrin Strecker**, **Laura Hasenkamp**, **Julia Götzl, Dr. Maria Patra**, **Dr. Denise Orozco**, **Dr. Frauke van Bebber und Dr. Joana McCarter**, es war eine tolle Zeit mit Euch und ich bin dankbar für unsere Freundschaft.
Dr. Eva Bentmann für deinen Input egal ob wissenschaftlich oder persönlich, dein Engagement und deine Hilfe, wenn ich sie gebraucht habe.

Allen Mitglieder des Haass Labors für die wissenschaftlichen und nicht wissenschaftlichen Diskussionen und die gute Arbeitsatmosphäre.

Meinen Uni Mädels, **Christina**, **Almut**, **Babsi** und **Silvia**, dafür dass wir nun schon seit 9 Jahren diesen Weg zusammen gehen und ich mich immer auf Euch verlassen kann.

Jeany Prinz, **Carina Lehmer, Denise Orozco, Franziska Schreiber** und **Dr. Benjamin Schwenk** für das Korrekturlesen meiner Arbeit.

Den Mitarbeitern der Alzheimer Gesellschaft München, besonders **Bianca Broda** und **Tobias Bartschinski**. Ihr habt mir gezeigt wie wichtig der Blick über den Tellerrand in der Forschung ist!

Felix Buggenthin, danke dass du da bist und immer ein offenes Ohr für meine Probleme hattest und sie dir auch noch beim 20. Mal mit Ruhe angehört hast.

Meiner Familie. Besonders **meinen Eltern**, die immer an mich geglaubt haben! Ohne Euch wäre ich niemals hier angekommen. Danke auch an meine **Großeltern** und meine **Tante Karin** für die Unterstützung, sowie an **Ute** und **Arno Buggenthin** für die Beruhigung meiner Nerven, wenn es mal wieder nötig war!